THE STUDY OF 8-HYDROXYQUINOLINE-2-CARBOXYLLIC ACID AND ITS METAL ION COMPLEXING PROPERTIES

F. Crisp McDonald, Jr.

A Thesis Submitted to the
University of North Carolina Wilmington in Partial Fulfillment
Of the Requirements for the Degree of
Master of Science

Department of Chemistry

University of North Carolina Wilmington

2005

Approved by

Advisory Committee

_____ _____

_____
Chair

Accepted by

_____
Dean, Graduate School

This thesis has been prepared in the style and format

consistent with

Inorganic Chemistry

TABLE OF CONTENTS

ABSTRACT

The metal ion coordinating properties of the ligand HQC (8-hydroxyquinoline-2-carboxylic acid) were studied by UV-visible spectroscopy and X-ray crystallography. The protonation constants of HQC were determined by monitoring absorbance of 5 x 10^{-5} *M* HQC at five different wavelengths in the range 210-300 nm as a function of pH. The protonation constants pK_1 and pK_2 were determined to be 10.14 and 3.92 at 25 ^{o}C in 0.1 M $NaClO_4$. The experiments were repeated with 5 x 10^{-5} *M* HQC and 5 x 10^{-5} *M* metal ion solutions. These experiments produced two apparent protonation constants (pK'_1 and pK'_2) that were shifted to lower pH by competition with the metal ion as compared with pK_1 and pK_2. These were used to calculate equilibrium constants for the metal ions (M) as:

$$M(HQC) + H^{+} \leftrightarrows M(HQC)H \qquad (pK'_1) \qquad [1]$$

$$M + HQC \leftrightarrows M(HQC) \qquad (\log[M] + pK_1 + pK_2 - pK'_1 - pK'_2) \qquad [2]$$

The HQC complexes also gave hydrolysis constants at higher pH according to:

$$M(HQC) + OH^{-} \leftrightarrows M(HQC)OH \qquad [3]$$

Log K_1 (eq. 2) was obtained in 0.1 *M* $NaClO_4$ at 25 ^{o}C for a selection of metal ions: Mg(II), 4.93; Ca(II), 6.16; Sr(II), 4.82; Ba(II), 4.10; La(III), 10.13; Gd(III), 9.89; Cu(II), 12.00; Zn(II), 9.10; Cd(II), 8.57; Pb(II), 11.35. The constants were remarkably high for a tridentate ligand with a donor set consisting of a pyridine nitrogen, and a phenolic and a carboxylic oxygen. These were discussed in terms of the high levels of preorganization of HQC, and contrasted with other similar ligands such as 8-hydroxyquinoline and dipicolinic acid. The high stability of HQC complexes is discussed in relation to its possible use in biomedical applications, such as the use of its Gd(III) complex as an MRI imaging agent.

The attachment of a proton to the HQC complexes as in equation 1 was of some interest. Accordingly, crystals of $[Zn((HQC)H)_2]$ $.2H_2O$ (**1**) and $[Cd((HQC)H)_2]$ $.2H_2O$ (**2**) were grown and the structures determined by X-ray crystallography. Crystals of **1** were triclinic, $P\bar{1}$, a = 7.152(3), b = 9.227(4), c = 15.629(7) Å, α = 103.978(7), β = 94.896(7), γ = 108.033(8)°, Z = 2, R = 0.0499. Crystals of **2** were triclinic, $P\bar{1}$, a = 7.0897(5), b = 9.1674(7), c = 16.0672(11) Å, α = 105.0240(10), β = 93.9910(10), γ = 107.1270(10)°, Z = 3, R = 0.033. The crystal structures showed that the protons present were indeed attached to the phenolic oxygens, which were coordinated to the metal ions. Of considerable interest was the very short O---O distance of 2.4-2.5 Å found for water molecules H-bonded to these protons, which is in the range for a very strong H-bond. The structures suggested that in the case of the Cd(II) complex (**2**) the proton was in one case actually attached to the water molecule to give a hydronium ion H-bonded to the non-protonated phenolic oxygen, while in the Zn(II) complex (**1**) the H-bond was actually symmetrical with the proton midway between the two oxygens. The significance of these short H-bonds is discussed in relation to their significance in biochemical processes.

ACKNOWLEDGMENTS

I would like to thank Dr. Hancock for sharing his immense knowledge of chemistry with me over the past three years. His and passion for his research daily inspires me. I would also like to thank Dr. Jones and Dr. Halkides for their input on my thesis and the questions they have answered, though many were off topic.

I would like to thank my friends, especially Bryan, Craig, and most of all Charley for their support during my graduate career. You have helped so much, there is no way I could possibly ever repay you.

To my family, I would like to thank you for all the love and support throughout my entire life.

And finally to my parents, you both have taught me that hard work and determination can help you to reach any goals you set for yourself, no matter the size. I am forever in debt for how much you have given me and I hope you both realize how special you both are.

LIST OF TABLES

LIST OF FIGURES

INTRODUCTION

Modern medicine focuses a great deal on metal-ligand interactions in the human body. This can range from antidotes for metal poisoning to more intricate studies such as magnetic resonance imaging (MRI) used to identify potential problems internally without the aide of surgery. The stability of this metal-ligand complex in the body is paramount. Gadolinium complexes, for instance, are used as MRI imaging agents. Gadolinium is also toxic to humans, so when gadolinium is introduced to the body it must be complexed with a ligand sufficiently enough that it will not be displaced by another metal found biologically in the body such as zinc. It is this concept that drives researchers to discover new ligands which preferentially bind to specific metals over others. This preferential binding can be facilitated by better preorganization of the ligand. Donald Cram first defined preorganization as; the more nearly a ligand is constrained to be in a specific conformation required to complex the metal ion[1].

Metals in medicine

As the study of physics has brought extraordinary breakthroughs to surgery, so has chemistry brought breakthroughs in medicine. The field of medicine in the recent past has shifted focus, from the ordinarily organic based research to a new trend of bioinorganic chemistry, which is not confined to therapeutic purposes but also diagnostic and supplemental. Some functions metals in medicine have in our body are (but are not limited to): mineral supplements, radiopharmaceuticals, chelation therapy, enzyme inhibitors, therapeutic agents, and diagnostic agents (MRI and X-ray).

Because studies have shown the benefits of metals in the human body, the market for mineral supplements has grown into a multibillion dollar industry. Some documented benefits of

supplements are: iron facilitates oxygen transport in blood, calcium builds and strengthens bones and teeth, zinc has been shown to inhibit viral replication, magnesium activates certain enzymes related to carbohydrate metabolism, and sodium and potassium drive the process of secondary active transport of glucose in intestinal cells to name a few.

Metal ligand complexes are the foremost combatant of cancer to date. Cisplatin, a platinum complex, is the most widely used anticancer drug (Figure 1). This platinum drug is very effective when combined with other forms of chemotherapy for treatment of advanced lung, colorectal, and ovarian cancers [2,3]. Other anticancer agents include titanium complex (bis(β-diketonato)Ti^{4+} which is in clinical trials to target colon cancer[4]. Gold complexes are also being investigated for their anticarcinogenic properties[5] as are both gallium[6] and ruthenium[7] complexes. Other facets of metals in medicine include the gold thiolato complexes which are being used clinically to treat very severe cases of rheumatoid arthritis[8]; bismuth which has been used for centuries to treat gastrointestinal disorders[9] and is now also being used as an antiulcer agent; and silver compounds which are found in medicine as an antimicrobial agent[10]. The Fe^{3+} complex of desferrioxamine is a proven treatment for malaria[11], potassium and zinc complexes are thought to be HIV-1 inhibitors in specific complexes[12], while iron-sodium nitroprusside is often used to lower blood pressure during heart attacks and surgery[13].

Some of the most important breakthroughs of metals in medicine are the diagnostic capabilities they now allow. Radiopharmaceuticals and MRI imaging agents are two such advances. Most radiopharmaceuticals are used for diagnostic imaging are strong γ-emitters such as ^{99}Tc, ^{201}Tl, ^{111}In, ^{67}Ga, ^{51}Co, ^{51}Cr, and ^{169}Yb. Other less intense β-emitters like ^{89}Sr, ^{153}Sm, and ^{186}Re are used for therapy[14]. Examples of these radiopharmaceuticals include: Ceretec, a Tc^{V} complex, which is used to evaluate strokes and Cardiolite, a Tc^{I} complex, is used in

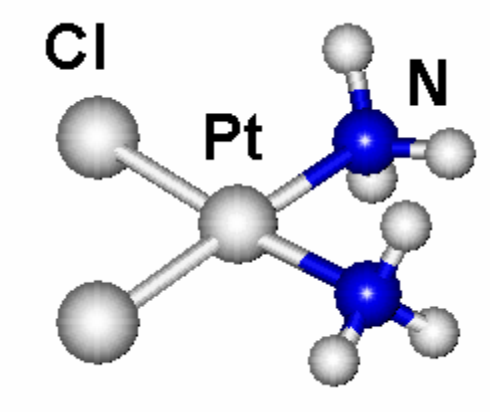

(a)

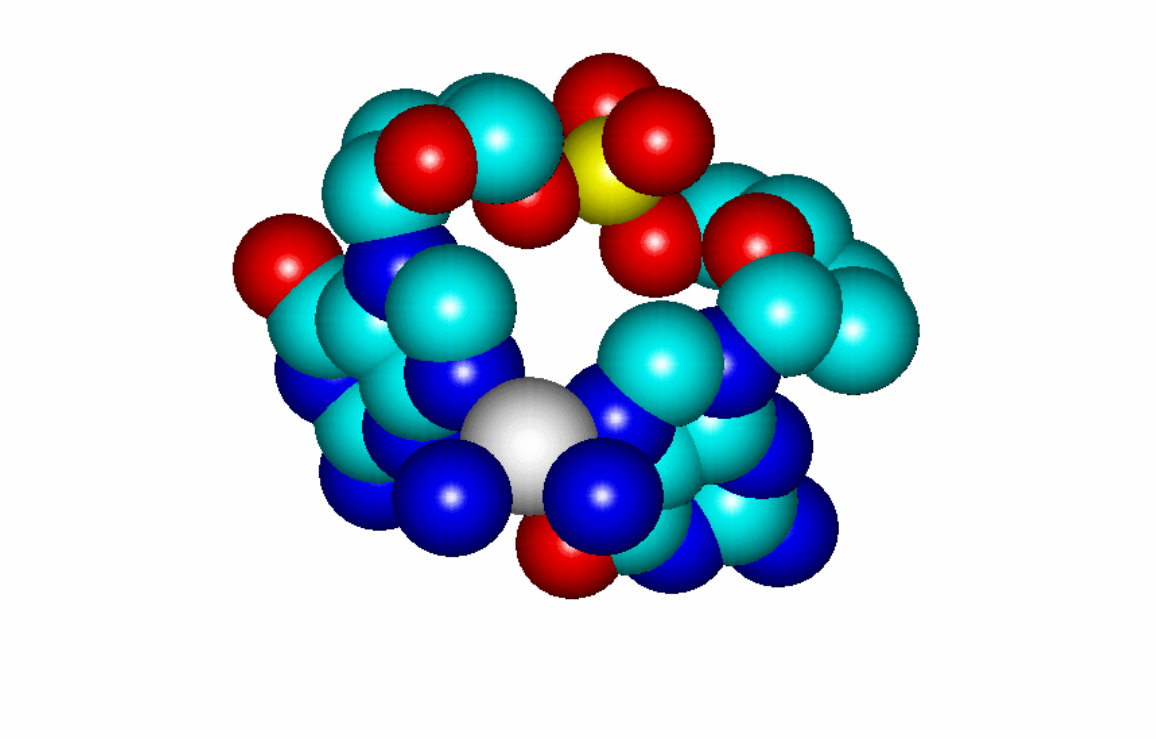

(b)

Figure 1. Structure of Cisplatin, a known anticancer drug based on platinum. The structure (a) shows the simplicity of the drug while (b) demonstrates how the Cisplatin binds to DNA.

myocardial perfusion imaging[15,16].

Magnetic Resonance Imaging (MRI) has possibly become the most powerful diagnostic imaging tool for the internal body organs. MRI is based on the principle of metals with a large number of unpaired electrons, like Gd^{3+}, Mn^{2+}, and Fe^{3+}, the most prevalent contrasting agents used, imposing a paramagnetic field on surrounding water molecules[17]. Diseases are detected by the difference in ^{1}H NMR resonances of H_2O between normal tissue and abnormal tissue. Gadolinium has four approved complexes which are used for clinical use (Figure 2). Manganese uses DTPA and DOTA, seen in Figure 2, although it also has another complex solely used for enhancing the contrast in the liver[18] (Figure 3).

Ligand design

Ligand design is based on six main principles; (1) the effect of neutral oxygen donors on metal ion size-based selectivity (which is of little importance to this study), (2) chelate ring size and metal ion size-based selectivity, (3) Hard/Soft Acid Base Theory, as it pertains to choice of donor atoms, (4) preorganization, and its effect on selectivity for metal ions of different sizes and coordinate geometries, (5) negative oxygen donors, and their promotion of selectivity for more acidic metal ions, and (6) coordination number, and its relationship to the denticity of ligands. The role of chelate ring size in selective binding of metal ions is that it controls selectivity based on metal ion size[20]. The lowest strain ring is that of cyclohexane. It has six carbons placed equidistant from each other with staggered hydrogens at axial and equatorial positions and equal bond lengths (Figure 4). This is true for organic chemistry where all the atoms are nearly the same size as the carbons. In the case of chelate rings, metal ions that are part of them vary in size from small metal ions such as Be^{2+} with an ionic radius of 0.27 Å to large metals such as

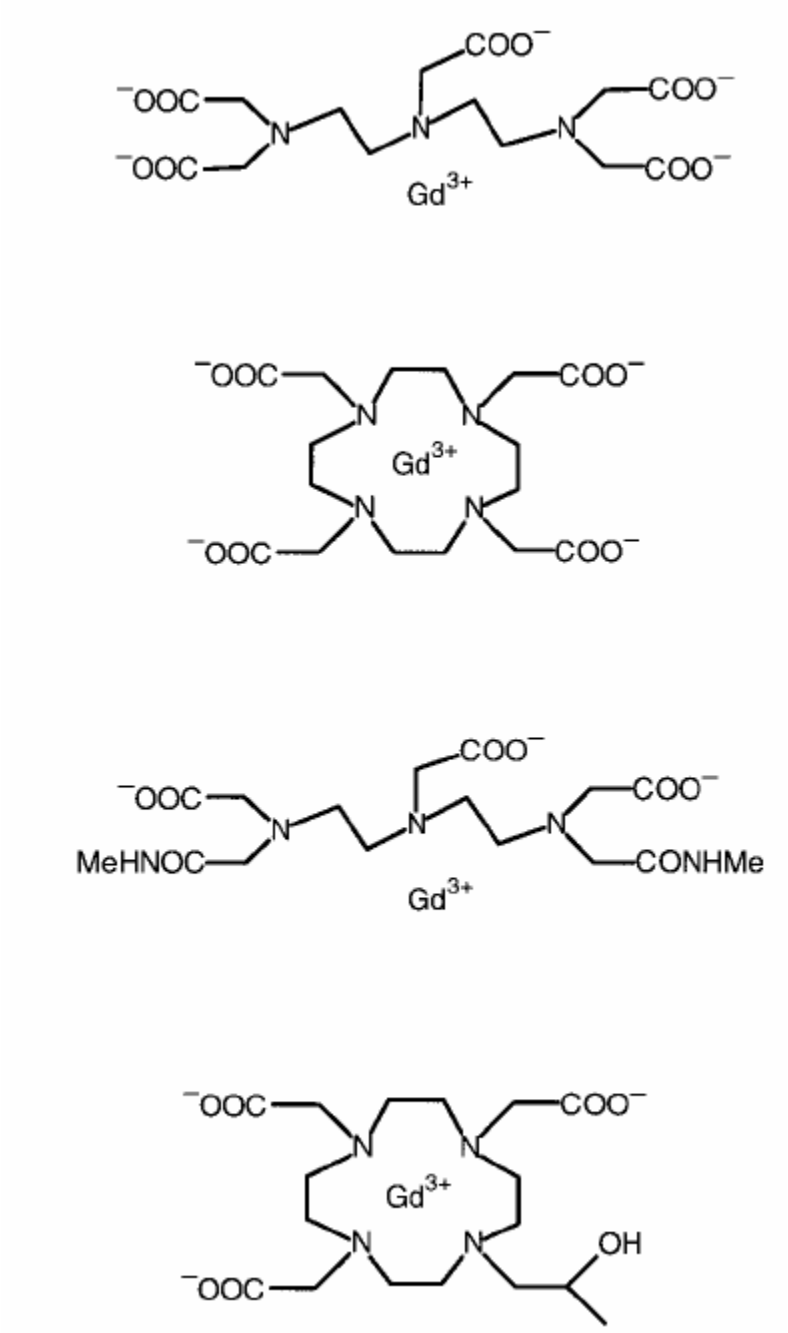

Figure 2. MRI imaging agents using gadolinium as complexing metal. Names from top to bottom: DTPA (Magnevist), DOTA (Dotarem), BMA-DTPA (Omniscan), and HP-DOTA (Prohance).

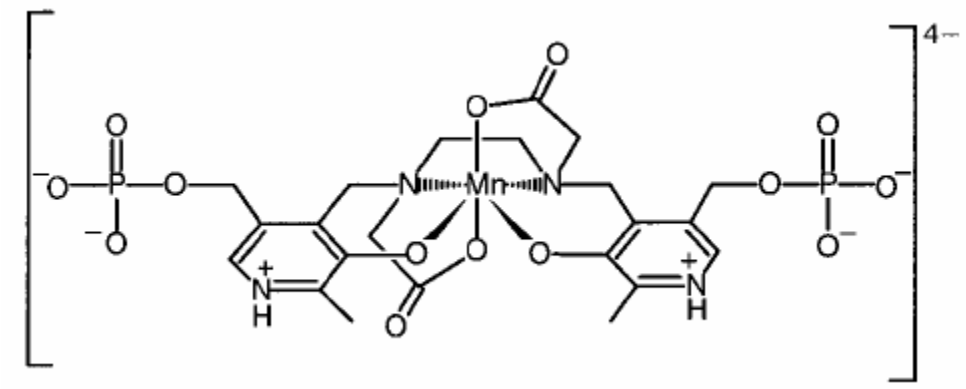

Figure 3. MRI imaging agent (Telescan) using manganese as the complexing metal[19].

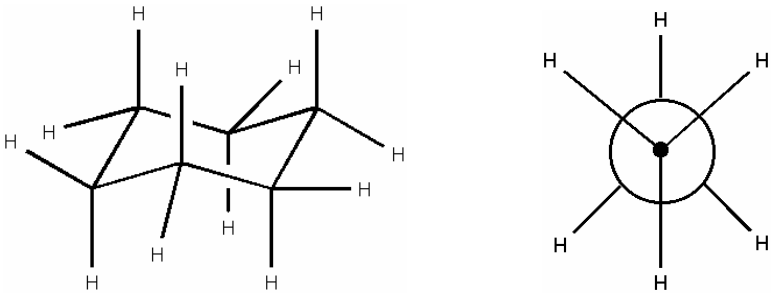

(a)

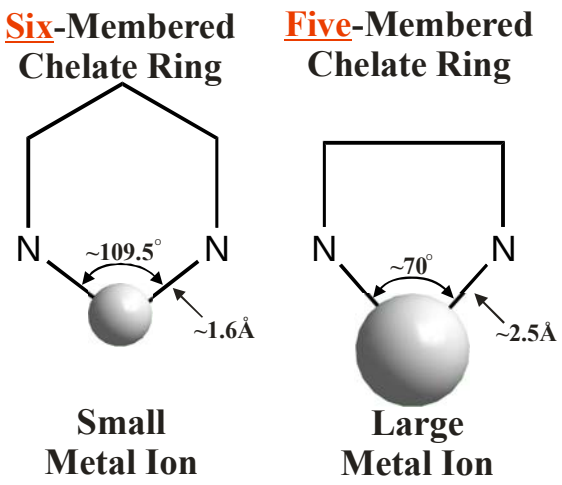

(b)

Figure 4. Shown is cyclohexane in the chair conformation demonstrating no eclipsing substituents (a). Small metals place less strain when forming six-membered rings while large metal ions prefer to be in five-membered rings[20].

Ba^{2+} with an ionic radius of 1.35 Å. This difference in size has varying effects on five-membered rings versus six membered rings. A five membered ring, like cyclopentane, is more sterically strained because the axial hydrogens partly eclipse one another. However, when a large metal ion is placed in the ring the hydrogens become staggered due to the change in bond angles. Large metal ions in five-membered rings are more stable. Not only does stability for the five-membered ring increase but the stability of the six membered ring decreases. This is because the hydrogens move from a staggered position to an eclipsed position, making the ligand sterically unfavorable (Figure 5).

Small metal ions, on the other hand, are closer to the size of a carbon atom, so when introduced into a six-membered ring, the bond angles change very little. Since the ring keeps its initial geometry it also remains stable. Conversely, when a small metal is part of a five-membered chelate ring it retains the unstable geometry of organic five membered rings, thus making it unfavorable. This means it is more probable the six-membered ring would favor small metal ions. 8-hydroxyquinoline-2-carboxyilic acid (HQC) forms two five membered rings when binding to metal ions and is expected to selectively favor larger metal ions.

Another aspect of ligand design that focuses on preferential binding for size is cavity size; the distance between donor atoms. If the cavity size is very small then a large metal will not be able to fit inside the cavity. This means there will be an increase in bond length between the metal and donor group, weakening the metal ligand bond which makes the complex less sterically favorable. If the cavity size is very large then the metal will not reach across to bind at all donor sites. HQC has a cavity measured from phenolate to carboxylate at 4.80 Å wide, as calculated by Molecular Mechanics (MM+) (Figure 6a). This means that, based on size only, smaller metal ions will not span across the gap and larger metals will not fit in the plane of HQC

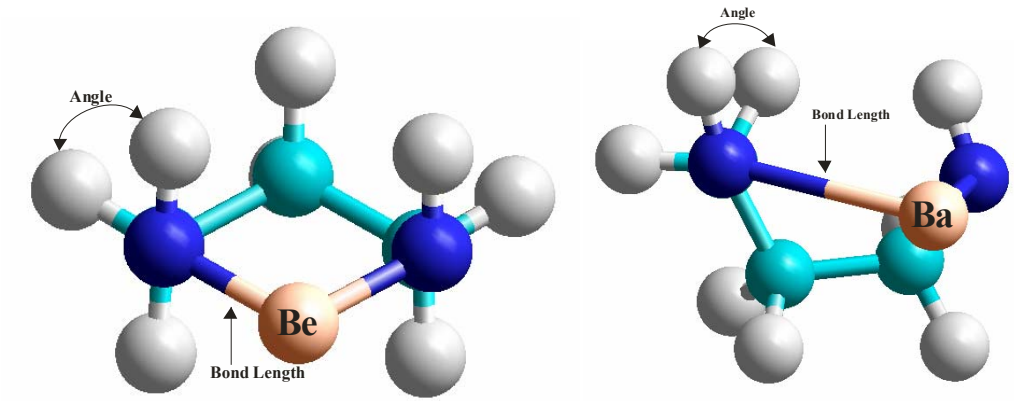

(a)

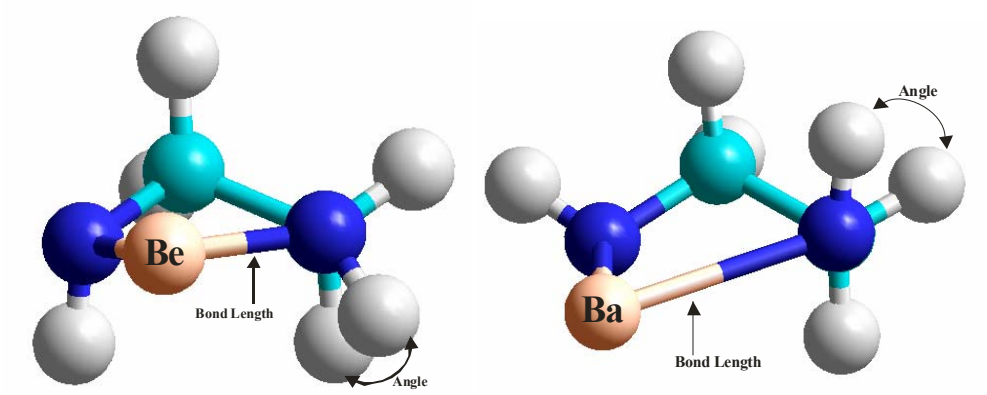

(b)

Figure 5. Smaller metal ions fit better into six-membered rings because there is less strain from eclipsing axial and equatorial hydrogens, beryllium in a six membered ring has 61.7º between hydrogens and a bond length of 1.65 Å while barium has 41.9º between hydrogens and a bond length of 2.68 Å (a). Larger metal ions fit better into five-membered rings for the same reason small metals fit into six-membered rings; beryllium in a five-membered ring has 27.0º between hydrogens and a bond length of 1.64 Å while barium has 55.6º between hydrogens and a bond length of 2.68 Å (b).

(Figure 6b). Molecular mechanics (MM+) functions were run in Hyperchem for each metal to test the total energy of each complex. This energy was then plotted against the ionic radius of the metal to give Figure 7, which demonstrates how larger metal ions are more thermodynamically stable in the HQC complex.

However ligand size is not the only determining factor for selective binding. Coordination number also plays a major role in preorganization. The coordination number is the number of binding sites on a metal. A ligand with more than one donor atom is considered to be a chelate, and denticity refers to the number of donor atoms a ligand has. The chelate effect is illustrated by the steady increase in log K_1, the formation constant for the complex, as the number of chelate rings in the chelating ligand increases, as seen in Table 1. This means that increasing denticity increases the formation constant of a complex.

Hard and Soft Acid Base Theory (HSAB)[21-28]

Changing the HSAB properties of the ligand can directly affect its selectivity. Pearson divided acids and bases into two categories, those polarizable or "soft ligands" and those that are not polarizable "hard ligands". Hard acids were determined to be metal ions of relatively small size but high oxidation state since their high oxidation state gives them low polarizability, shown in yellow (Figure 8). Conversely, soft acids have relatively large size and low oxidation state making them easily polarized, shown in red (Figure 8). Intermediate metals are shown in blue and display characteristics of both hard and soft acids. Pearson deduced from this trend that hard acids prefer to bind to hard bases and soft acids prefer binding to soft bases. Hard bases are those with highly electronegative donor atoms, chiefly O and F, while soft bases have donor atoms such as C, S, P, and I. Intermediate bases have donor atoms such as N. This is summarized in Figure 9.

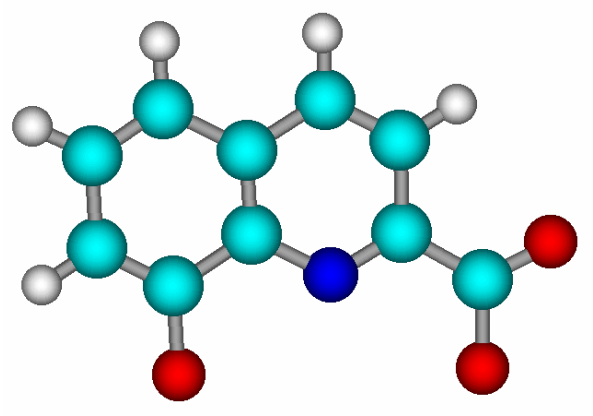

(a)

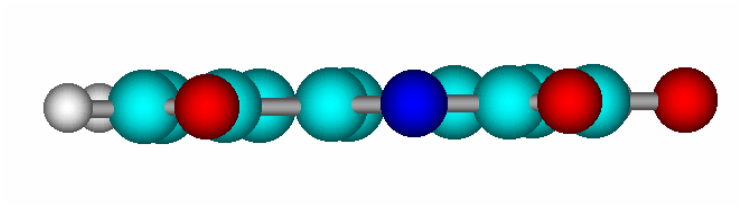

(b)

Figure 6. Hyperchem generated structure of 8-hydroxyquinoline-2-carboxylic acid showing donor groups, cavity size (a), and the plane the ligand lies in (b).

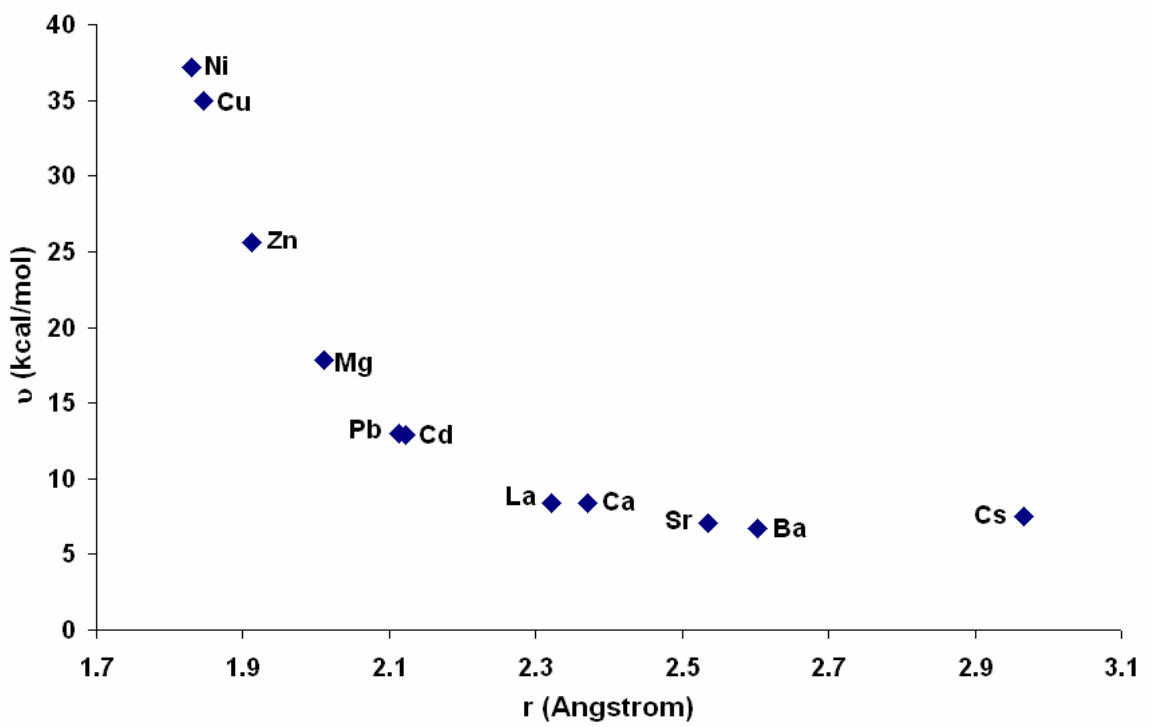

Figure 7. Strain energy (v) of $[M(HQC)(H_sO)_2]^{n+}$ complexes as a function of M-L bond length, calculated using the MM+ force field.

Table 1. The chelate effect for complexes of Ni^{2+} with polyamines[29].

polyamine	EN	DIEN	TRIEN	TETREN	PENTEN
denticity, n	2	3	4	5	6
log β_n (NH_3)	5.08	6.85	8.12	8.93	9.08
log K_1 (polyamine)	7.47	10.7	14.4	17.4	19.1

Where:

Ionic strength = 0.5 M

EN $NH_2CH_2CH_2NH_2$

DIEN $NH_2(CH_2CH_2NH)_2H$

TRIEN $NH_2(CH_2CH_2NH)_3H$

TETREN $NH_2(CH_2CH_2NH)_4H$

PENTEN $NH_2(CH_2CH_2NH)_5H$

$\log \beta_n(NH_3) = \log(K_1 \times K_2 \text{ ----- } \times K_n)$

Note that the chelate effect increases with the increase of denticity of the ligand.

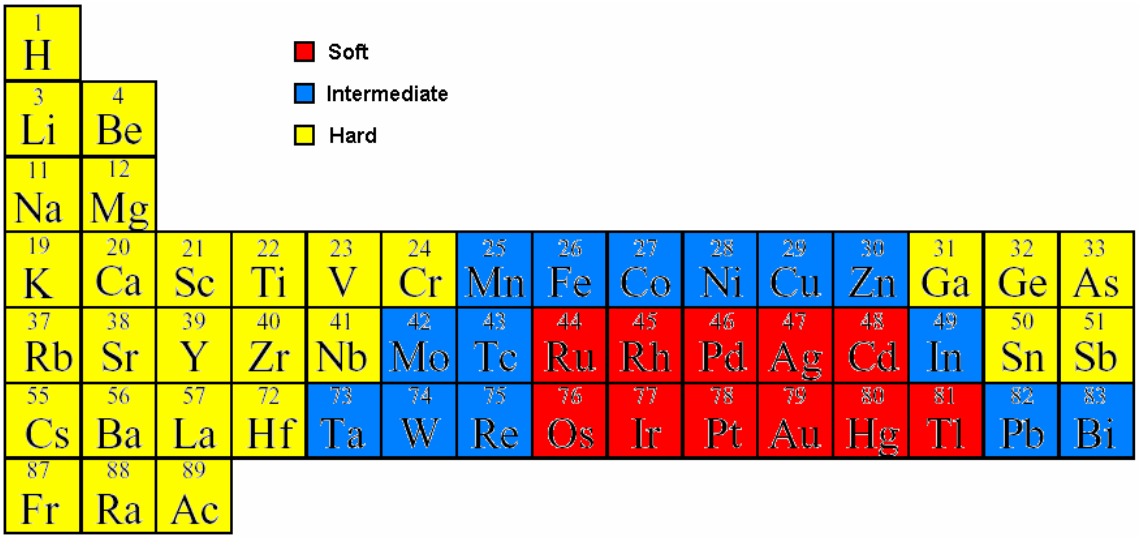

Figure 8. Periodic table of HSAB[22-27].

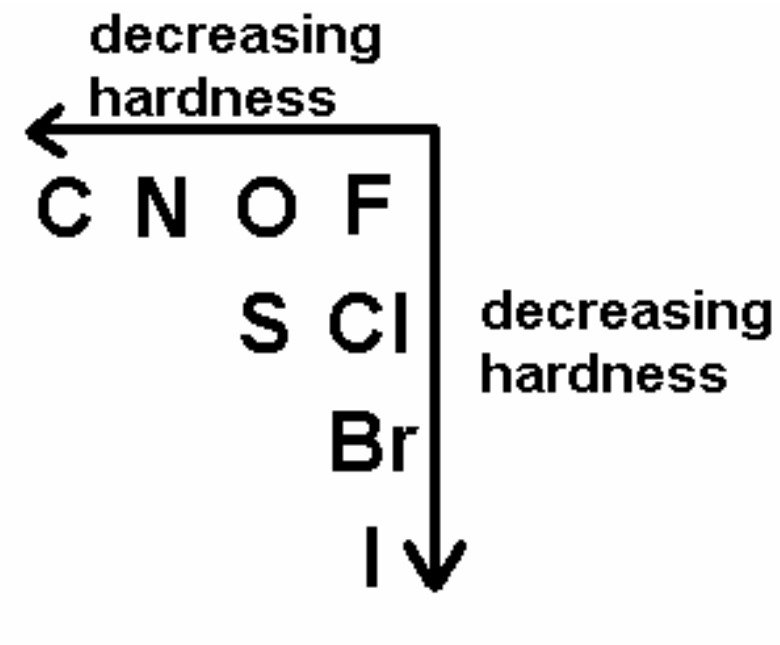

Figure 9. Trend of ligand hardness.

Gadolinium(III) is considered to be a hard metal ion in the HSAB classification with a higher affinity for hard ligands. It can be seen that the formation constant of $[In(H_2O)_8]^{2+}(aq)$ is greatest with the hardest ligand F^- (Table 2) and the same can be postulated for gadolinium. The trend of decreasing hardness can be seen in Figure 9. In our ligand design efforts for Gd^{3+} we should thus try to include as many negative O-donors as possible, with intermediate N-donors also included.

Many metals obey the trends predicted by HSAB, apparent in the formation constants of both hard and soft acids with both hard and soft ligands (Table 2). Ag^+ has a very high affinity for I^- over F^- making it a soft metal, which holds true to the periodic relationships seen in Figure 8. Since Pb^{2+} shows preferences for neither hard nor soft ligands it is deemed intermediate. In^{3+} has a definite affinity for hard ligand over soft so therefore it is a hard Lewis acid.

Table 2. Log formation constants of metal ions with halide ligands[21-28].

Log K_1	F^-	Cl^-	Br^-	I^-	Classification
Ag^+	0.4	3.31	4.68	6.58	Soft, or (b)
Pb^{2+}	1.26	0.90	1.06	1.30	Intermediate
In^{3+}	4.6	2.32	2.04	1.64	Hard. or (a)

EXPERIMENTAL

All chemicals and reagents used were of analytical grade and purchased from commercial sources and used without further purification. Deionized water was used to prepare all solutions. A stock solution of 0.1 M $HClO_4$ was made to be used in titrations as well as a solution of 0.1 M NaOH. A stock solution of 7.929 x 10^{-4} M HQC was made to be used for all titrations.

UV-Visible spectra were recorded using Cary Win UV Scan Application version 02.00(5) software which controlled a Varian 300 Cary 1E UV-Visible Spectrophotometer in absorbance mode with wavelength range set at 190.00 nm – 350.00 nm. Scan controls were set at baseline (zero/baseline correction), average time (0.100 s), data interval (1.000 s), scan rate (600.00 nm/min), spectral bandwidth (2.0 nm), double beam mode, and changeover (360.00 nm). The reference cell used was a 1.000 cm, 3.0 mL quartz cell and the flow cell used was also a 1.000 cm quartz cell. 5.00 mm R-3603 Tygon tubing was used to connect the flow circuit. A VWR sym**pH**ony™ SR60IC pH meter with a VWR sym**pH**ony™ gel epoxy semi-micro combination pH electrode was used for all pH readings. pH meter was calibrated prior to every use with the % calibration limit set at 95.0%. Buffers used for standardization were 4.00, 7.00, and 10.00. All pH reading were measured to ±0.01 pH units and kept at a constant temperature using a 25 gallon tank and a Fisher Scientific Isotemp Immersion Circulator Model 730 for thermoregulation, set at 25ºC ± 0.5ºC and limit adjust set at 55. The peristaltic pump used for the circulation in this analysis was a VWR mini-pump variable flow set to forward at the maximum level (10) while system was set to fast.

The system was flushed with deionized water for 5.0 minutes prior to recording blank. Reference cell was filled with the same deionized water throughout the entire titration. Once a

baseline had been established the water was purged out with air and the sample was run through the system. All solutions were kept at $I = 0.10$ using $NaClO_4$. The ionic strength must be kept constant since log K changes with changing I according to the Debye-Hückel equation. The perchlorate ion was chosen over nitrate since nitrates absorb near 200 nm.

To run the system, 50 mL of the sample was placed in a 100 mL beaker and suspended with a clamp in the thermoregulated tank. The calibrated pH electrode and Tygon tubes for solution flowing in and out of the cell were immersed in the 50 mL sample. The peristaltic pump was then turned on and allowed to equilibrate for 10 minutes, making sure that no air was trapped in the flow line or flow cell (Figure 10).

HQC pK_a titration

50 mL of a solution of 2 x10^{-5} M HQC in a 0.500 L volumetric (12.610 mL of stock 7.929 x10^{-4} M HQC) and 0.1 M $NaClO_4$ (6.122 g). The solution was then brought to pH = 12.00 by using 0.660 mL 10.00 M NaOH with pH calibration at 98.0%. The absorbance at wavelengths 230, 240, 250, 265, and 280 were recorded and plotted against pH to determine pK_a.

For each titration acid (0.1 M HClO4) was titrated into the sample cell so that a pH change of 0.5 occurred between each spectrum taken. In the case of the more acidic metal ions, which initiated at a lower pH, the titrant was 0.1 M NaOH and again a spectrum was taken every 0.5 pH units. Since the first protonation event of HQC occurs at 10.14 and there is little chance this protonation event would shift to a more basic pH, it was assumed that no noteworthy protonation event for this study would be present above pH 11.00. For each titration's spectra, the absorbance at wavelengths 230, 240, 250, 265, and 280 were recorded and plotted against pH to determine pK_a.

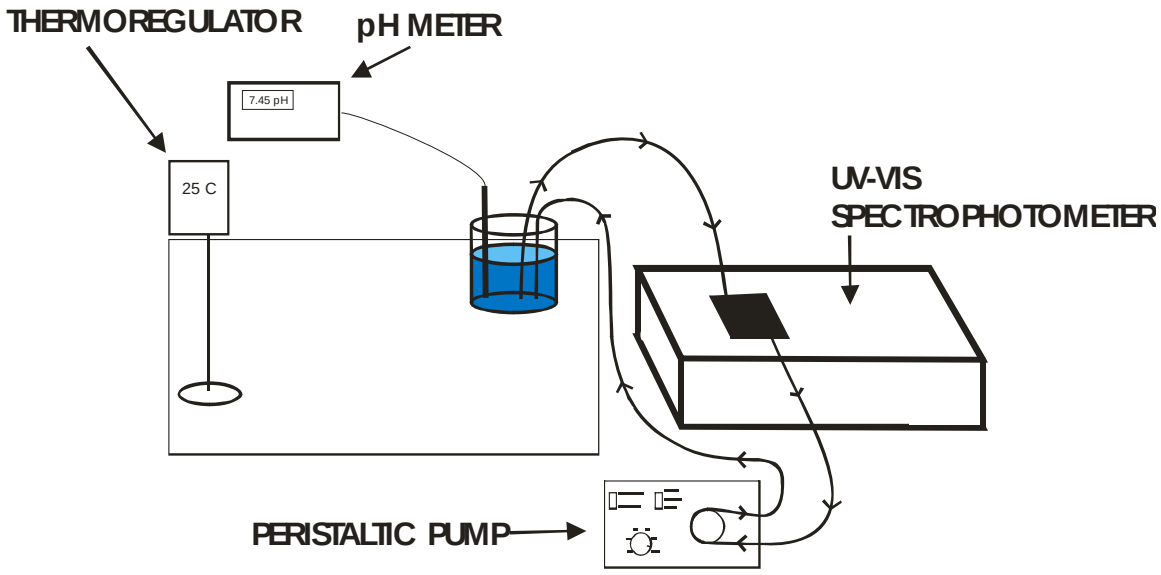

Figure 10. Flow cell and UV-Vis apparatus.

Titration of HQC and Calcium

50 mL of a solution of 2 x10^{-5} M HQC and 0.0333 M $Ca(ClO_4)_2$ was placed in a 100 mL beaker. The solution was then brought to pH = 11.00 by using 0.025 mL 10.00 M NaOH with pH calibration at 95.6%. pH was not taken to 12.00 due to the propensity for calcium hydroxide to form at elevated pHs and thus precipitate out of solution.

Titration of HQC and Magnesium

50 mL of a solution of 2 x10^{-5} M HQC and 0.0333 M $Mg(ClO_4)_2$ was placed in a 100 mL beaker. The solution was then brought to pH = 9.50 by using 0.035 mL 10.00 M NaOH with pH calibration at 98.0%. pH was not taken to 12.00 since the likelihood of a stable complex of HQC-Mg is very unlikely at a pH greater than 10.0.

Titration of HQC and Strontium

50 mL of a solution of 2 x10^{-5} M HQC and 0.0333 M $Sr(ClO_4)_2$ was placed in a 100 mL beaker. The solution was then brought to pH = 10.96 by using 0.030 mL 10.00 M NaOH with pH calibration at 97.9%.

Titration of HQC and Barium

50 mL of a solution of 2 x10^{-5} M HQC and 0.0333 M $Ba(ClO_4)_2$ was placed in a 100 mL beaker. The solution was then brought to pH = 11.10 by using 0.030 mL 10.00 M NaOH with pH calibration at 97.1%.

Titration of HQC and Zinc

50 mL of a solution of 2 x10^{-5} M HQC and 2 x10^{-5} M $Zn(ClO_4)_2$ was placed in a 100 mL beaker. The solution was then brought to pH = 10.95 by using 0.030 mL 10.00 M NaOH with pH calibration at 97.0%.

Titration of HQC and Cadmium

50 mL of a solution of 2 x10^{-5} M HQC and 2 x10^{-5} M $Cd(ClO_4)_2$ was placed in a 100 mL beaker. The solution was then brought to pH = 11.04 by using 0.030 mL 10.00 M NaOH with pH calibration at 96.0%.

Titration of HQC and Lanthanum

50 mL of a solution of 2 x10^{-5} M HQC and 2 x10^{-5} M $La(ClO_4)_2$ was placed in a 100 mL beaker. The solution was then brought to pH = 2.02 by using 0.150 mL 0.1 M $HClO_4$ with pH calibration at 96.0%. Perchloric acid was used to change pH over sodium hydroxide because lanthanum forms hydroxides very easily in basic conditions, therefore starting the titration at a more acidic pH and raising the pH gradually the complex would be allowed to form before precipitation occurred.

Titration of HQC and Lead

50 mL of a solution of 2 x10^{-5} M HQC and 2 x10^{-5} M $Pb(ClO_4)_2$ was placed in a 100 mL beaker. The solution was then brought to pH = 10.81 by using 0.020 mL 10.00 M NaOH with pH calibration at 96.0%.

Titration of HQC and Copper

50 mL of a solution of 2 x10^{-5} M HQC and 2 x10^{-5} M $Cu(ClO_4)_2$ was placed in a 100 mL beaker. The solution was then brought to pH = 10.86 by using 0.020 mL 10.00 M NaOH with pH calibration at 96.2%.

Titration of HQC and Gadolinium

50 mL of a solution of 2 x10^{-5} M HQC and 2 x10^{-5} M $Gd(ClO_4)_2$ was placed in a 100 mL beaker. The solution was then brought to pH = 2.04 by using 2.150 mL 0.1 M $HClO_4$ and 0.225 mL 11.7 M $HClO_4$ with pH calibration at 97.6%. Perchloric acid was used to change pH instead of sodium hydroxide because gadolinium, like lanthanum, forms hydroxides very easily in basic conditions, therefore starting the titration at a more acidic pH and raising the pH gradually the complex would be allowed to form before precipitation occurred.

Titration of HQC and Nickel

50 mL of a solution of 2 x10^{-5} M HQC and 2 x10^{-5} M $Ni(ClO_4)_2$ was placed in a 100 mL beaker. The solution was then brought to pH = 11.03 by using 0.030 mL 10.00M NaOH with pH calibration at 97.7%.

Crystallization of HQC and Metals ($Cd^{2+}$and Zn^{2+})

All recrystallizations were prepared in a 1:1 ratio of HQC : metal, where metal = Cd^{2+}or Zn^{2+}. The HQC was placed in ~20 mL n-butanol, in a 50mL beaker, and sonicated until completely dissolved (5-10 minutes). The metal was placed in ~20mL of deionized water, in a 50mL beaker, and sonicated until completely dissolved (5-10 minutes). The metal solution was then added drop wise to the side of the of 50 mL beaker containing the ligand so as not to disturb the air/solvent interface. After adding all the metal solution to the ligand, parafilm was applied to the top of the beaker with small holes punched out. The stratified solutions were then left to

recrystallize on a shelf. The solutions were left alone for one month to allow sufficient time for crystal growth. The crystals were then extracted using vacuum filtration with no rinse and placed in a small vial for storage. Infrared spectroscopy was used to characterize the HQC-metal complex apart from the free ligand. X-ray crystallographic analyses of crystals were carried out at the Department of Chemistry at Texas A & M.

RESULTS

The vast majority of formation constants are determined by glass electrode potentiometry. However, UV-Vis spectroscopy allows for accurate determination of pK_a and/or log K values at extremely low concentrations where the precipitation of metal hydroxides becomes nearly irrelevant. This method is based on the premise that the $\pi \rightarrow \pi^*$ transitions in the ligand are affected by protonation or complex formation. Specifically, the π orbitals in the free ligand absorb specific wavelengths of light, as the pH decreases the ligand is protonated which causes an absorbance at a different wavelength. The pH continues to lower, due to the acid titration, and the ligand is protonated a second time, noted by another correlating shift in absorbance. For example, in HQC both the phenol and carboxyl donor groups have protons which are removed at higher pH. Since the majority of titrations began at an elevated pH and were titrated with acid, the protonation of both these sites can be observed by noting spectral changes at specific pHs. These shifts are an indication that the ground state π electrons of the ligand absorb light at a different wavelength when excited to the π^* excited state (Figure 11).

All absorbances of the UV-Vis titrations were plotted at three wavelengths as a function of pH. Throughout the course of the titration the absorbance at these selected wavelengths changed as a function of the metal-ligand complex formation/deterioration. In this experiment both free hydrogen ions and hydroxides are in constant competition with HQC for binding sites on the metal and ligand. The competition of H^+ ions and OH^- ions for binding on the ligand and/or metal cause significant changes in the absorbance. This can be seen in the shifts in spectra over the course of a titration. Two main shifts are present. A hypsochromic shift, a shift of longer wavelength to shorter wavelength, occurs initially signaling the protonation of the phenolate. It is postulated that this shift is hypsochromic in response to the loss of a resonance

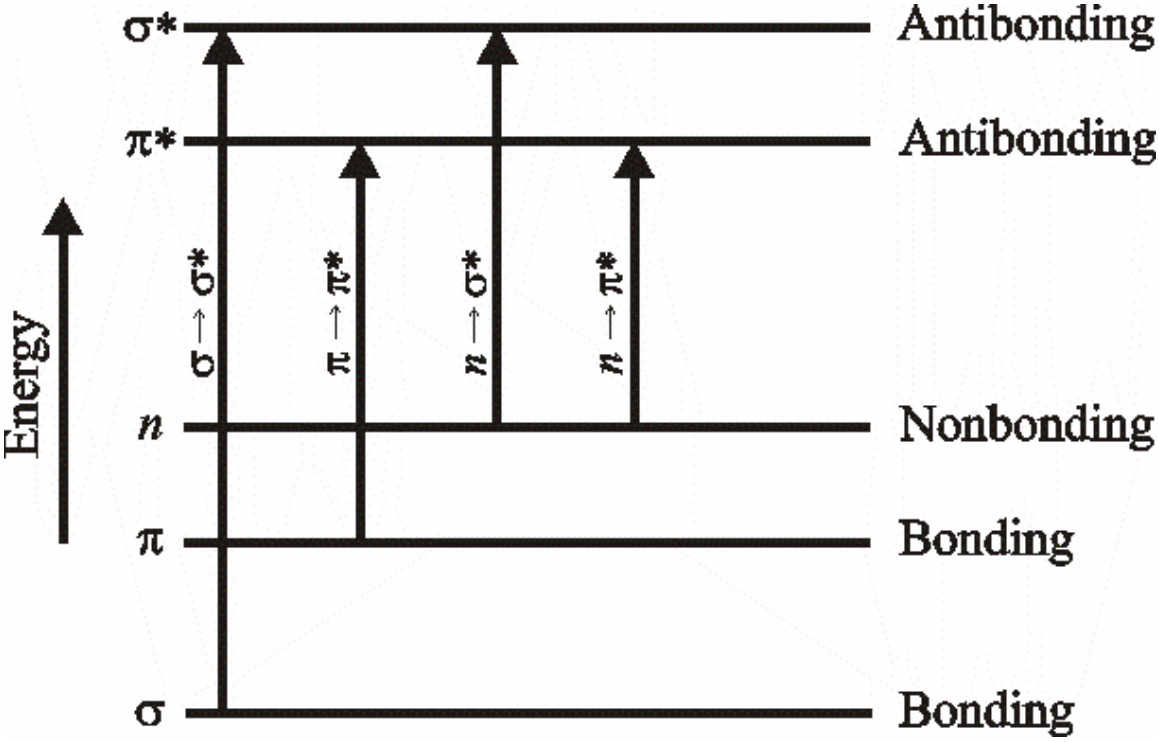

Figure 11. Electronic molecular energy levels.

structure since the π electrons can no longer delocalize onto the negative phenol. This decrease in wavelength and increase in energy is directly related to the difference in highest occupied molecular orbital (HOMO) and lowest unoccupied molecular orbital (LUMO) of the ligand and the protonated ligand. This increase in energy between the excited states of unprotonated phenol compared to protonated phenol can be observed in the spectral shifts. The second shift is bathochromic, shifting from a shorter wavelength to longer wavelength or a decrease in energy. This could be caused by the protonation of the pyridine nitrogen allowing the π electron to move out of the ring onto the hydrogen. This shift, like the hypsochromic shift is related to the change in energy between the HOMO and LUMO.

HQC Titration

The titration of HQC with no metals present was reported as a function of absorbance versus pH and follows Equation 1 and 2.

$$L^{2-} + H^{+} \overset{pK_1}{\Longleftrightarrow} LH^{-} \tag{1}$$

$$LH^{-} + H^{+} \overset{pK_2}{\Longleftrightarrow} LH_2 \tag{2}$$

For every absorbance scan (Figure 12a), pH values were also recorded and plotted as corrected absorbance (Equation 3) versus pH using EXCEL (Figure 12b). Though five separate wavelengths were documented, only three were used to determine pK_a 240 nm, 250 nm, and 265 nm. The 230 nm wavelength was not used since there was interfering absorbance from the perchlorate anion at this wavelength. The 280 nm band was not used because of its proximity to an isosbestic point in the spectrum. This left very little change in absorbance where even slight deviations could cause large errors. Using Equation (3), recorded

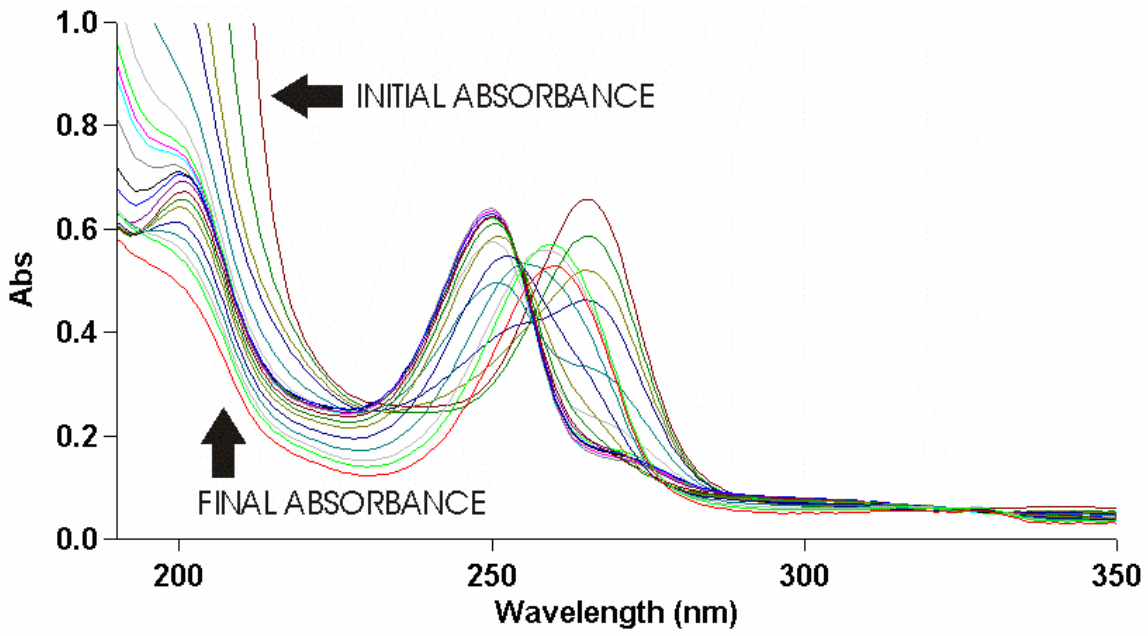

(a)

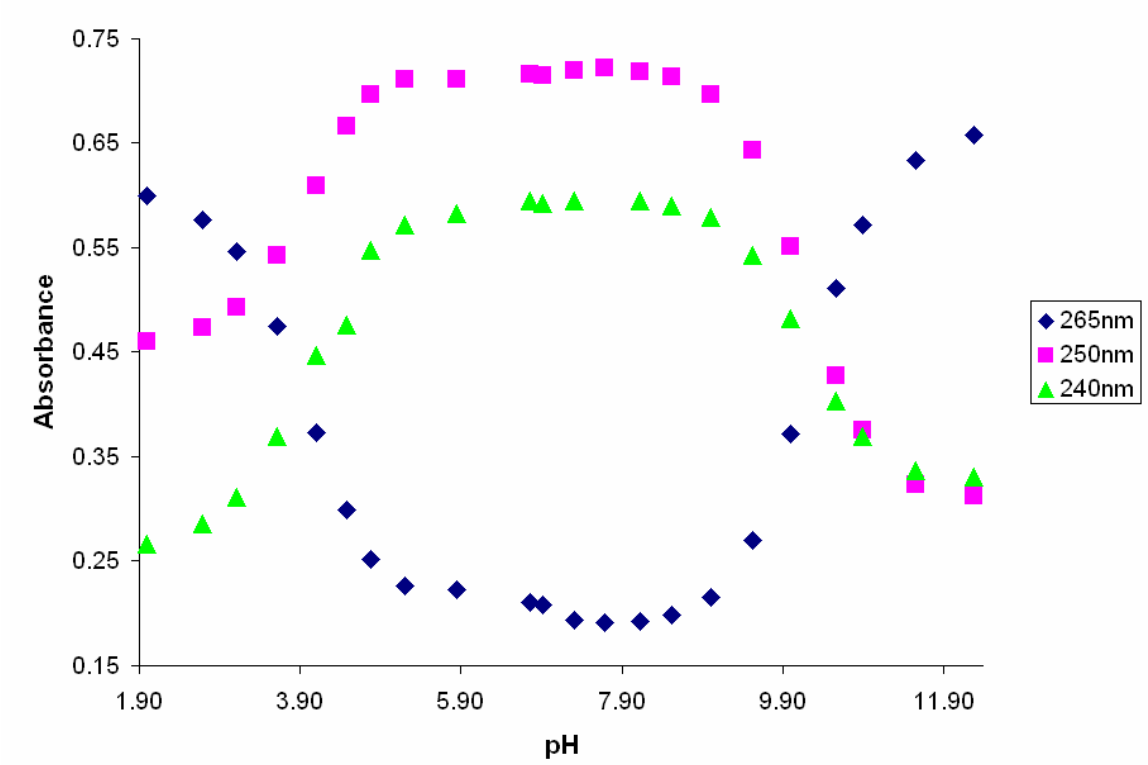

(b)

Figure 12. HQC alone UV-Vis spectra (a) and peak shifts at wavelengths 240nm, 250nm, and 265 nm (b).

absorbance values were corrected for dilution after each addition of titrant.

$$A_{corr} = \frac{A \cdot V_{total}}{V_{initial}} \quad (3)$$

At higher pH a peak maximum was observed at 265 nm. As 0.1 M $HClO_4$ was added in this peak moved across an isosbestic point at 257 nm creating a new peak maximum at 250 nm. This isosbestic point indicates all species associated with this shift are of the same equilibrium equation. This change was directly related to the protonation of the phenolate donor group on HQC. The peak at 250 nm then slowly shifted back up to 260 nm as the pH approached 2.00. This shift indicated the pyridine had been protonated.

$\bar{n}$ calculations were performed for each absorbance shift at wavelengths 240nm, 250nm, and 265nm. $\bar{n}$ values show the fractionation of two species in equilibrium. $\bar{n}_1$ corresponds directly to the first protonation event; the protonation of the phenol (Equation 4). $\bar{n}_2$ corresponds directly to the second protonation event; the protonation of the pyridine (Equation 5). These $\bar{n}$ values can be separated for this ligand because there is a large difference in pH for protonation constants. This means there are only two species in equilibrium at any given pH. An $\bar{n}$ calculation was performed for each change in absorbance (Figures 13, 14, and 15) using equation for A_{corr}.

$$\bar{n}_1 = \frac{A_{corr} - A_{ini_1}}{A_{inf_1} - A_{ini_1}} \quad (4)$$

$$\bar{n}_2 = \frac{A_{corr} - A_{ini_2}}{A_{inf_2} - A_{ini_2}} \quad (5)$$

Once both $\bar{n}$ curves have been fitted, both K_1 and K_2 can be derived from their respective equation:

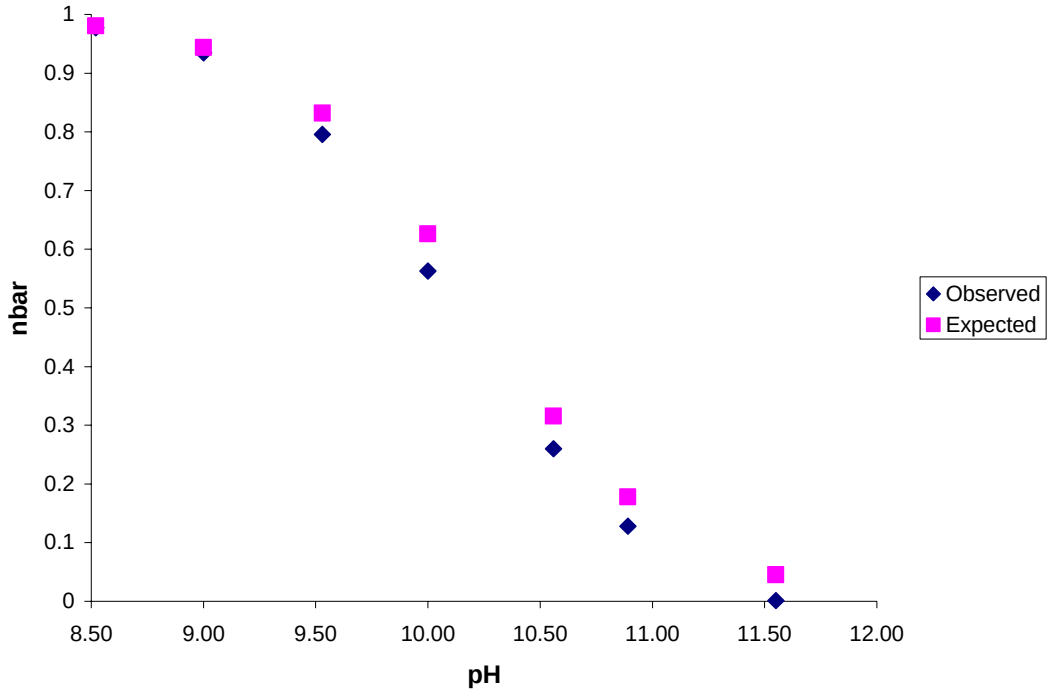

(a)

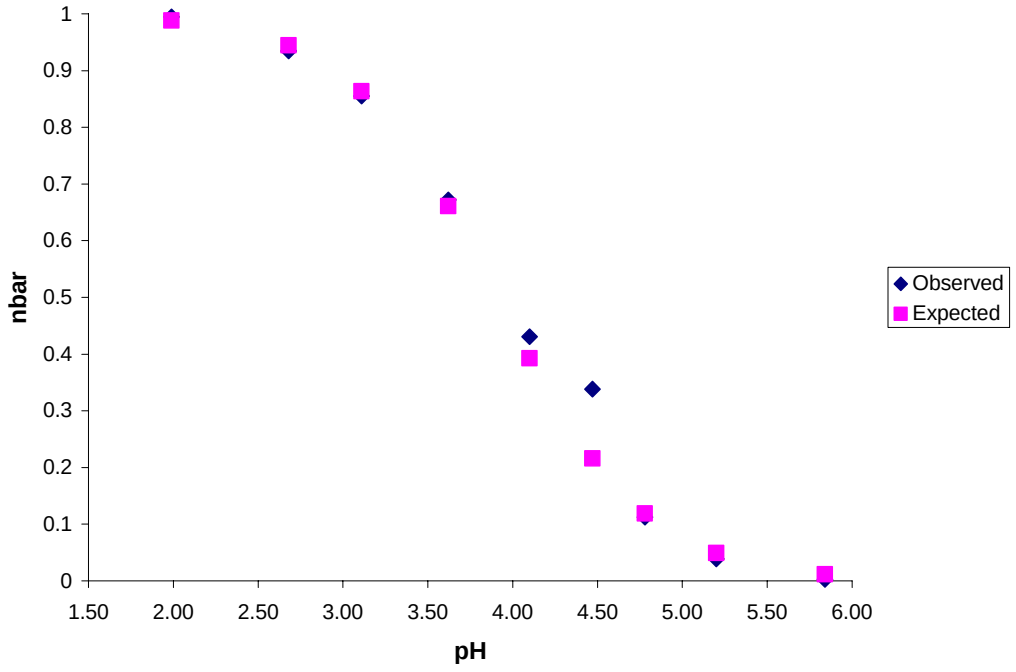

(b)

Figure 13. Plot of $\bar{n}$ as a function of pH for HQC-H^+ complex at 240nm (a) represents pK_1, the protonation of the phenolate on HQC and (b) represents pK_2, the protonation of the pyridine on HQC.

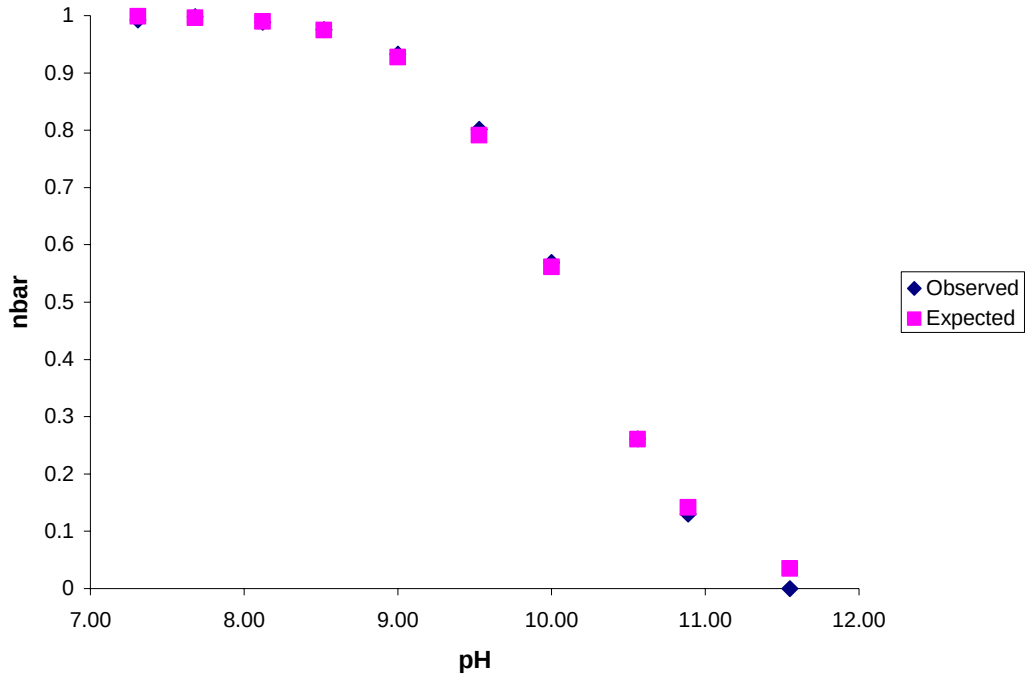

(a)

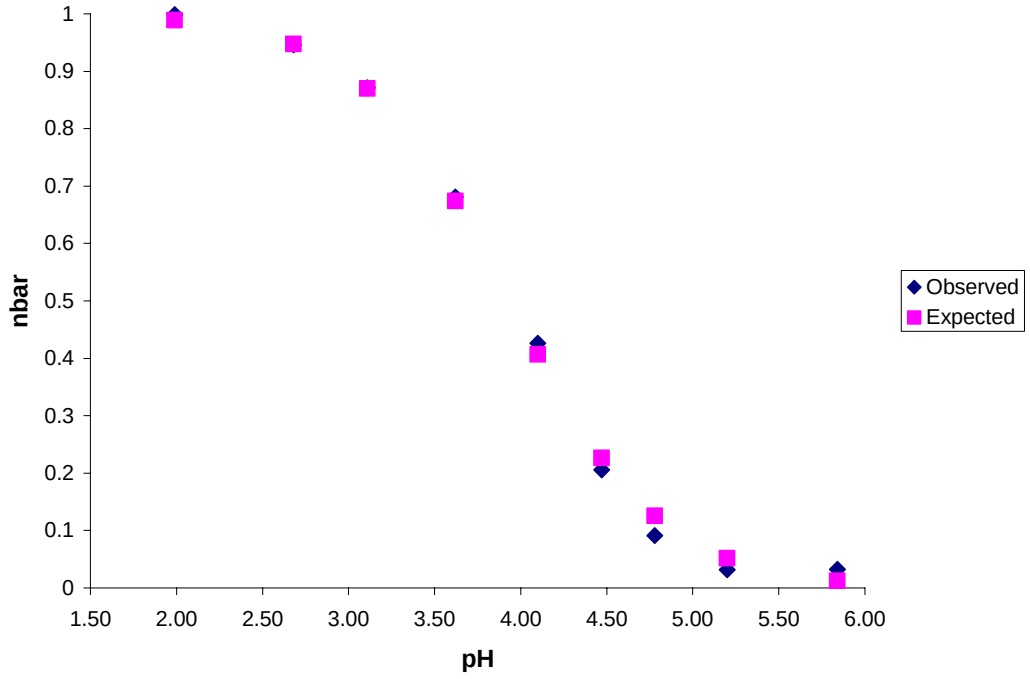

(b)

Figure 14. Plot of $\bar{n}$ as a function of pH for HQC-H^+ complex at 250nm (a) represents pK_1, the protonation of the phenolate on HQC and (b) represents pK_2, the protonation of the pyridine on HQC.

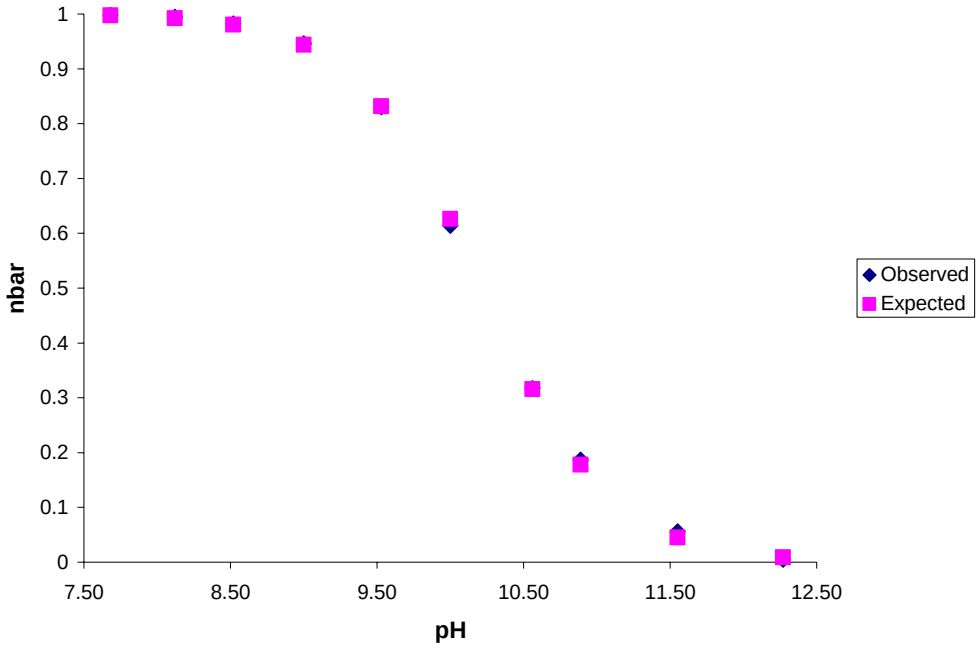

(a)

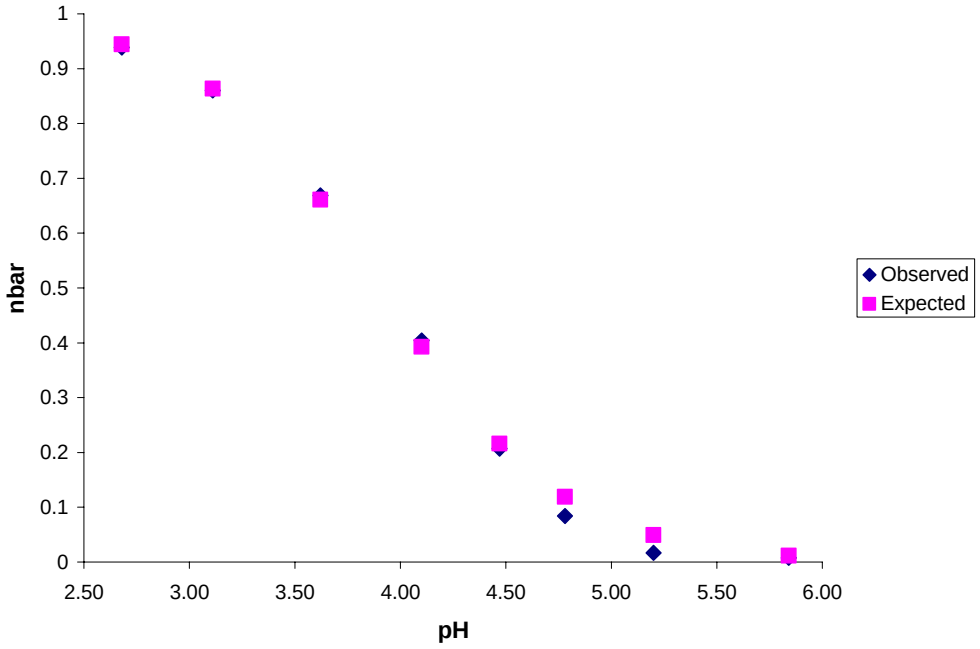

(b)

Figure 15. Plot of $\bar{n}$ as a function of pH for HQC-H^+ complex at 265nm (a) represents pK_1, the protonation of the phenolate on HQC and (b) represents pK_2, the protonation of the pyridine on HQC.

$$K_1 = \frac{\bar{n}_1}{[H^+](1-\bar{n}_1)} \tag{6}$$

$$K_2 = \frac{\bar{n}_2}{[H^+](1-\bar{n}_2)} \tag{7}$$

Both Equation (6) and (7) are equilibrium expressions for a respective protonation event. From the K_a's, pK_1 and pK_2 can be calculated simply by taking the negative logarithm of K_1 and K_2 as seen in equation 8 and 9:

$$pK_1 = -\log K_1 \tag{8}$$

$$pK_2 = -\log K_2 \tag{9}$$

For HQC pK_1 was calculated to be 10.14, which was the pH the phenol was protonated on the free ligand, and pK_2 was calculated to be 3.94, which was the pH where the pyridine was protonated on the free ligand. From the K_a's, the overall stability constants, β, can be calculated using the following equations:

$$\beta_1 = K_1 \tag{10}$$

$$\beta_2 = K_1 K_2 \tag{11}$$

The total ligand concentration, $[L]_{total}$, in the sample solution was also calculated using Equation (12).

$$[\mathrm{L}]_{\mathrm{total}} = \frac{[\mathrm{L}]_{\mathrm{ini}} \cdot \mathrm{V}_{\mathrm{ini}}}{\mathrm{V}_{\mathrm{total}}} \tag{12}$$

For metal complexes both the $\bar{n}$ values and the total ligand concentration were known, the distribution between the complexed ligand, [ML] and the free ligand, [L], was calculated using Equations (13) and (14).

$$[\mathrm{ML}] = \bar{n} \cdot [\mathrm{L}]_{\mathrm{total}} \tag{13}$$

$$[L] = [L]_{total} - [ML] \quad (14)$$

The total hydrogen ion concentration, $[H^+]$, in the sample solution was calculated using Equation (15).

$$[H^+] = 10^{-pH} \quad (15)$$

Finally, the stability constant (log *K*) for each metal ion with HQC was calculated using Equation (16). ([M] = concentration of free metal ion = M_{total} – [ML])

$$\text{Log } K \text{ (HQC-M}^{n+}) = \Delta \text{ p}K_1 + \Delta \text{ p}K_2 + \log [M] \quad (16)$$

Equation (16) is based on the principle that as the ligand hold the metal more tightly the complex becomes increasingly harder to protonate. This leads to a decrease in pK_a and as the difference in pK_a of the complex becomes lower the formation constant becomes greater. This is demonstrated in the shift in pK_a's for the HQC – Ca complex as compared to the free ligand in Figure 16. To ensure that each ligand - metal complex had broken apart completely the absorbances of the free ligand at pH 2.00 were compared to that of the metal ligand complex at the same pH.

Metal titrations

The acid titration of the HQC – calcium complex initiated at pH 10.87 and ended at pH 1.48. Both the spectra for this titration and the plot of absorbance versus peak shift show how the peak maximum moves throughout the course of the titration (Figure 17). The $\bar{n}$ plots of pK_1 and pK_2 were combined into one figure to demonstrate both protonations concurrently. From these $\bar{n}$ plots one can recognize the $\bar{n}$ observed data, gathered experimentally, agrees with the $\bar{n}$ theoretical data (Figure 18). Using equation 8, pK_1 was calculated to be 7.09 and using equation 9, pK_2 was calculated to be 2.47. In order to calculate the formation constant of

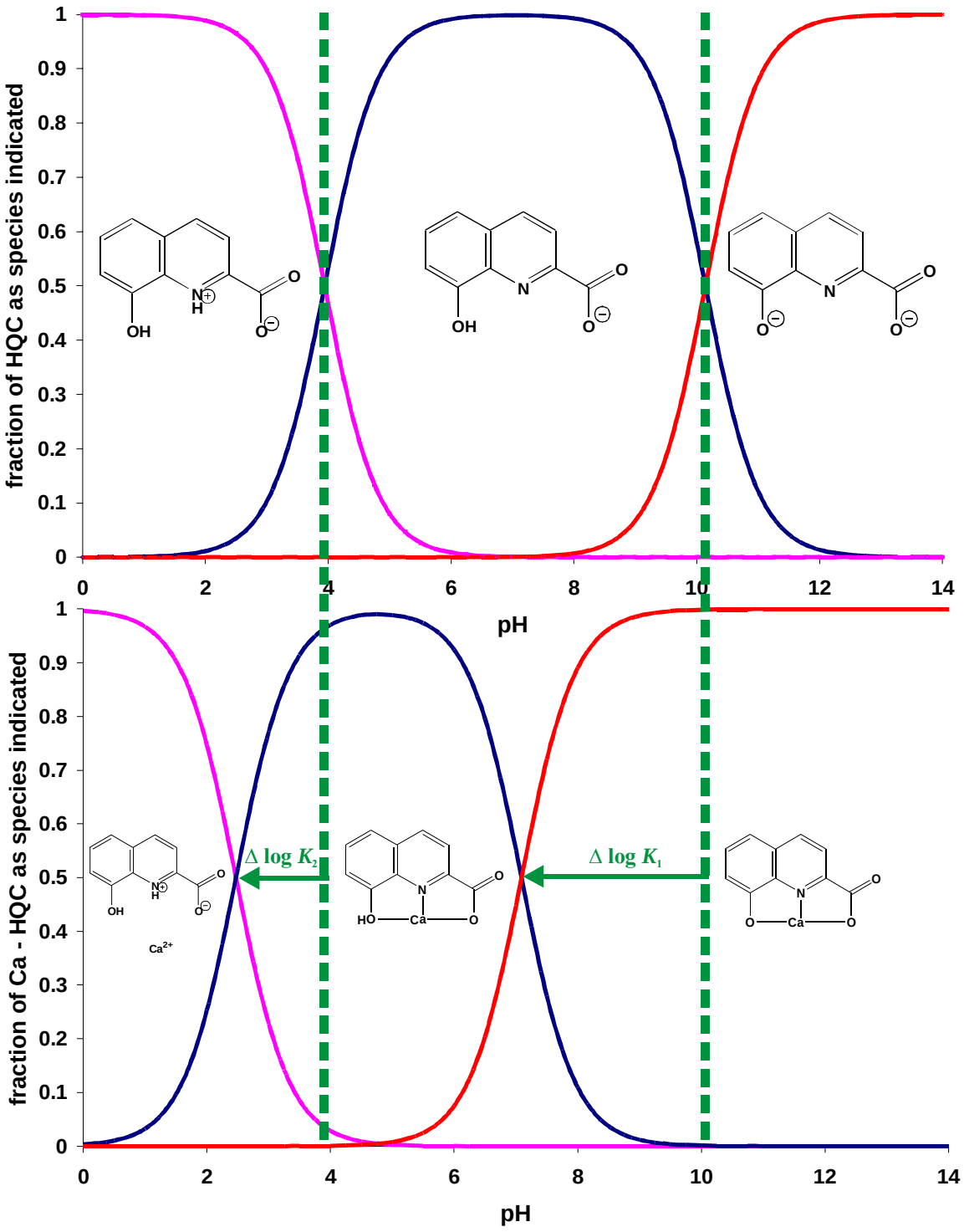

Figure 16. Demonstration of how pK_a's change with the introduction of a metal into the complex.

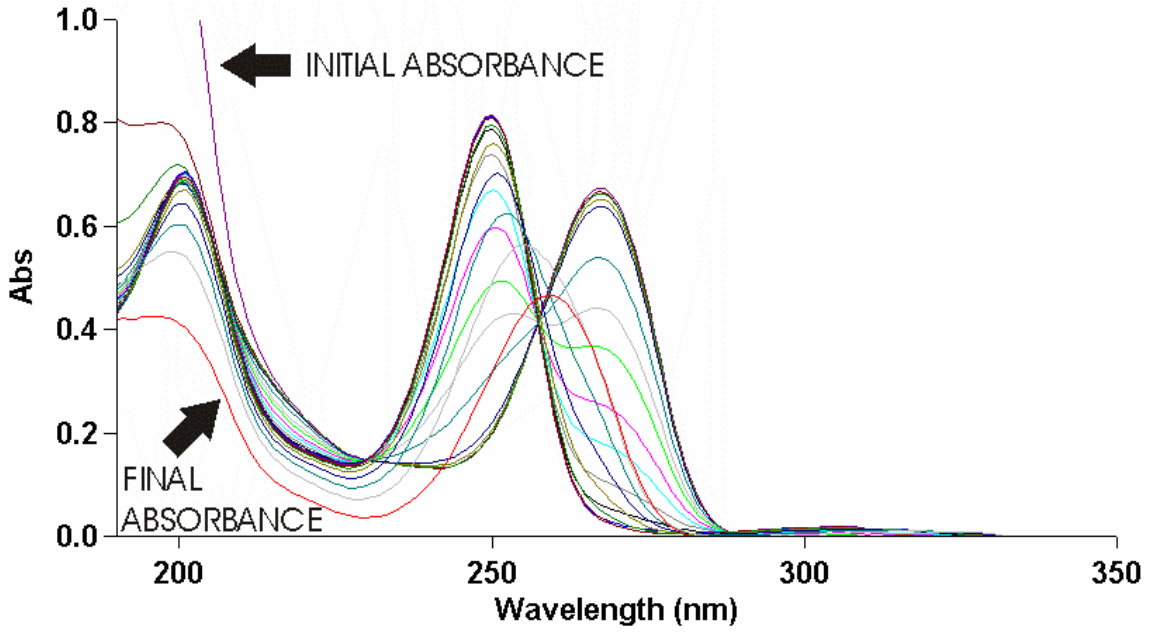

(a)

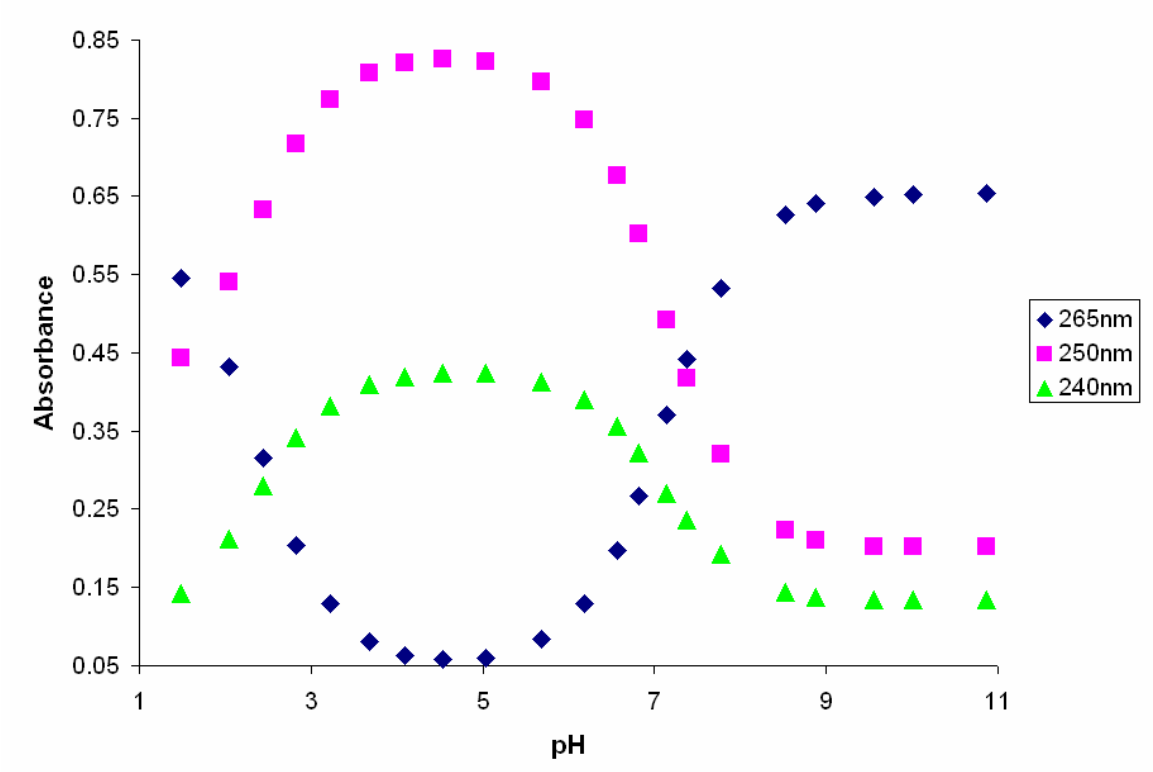

(b)

Figure 17. HQC and calcium UV-Vis spectra (a) and peak shifts at wavelengths 240nm, 250nm, and 265 nm (b).

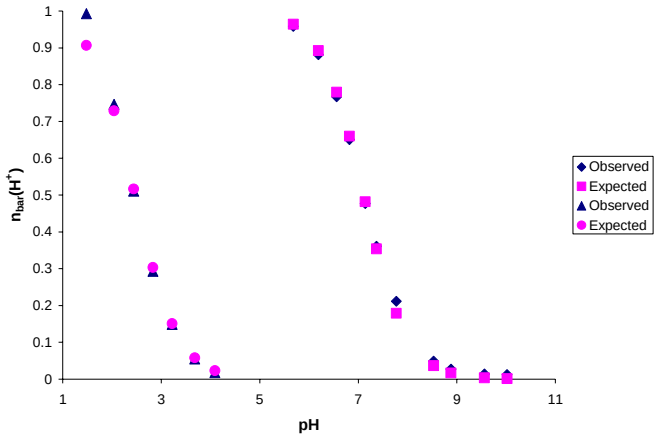

(a)

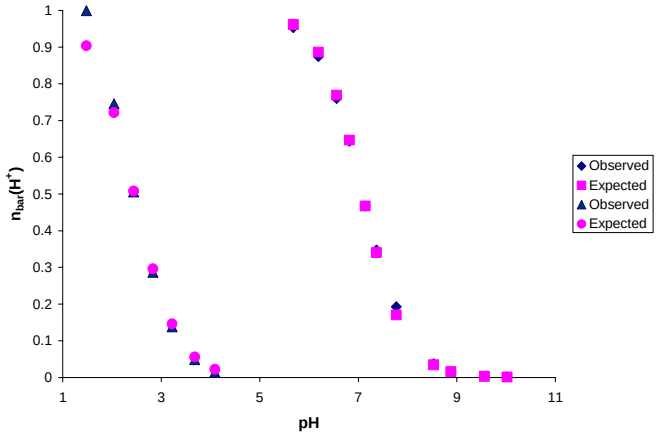

(b)

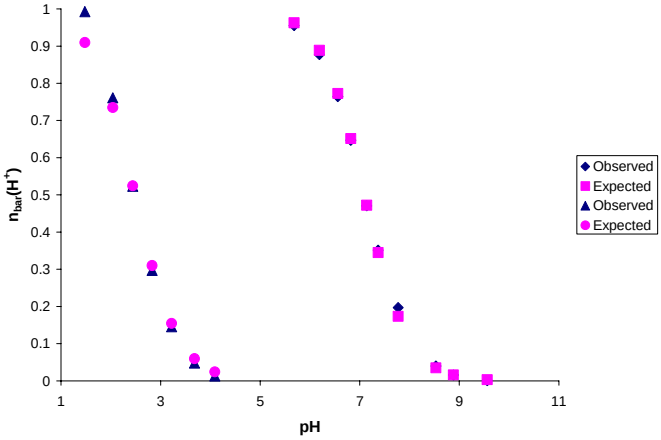

(c)

Figure 18. Observed $\bar{n}$ graphs of HQC and calcium at (a) 240nm, (b) 250nm, and (c) 265nm plotted against expected $\bar{n}$ values.

calcium and HQC, the sum of differences between pK_1 and pK_2 of the free and complexed ligand was determined using equation 16, the resulting value was 6.00.

The acid titration of the HQC – magnesium complex began at pH 9.50 and ended at pH 1.52. Both the spectra of this titration and the plot of absorbance versus peak shift show how the peak maximum moves throughout the course of the titration (Figure 19). The $\bar{n}$ plots of pK_1 and pK_2 were combined into one figure to demonstrate both protonations concurrently. From these $\bar{n}$ plots one can recognize the $\bar{n}$ observed data, gathered experimentally, agrees with the $\bar{n}$ theoretical data (Figure 20). Using equation 8, pK_1 was calculated to be 7.43 and using equation 9, pK_2 was calculated to be 3.71. In order to calculate the formation constant of magnesium and HQC, the sum of differences between pK_1 and pK_2 of the free and complexed ligand was determined using equation 16, the resulting value was 4.42.

The acid titration of the HQC – strontium complex began at pH 10.92 and ended at pH 1.59. Both the spectra of this titration and the plot of absorbance versus peak shift show how the peak maximum moves throughout the course of the titration (Figure 21). The $\bar{n}$ plots of pK_1 and pK_2 were combined into one figure to demonstrate both protonations concurrently. From these $\bar{n}$ plots one can recognize the $\bar{n}$ observed data, gathered experimentally, agrees with the $\bar{n}$ theoretical data (Figure 22). Using equation 8, pK_1 was calculated to be 7.69 and using equation 9, pK_2 was calculated to be 3.36. In order to calculate the formation constant of strontium and HQC, the sum of differences between pK_1 and pK_2 of the free and complexed ligand was determined using equation 16, the resulting value was 4.51.

The acid titration of the HQC – barium complex started at pH 10.94 and ended at pH 1.58. Both the spectra of this titration and the plot of absorbance versus peak shift show how the peak maximum moves throughout the course of the titration (Figure 23). The $\bar{n}$ plots of pK_1 and

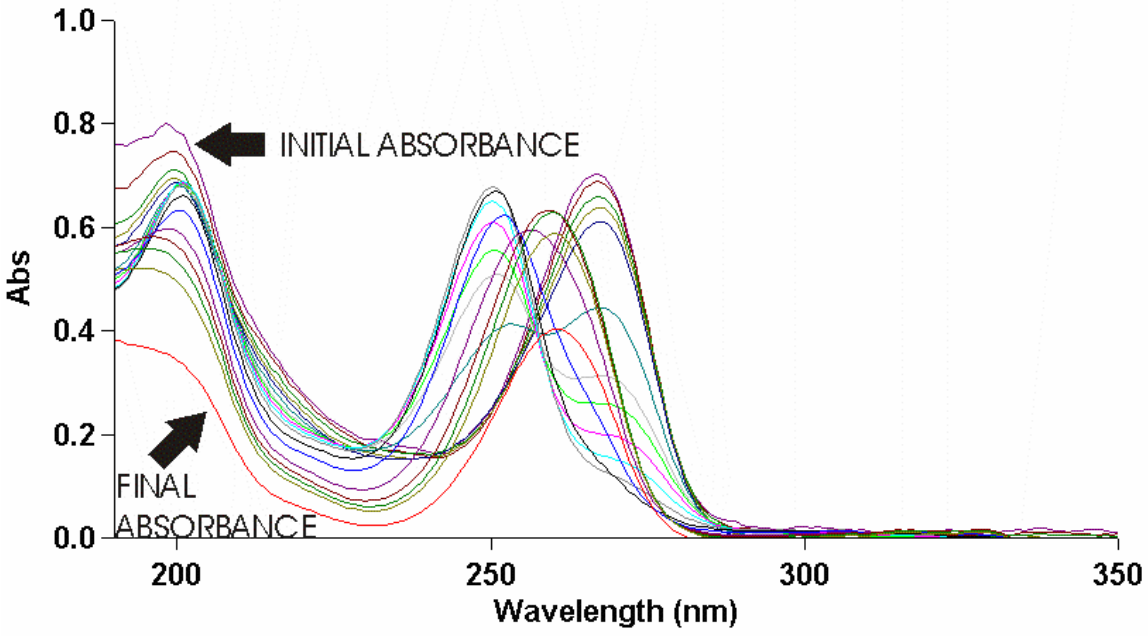

(a)

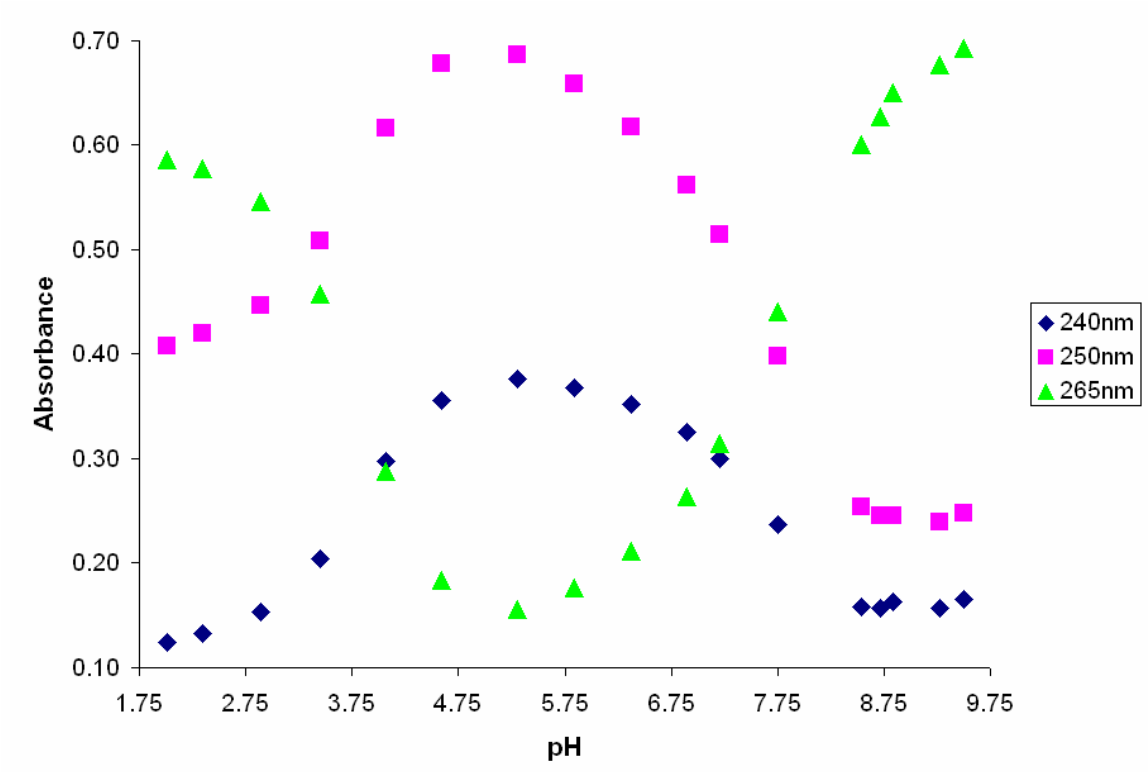

(b)

Figure 19. HQC and magnesium UV-Vis spectra (a) and peak shifts at wavelengths 240nm, 250nm, and 265 nm (b).

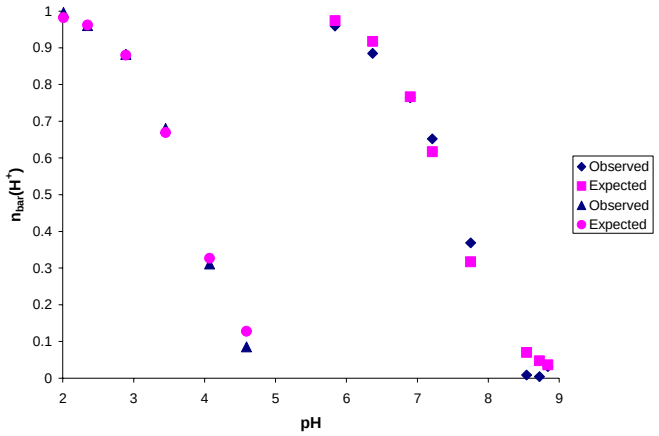

(a)

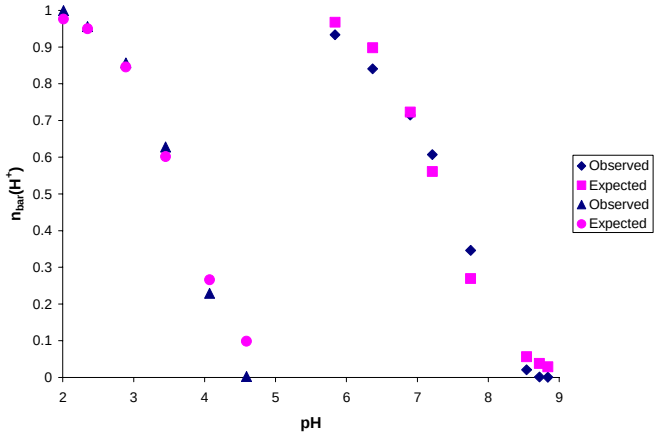

(b)

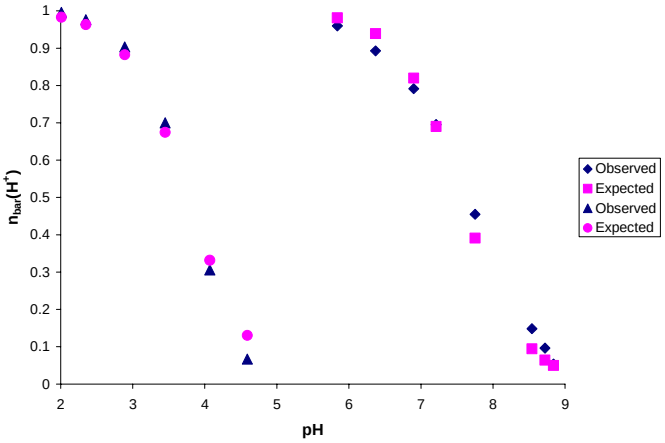

(c)

Figure 20. Observed $\bar{n}$ graphs of HQC and magnesium at (a) 240nm, (b) 250nm, and (c) 265nm plotted against expected $\bar{n}$ values.

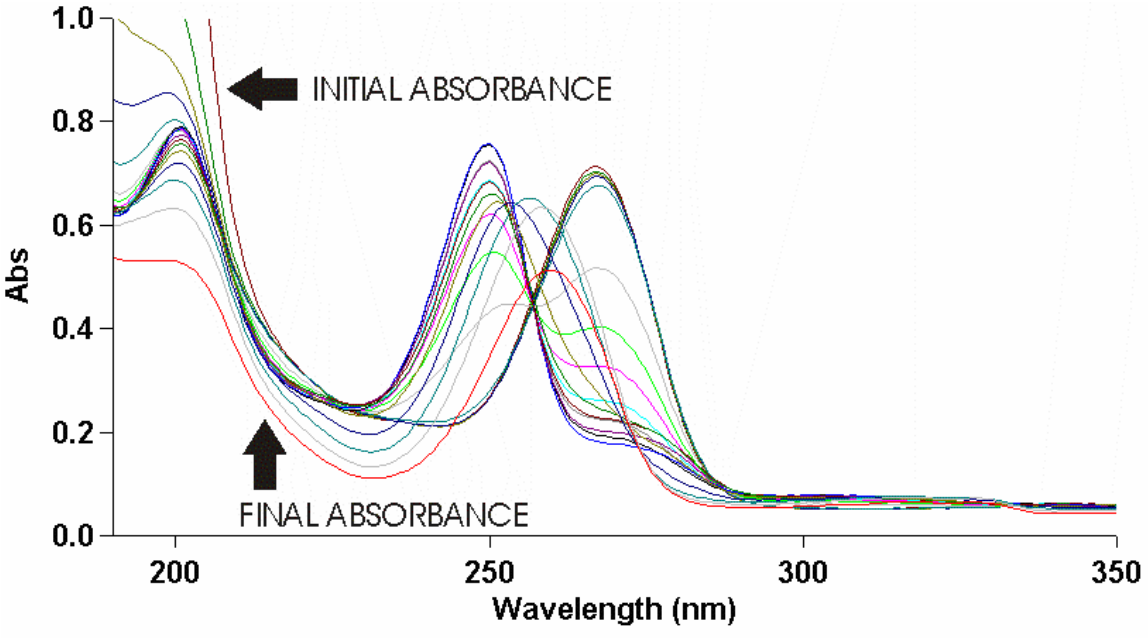

(a)

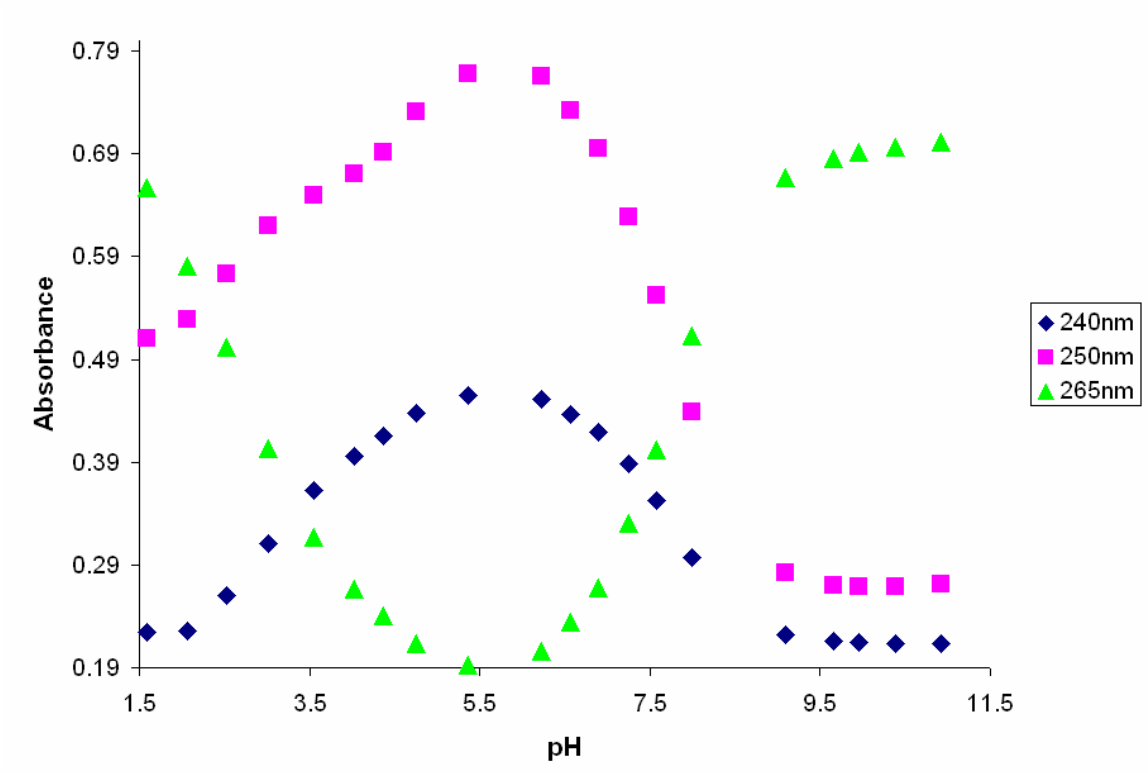

(b)

Figure 21. HQC and strontium UV-Vis spectra (a) and peak shifts at wavelengths 240nm, 250nm, and 265 nm (b).

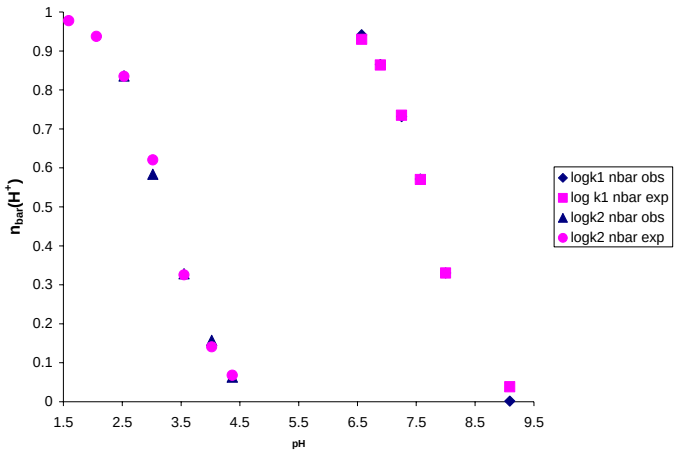

(a)

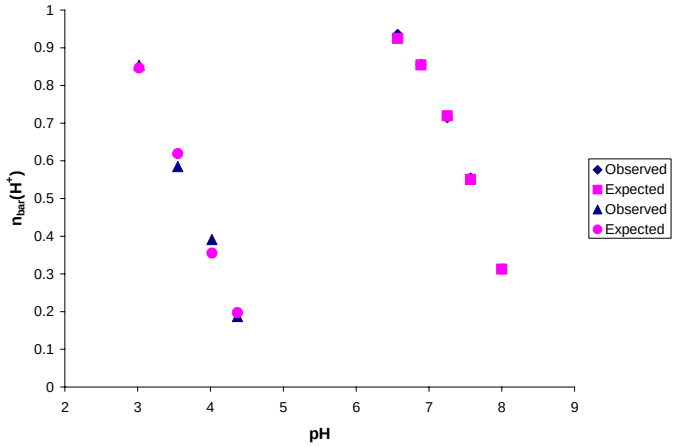

(b)

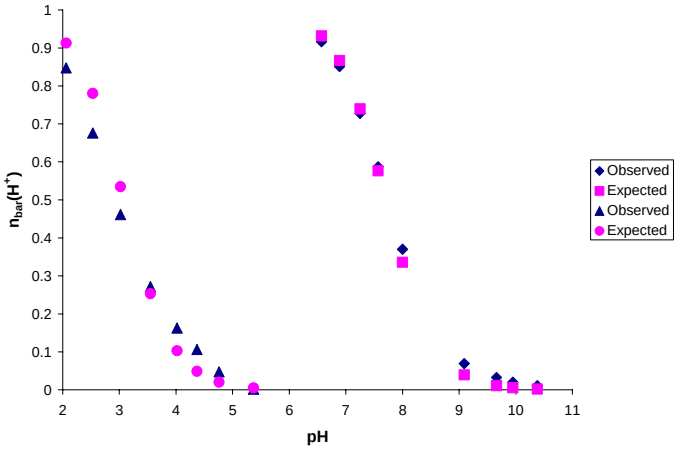

(c)

Figure 22. Observed $\bar{n}$ graphs of HQC and strontium at (a) 240nm, (b) 250nm, and (c) 265nm plotted against expected $\bar{n}$ values.

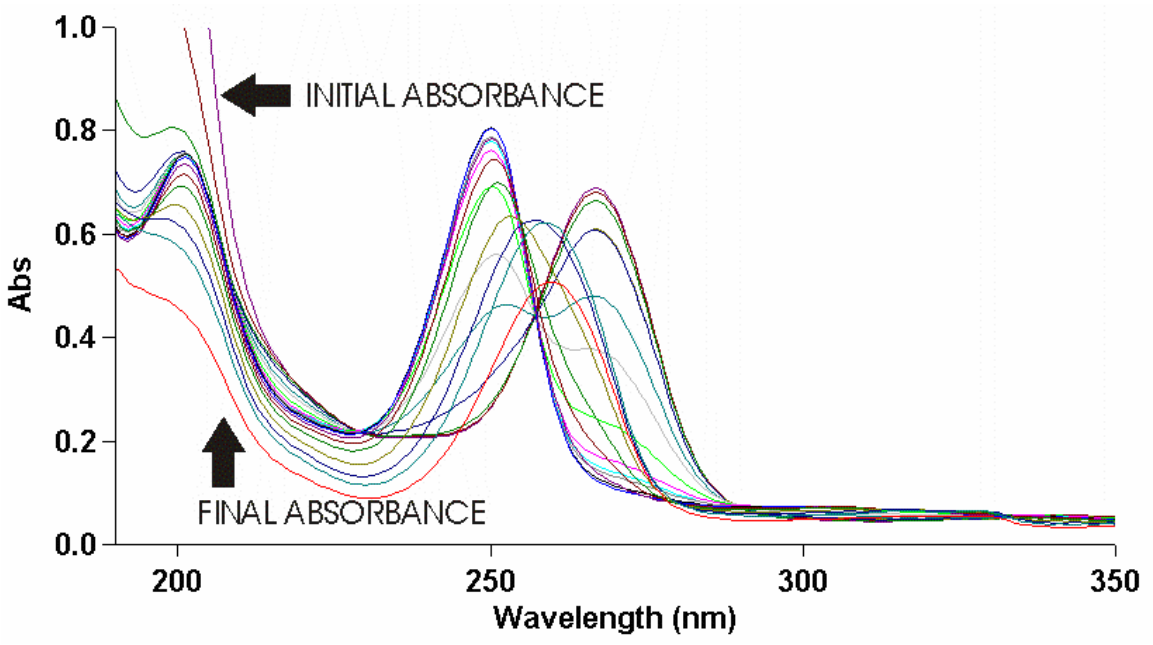

(a)

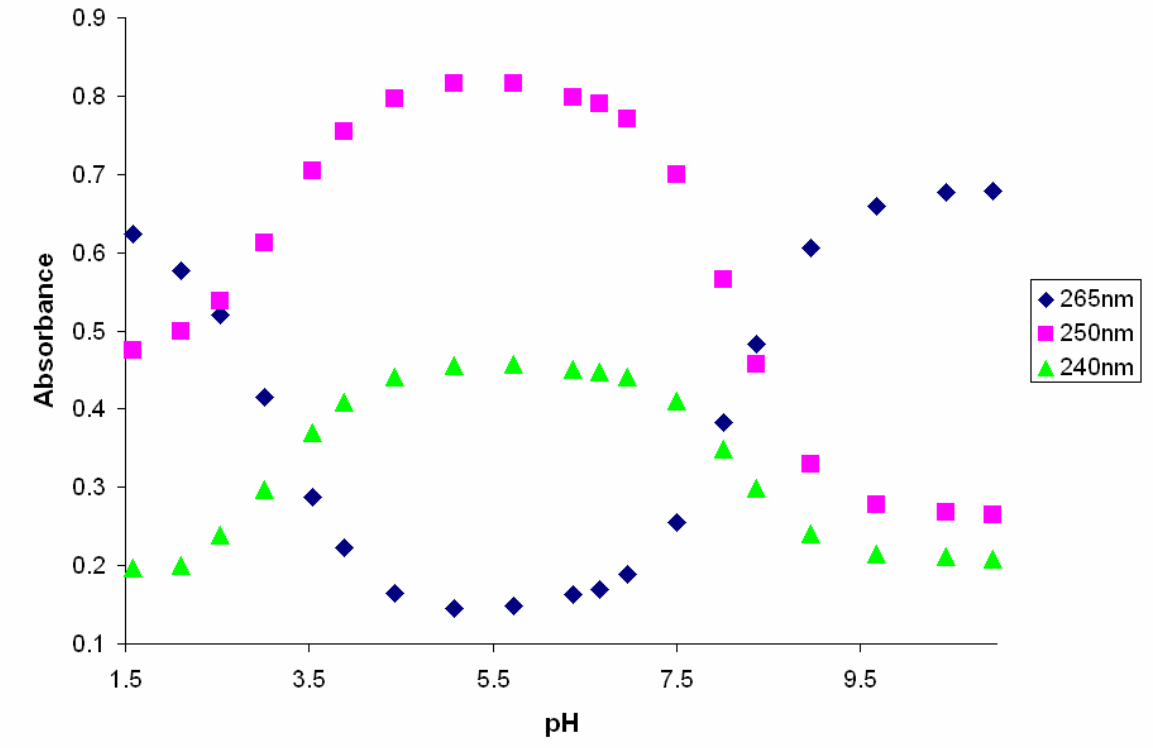

(b)

Figure 23. HQC and barium UV-Vis spectra (a) and peak shifts at wavelengths 240nm, 250nm, and 265 nm (b).

pK_2 were combined into one figure to demonstrate both protonations concurrently. From these $\bar{n}$ plots one can recognize the $\bar{n}$ observed data, gathered experimentally, agrees with the $\bar{n}$ theoretical data (Figure 24). Using equation 8, pK_1 was calculated to be 8.14 and using equation 9, pK_2 was calculated to be 3.49. In order to calculate the formation constant of barium and HQC, the sum of differences between pK_1 and pK_2 of the free and complexed ligand was determined using equation 16, the resulting value was 3.93.

The acid titration of the HQC – zinc complex started at pH 10.90 and ended at pH 1.99. Both the spectra of this titration and the plot of absorbance versus peak shift show how the peak maximum moves throughout the course of the titration (Figure 25). The $\bar{n}$ plots of pK_1 and pK_2 were combined into one figure to demonstrate both protonations concurrently. From these $\bar{n}$ plots one can recognize the $\bar{n}$ observed data, gathered experimentally, agrees with the $\bar{n}$ theoretical data (Figure 26). Using equation 8, pK_1 was calculated to be 6.13 and using equation 9, pK_2 was calculated to be 3.85. In order to calculate the formation constant of zinc and HQC, the sum of differences between pK_1 and pK_2 of the free and complexed ligand was determined using equation 16, the resulting value was 9.10.

The base titration of the HQC – lanthanum complex started at pH 2.13 and ended at pH 11.65. It is noted again that this titration was run from acidic to basic conditions to prevent the initial precipitation of lanthanum. Both the spectra of this titration and the plot of absorbance versus peak shift show how the peak maximum moves throughout the course of the titration (Figure 27). The $\bar{n}$ plots of pK_1 and pK_2 were combined into one figure to demonstrate both protonations concurrently. From these $\bar{n}$ plots one can recognize the $\bar{n}$ observed data, gathered experimentally, agrees with the $\bar{n}$ theoretical data (Figure 28). Using equation 8, pK_1 was calculated to be 4.89 and using equations 9, pK_2 was calculated to be 2.91. In order to calculate

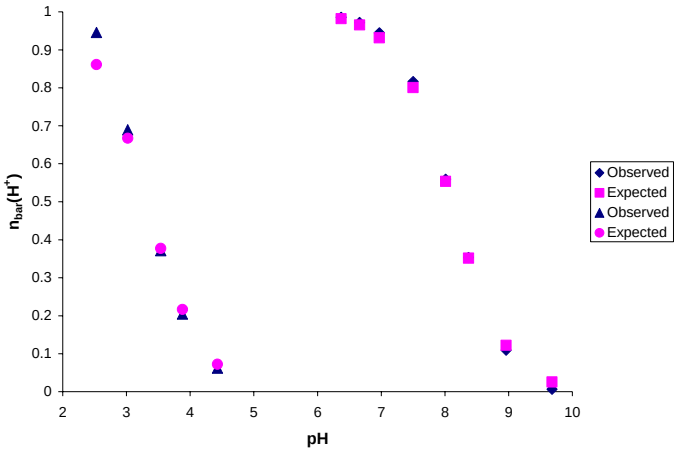

(a)

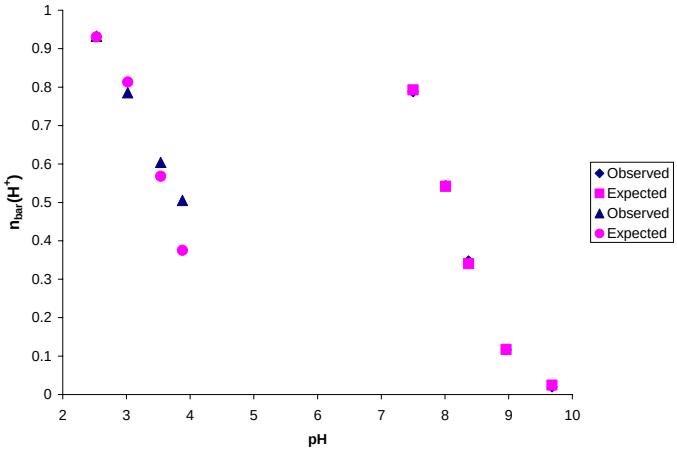

(b)

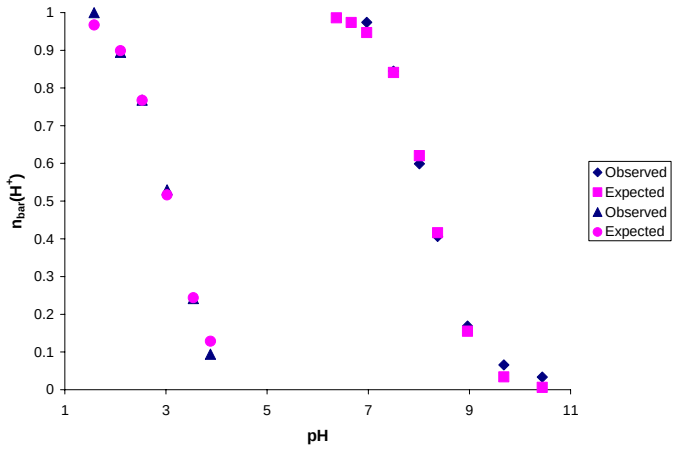

(c)

Figure 24. Observed $\bar{n}$ graphs of HQC-Barium at (a) 240nm, (b) 250nm, and (c) 265nm plotted against expected $\bar{n}$ values.

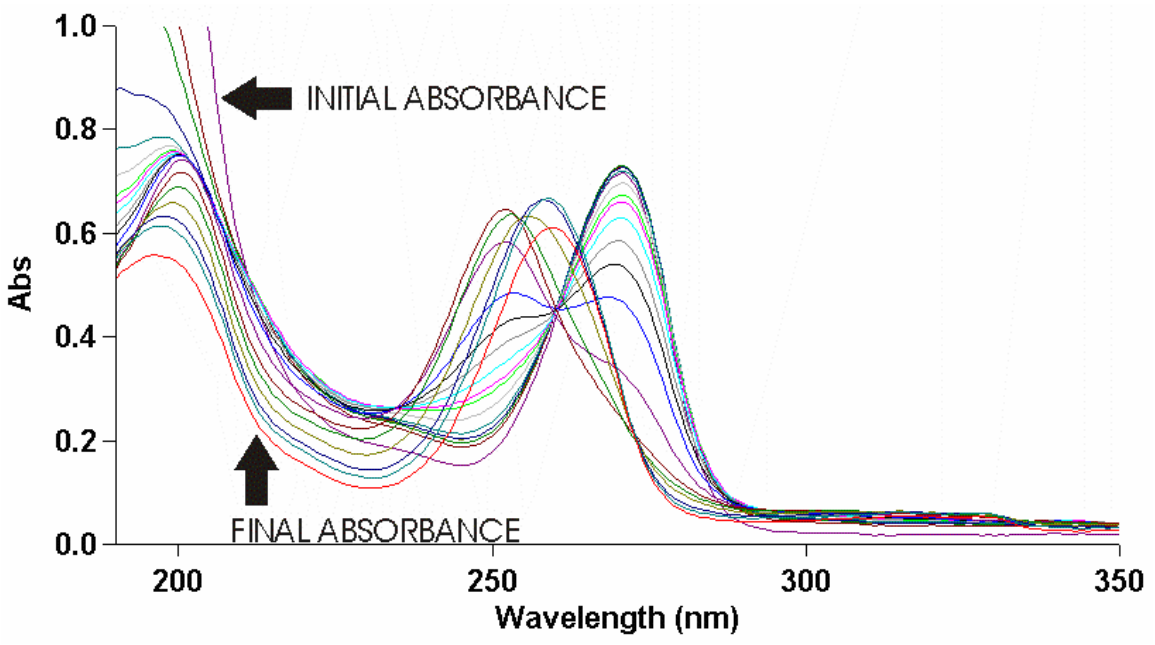

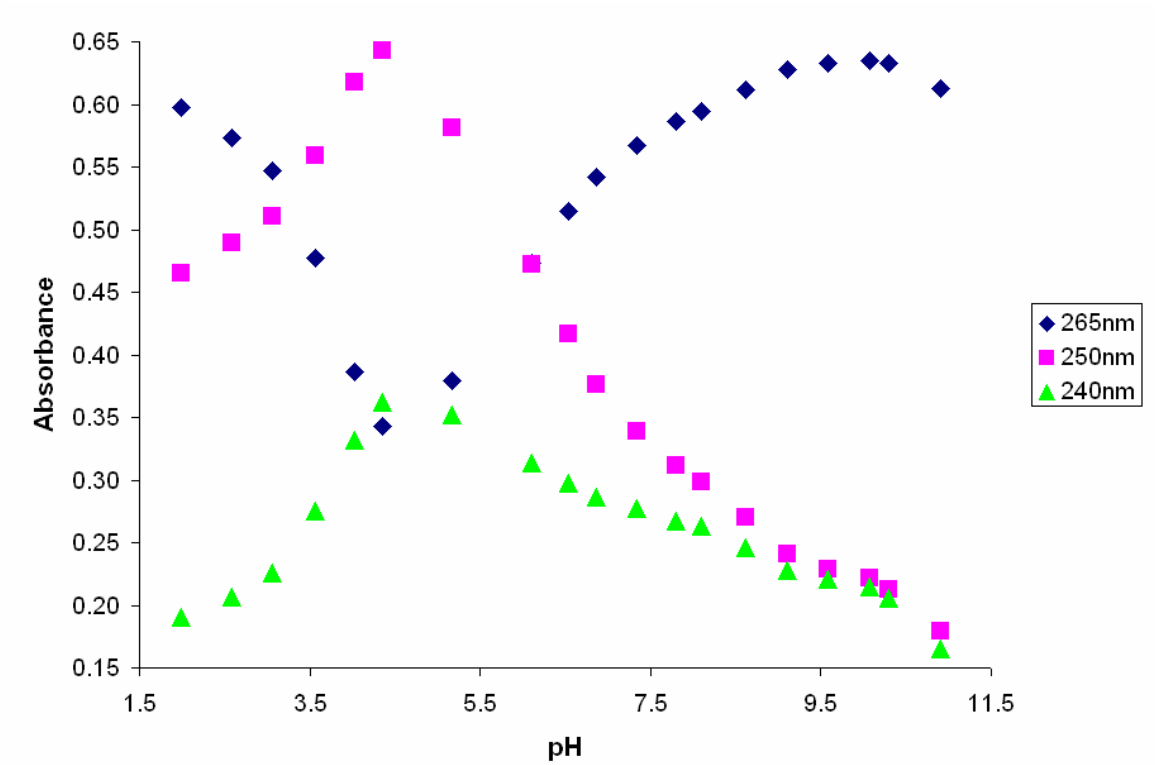

(a)

(b)

Figure 25. HQC and zinc UV-Vis spectra (a) and peak shifts at wavelengths 240nm, 250nm, and 265 nm (b).

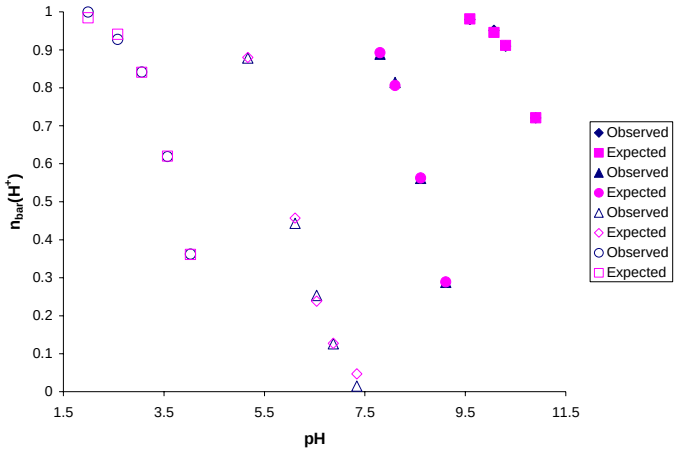

(a)

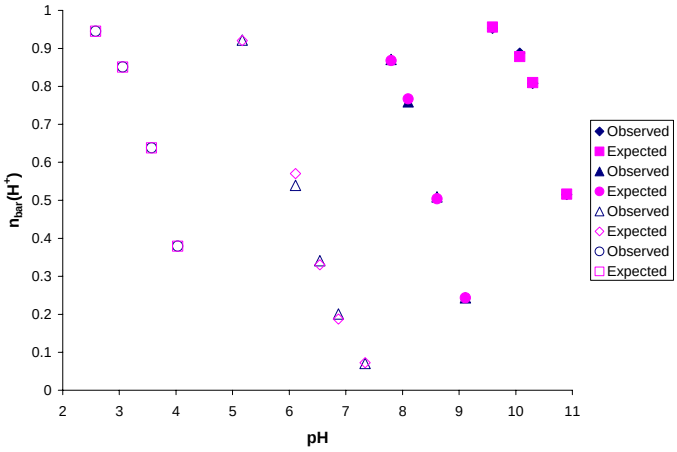

(b)

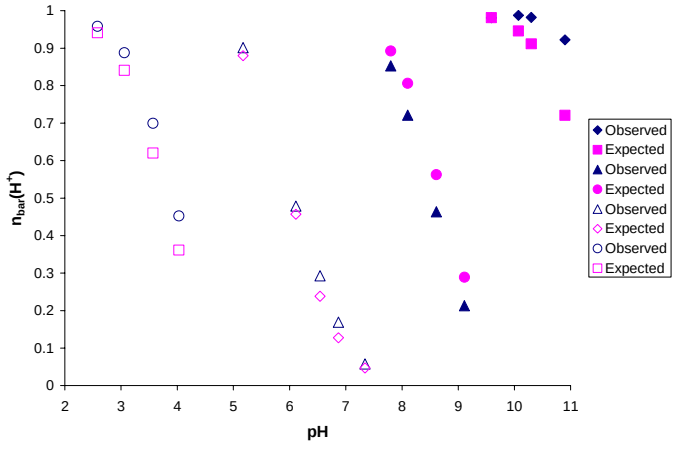

(c)

Figure 26. Observed $\bar{n}$ graphs of HQC and zinc at (a) 240nm, (b) 250nm, and (c) 265nm plotted against expected $\bar{n}$ values.

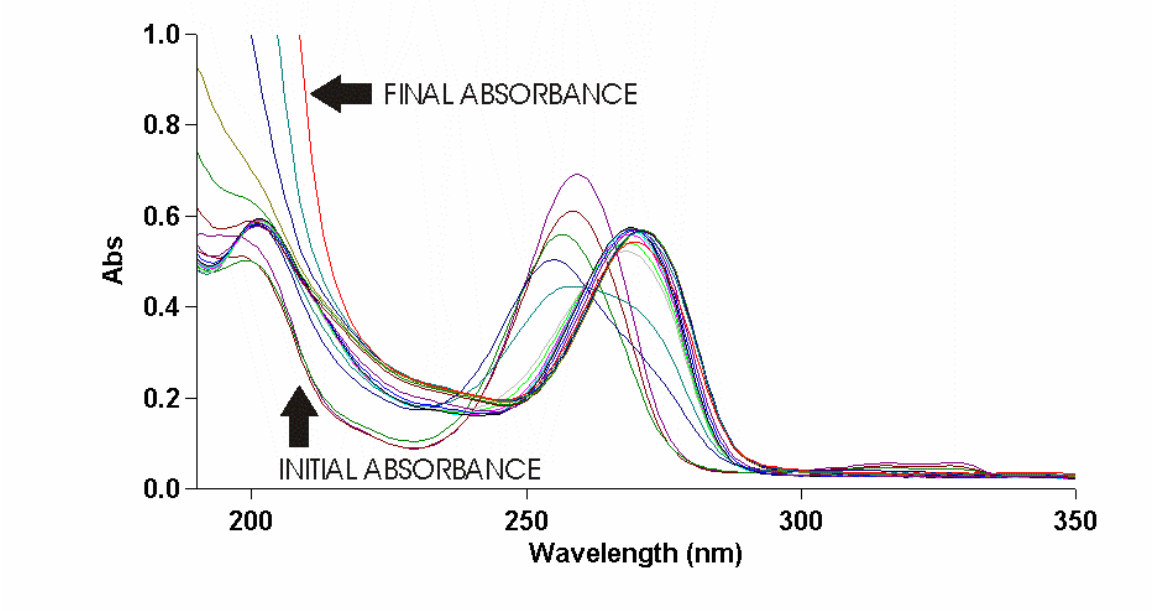

(a)

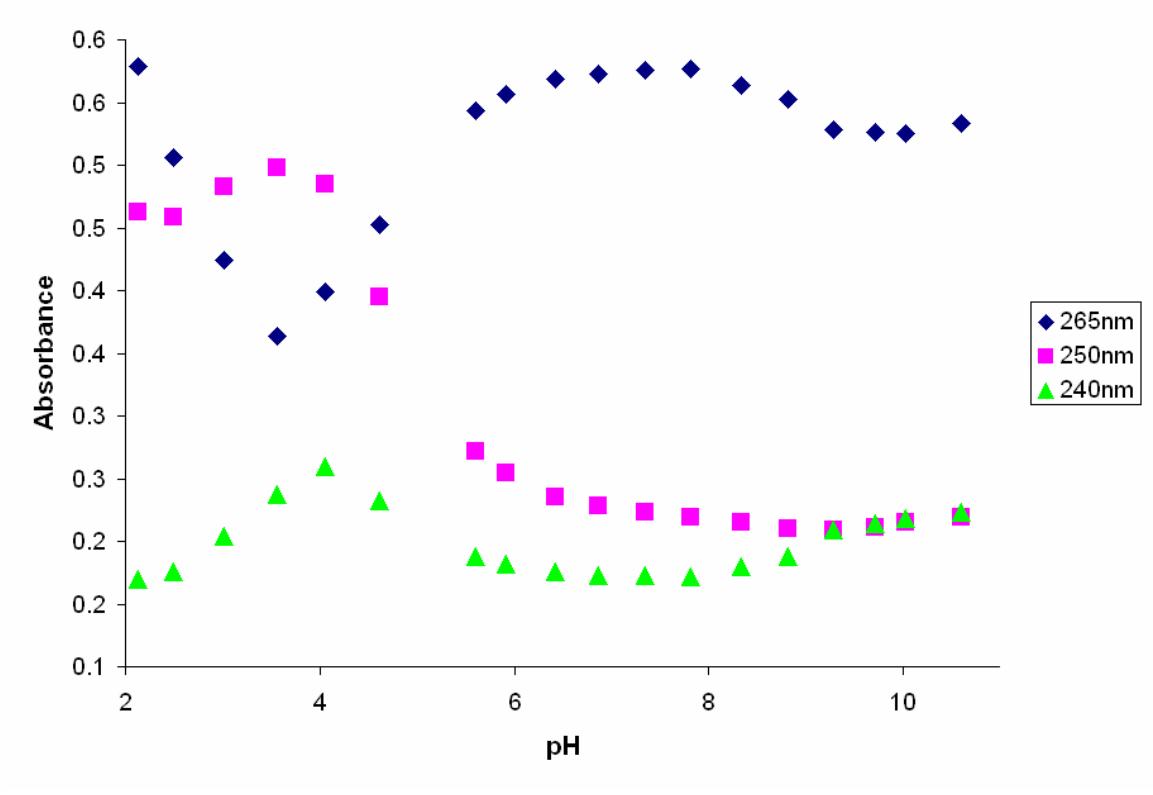

(b)

Figure 27. HQC and lanthanum UV-Vis spectra (a) and peak shifts at wavelengths 240nm, 250nm, and 265 nm (b).

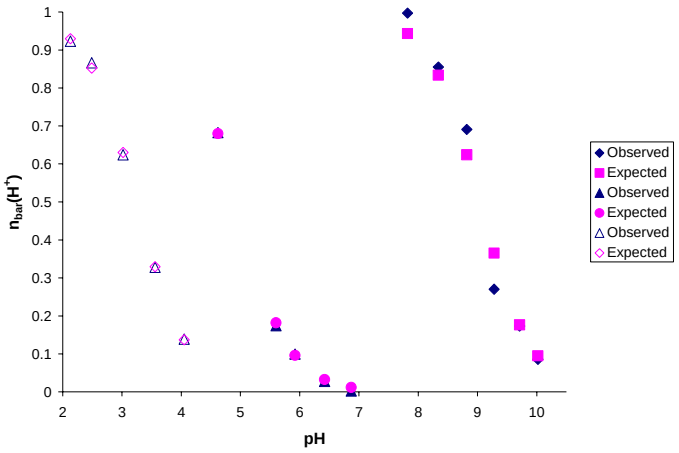

(a)

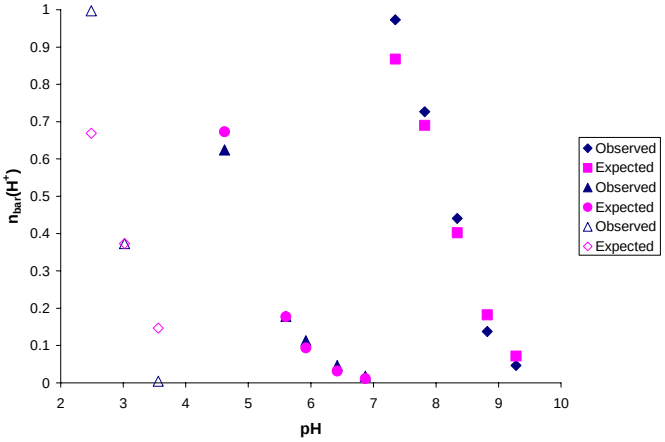

(b)

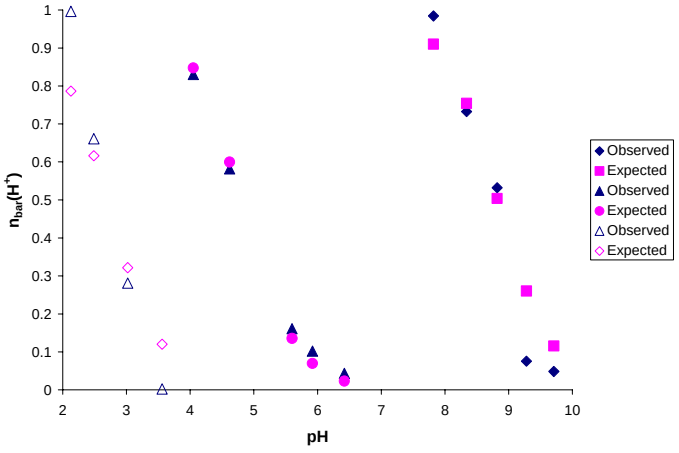

(c)

Figure 28. Observed $\bar{n}$ graphs of HQC and lanthanum at (a) 240nm, (b) 250nm, and (c) 265nm plotted against expected $\bar{n}$ values.

the formation constant of lanthanum and HQC, the sum of differences between pK_1 and pK_2 of the free and complexed ligand was determined using equation 16, the resulting value was 11.28.

The acid titration of the HQC – cadmium complex started at pH 11.04 and ended at pH 1.56. Both the spectra of this titration and the plot of absorbance versus peak shift show how the peak maximum moves throughout the course of the titration (Figure 29). The $\bar{n}$ plots of pK_1 and pK_2 were combined into one figure to demonstrate both protonations concurrently. From these $\bar{n}$ plots one can recognize the $\bar{n}$ observed data, gathered experimentally, agrees with $\bar{n}$ theoretical data (Figure 30). Using equation 8, pK_1 was calculated to be 6.75 and using equation 9, pK_2 was calculated to be 3.76. In order to calculate the formation constant of cadmium and HQC, the sum of differences between pK_1 and pK_2 of the free and complexed ligand was determined using equation 16, the resulting value was 8.57.

The acid titration of the HQC – nickel complex began at pH 10.97 and ended at pH 1.59. Both the spectra of this titration and the plot of absorbance versus peak shift show how the peak maximum moves throughout the course of the titration (Figure 31). The $\bar{n}$ plots of pK_1 and pK_2 were combined into one figure to demonstrate both protonations concurrently. From these $\bar{n}$ plots one can recognize the $\bar{n}$ observed data, gathered experimentally, agrees with the $\bar{n}$ theoretical data (Figure 32). Using equation 8, pK_1 was calculated to be 5.64 and using equation 9, pK_2 was calculated to be 2.86. In order to calculate the formation constant of nickel and HQC, the sum of differences between pK_1 and pK_2 of the free and complexed ligand was determined using equation 16, the resulting value was 10.58.

The base titration of the HQC – gadolinium complex began at pH 2.04 and ended at pH 11.05. It is noted again that this titration was run from acidic to basic conditions to prevent the initial precipitation of gadolinium. Both the spectra of this titration and the plot of absorbance

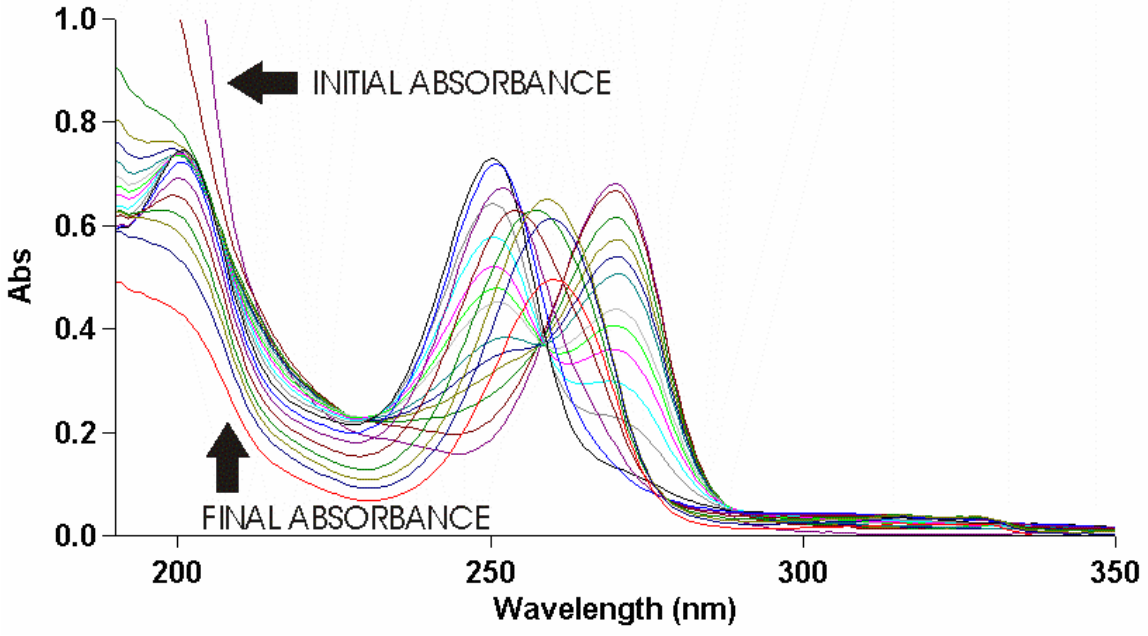

(a)

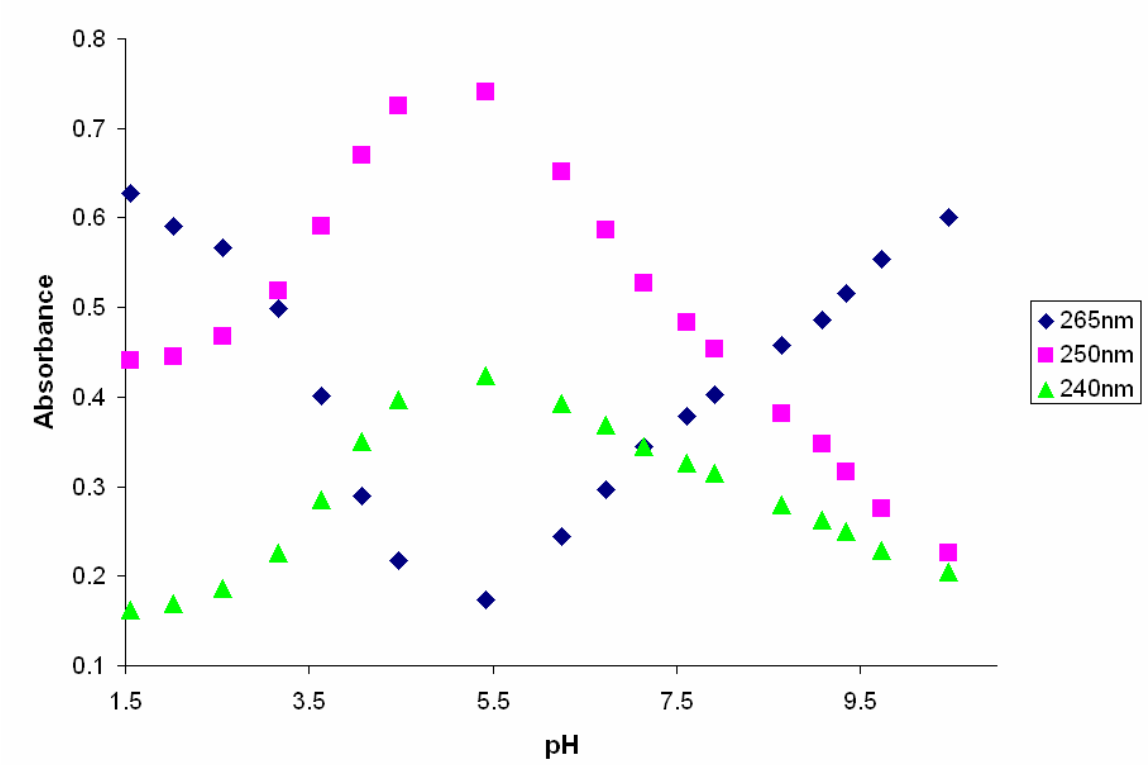

(b)

Figure 29. HQC and cadmium UV-Vis spectra (a) and peak shifts at wavelengths 240nm, 250nm, and 265 nm (b).

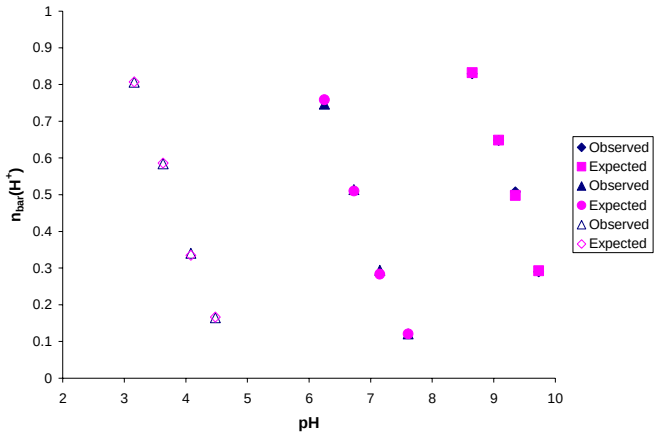

(a)

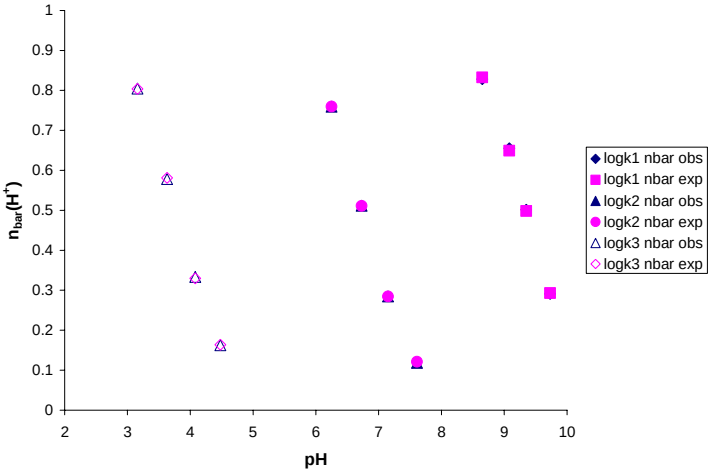

(b)

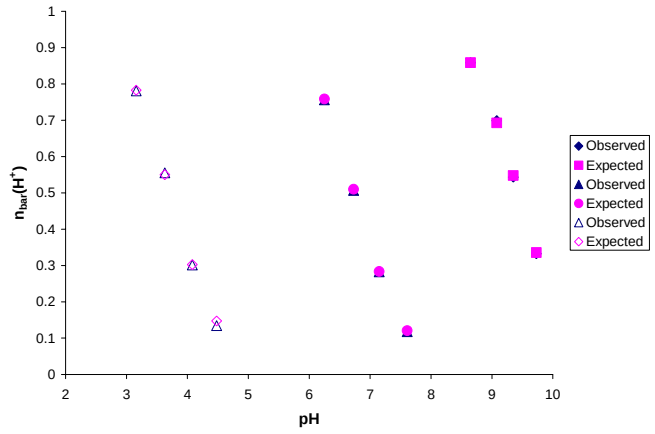

(c)

Figure 30. Observed $\bar{n}$ graphs of HQC and cadmium at (a) 240nm, (b) 250nm, and (c) 265nm plotted against expected $\bar{n}$ values.

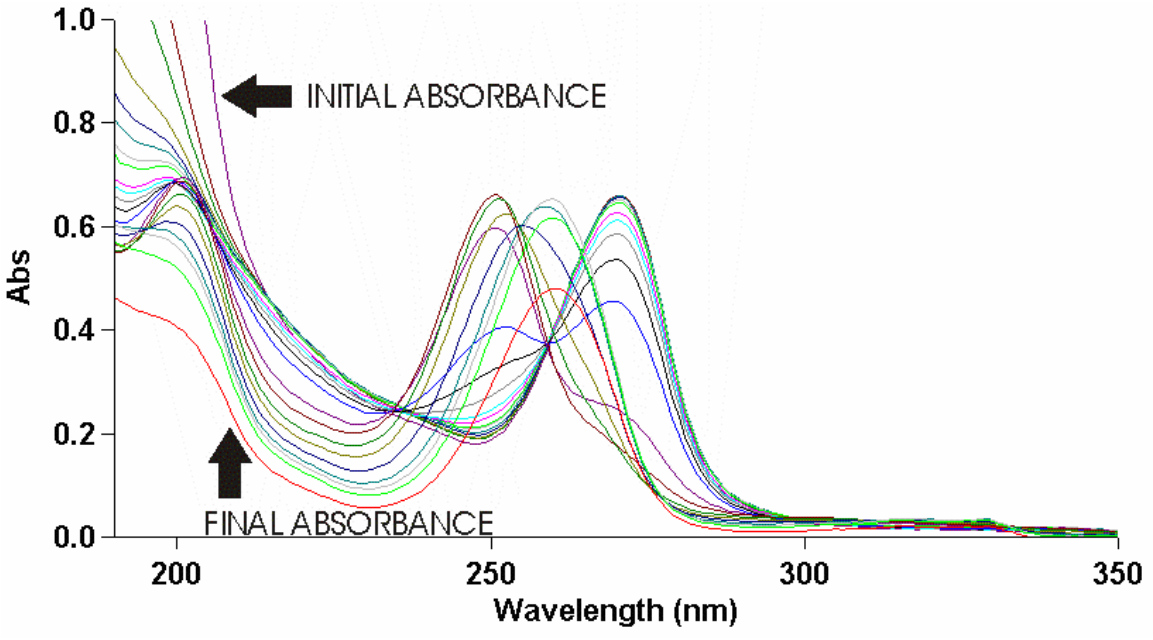

(a)

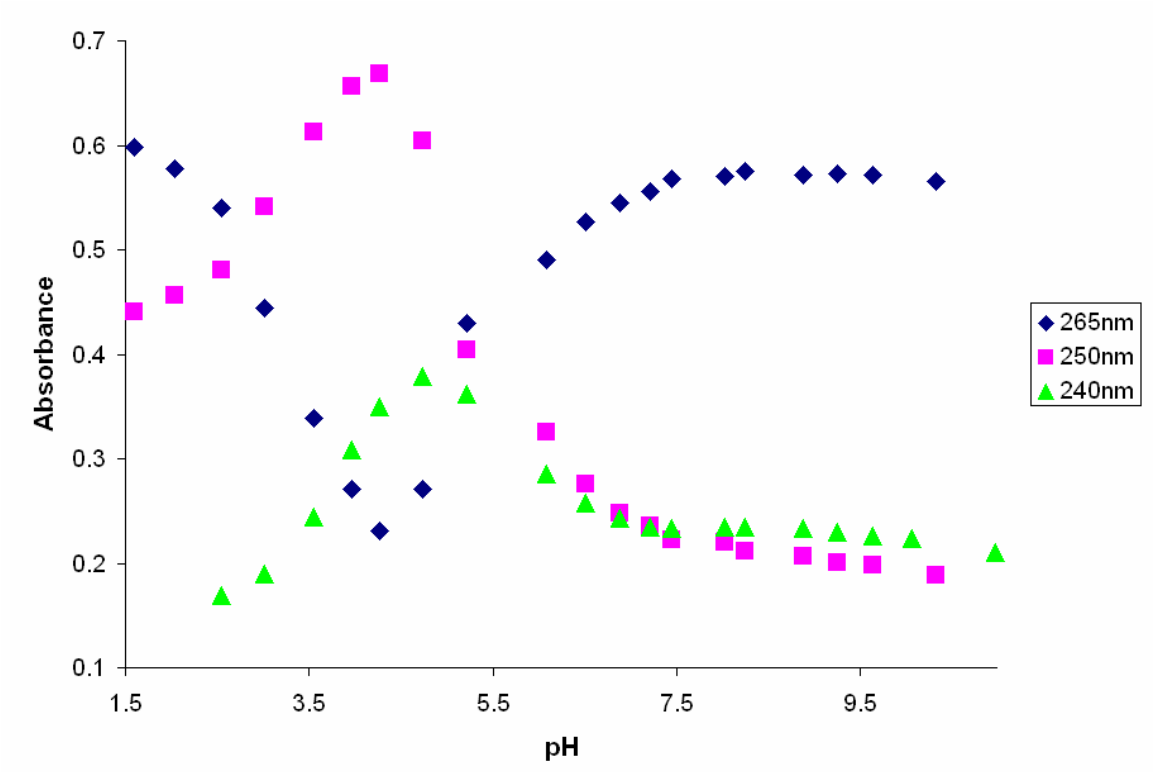

(b)

Figure 31. HQC and nickel UV-Vis spectra (a) and peak shifts at wavelengths 240nm, 250nm, and 265 nm (b).

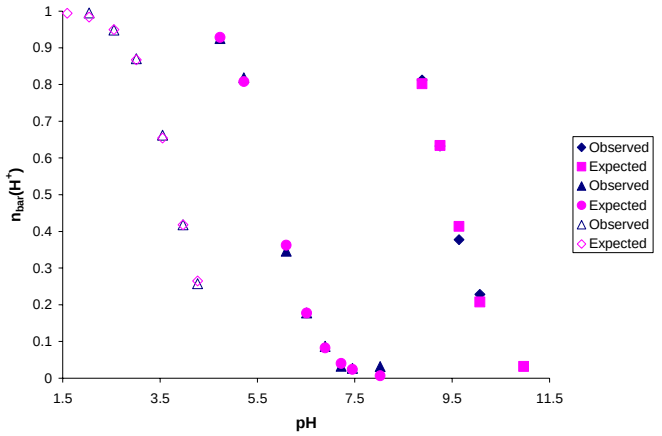

(a)

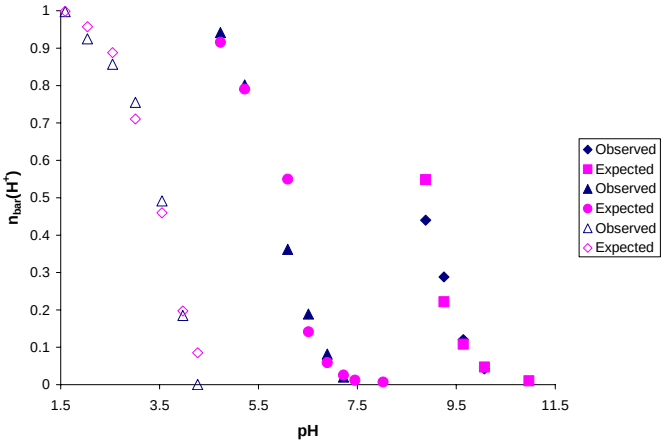

(b)

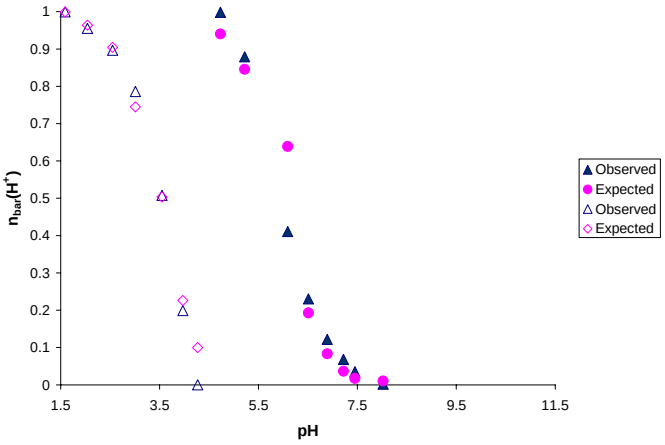

(c)

Figure 32. Observed $\bar{n}$ graphs of HQC and nickel at (a) 240nm, (b) 250nm, and (c) 265nm plotted against expected $\bar{n}$ values.

versus peak shift show how the peak maximum moves throughout the course of the titration (Figure 33). The $\bar{n}$ plots of pK_1 and pK_2 were combined into one figure to demonstrate both protonations concurrently. From these $\bar{n}$ plots one can recognize the $\bar{n}$ observed data, gathered experimentally, agrees with the $\bar{n}$ theoretical data (Figure 34). Using equation 8 pK_1 was calculated to be 5.93 and using equation 9, pK_2 was calculated to be 3.26. In order to calculate the formation constant of gadolinium and HQC, the sum of differences between pK_1 and pK_2 of the free and complexed ligand was determined using equation 16, the resulting value was 9.89.

The acid titration of the HQC – lead complex started at pH 10.78 and ended at pH 1.92. Both the spectra of this titration and the plot of absorbance versus peak shift show how the peak maximum moves throughout the course of the titration (Figure 35). The $\bar{n}$ plots of pK_1 and pK_2 were combined into one figure to demonstrate both protonations concurrently. From these $\bar{n}$ plots one can recognize the $\bar{n}$ observed data, gathered experimentally, agrees with the $\bar{n}$ theoretical data (Figure 36). Using equation 8, pK_1 was calculated to be 3.92 and using equation 9, pK_2 was calculated to be at least 3.92. The actual pK_2 of the HQC – Pb complex was not observed experimentally because the lead in the complex coordinated so strongly it shifted pK_2 to a pH < 1.5. Since the phenolate is more basic and would be protonated first, it can be assumed that the greatest pK_2 could be is a value equal to pK_1. In order to calculate the formation constant of lead and HQC, the sum of differences between pK_1 and pK_2 of the free and complexed ligand was determined using equation 16, the resulting value was 11.24.

The acid titration of the HQC – copper complex started at pH 10.78 and ended at pH 1.98. Both the spectra of this titration and the plot of absorbance versus peak shift show how the peak maximum moves throughout the course of the titration (Figure 37). The $\bar{n}$ plots of pK_1 and pK_2 were combined into one figure to demonstrate both protonations concurrently. From

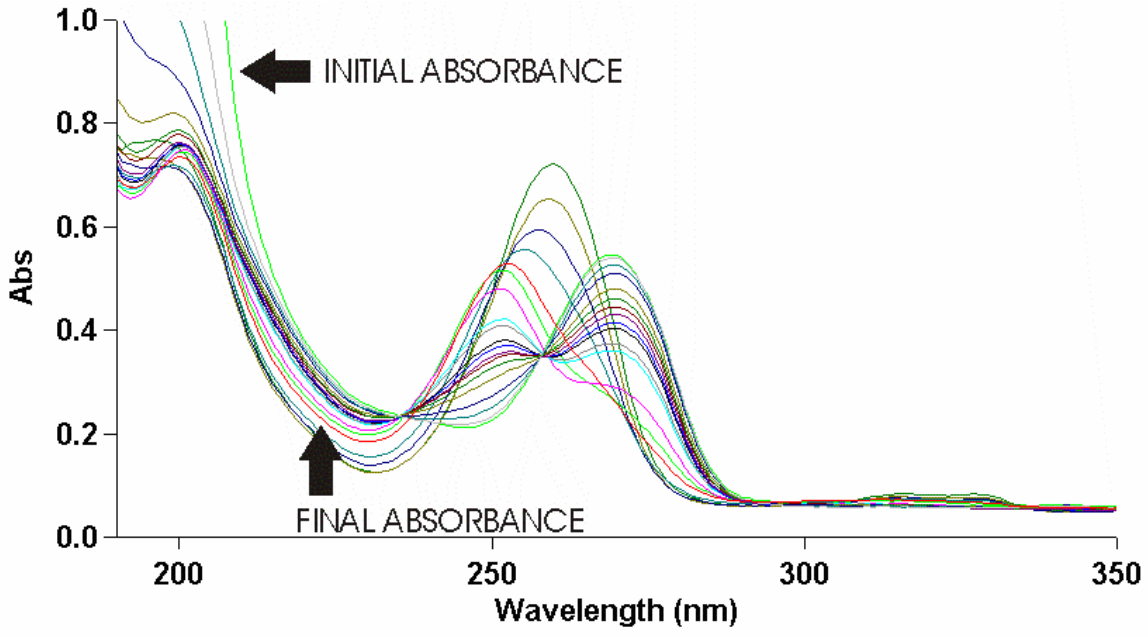

(a)

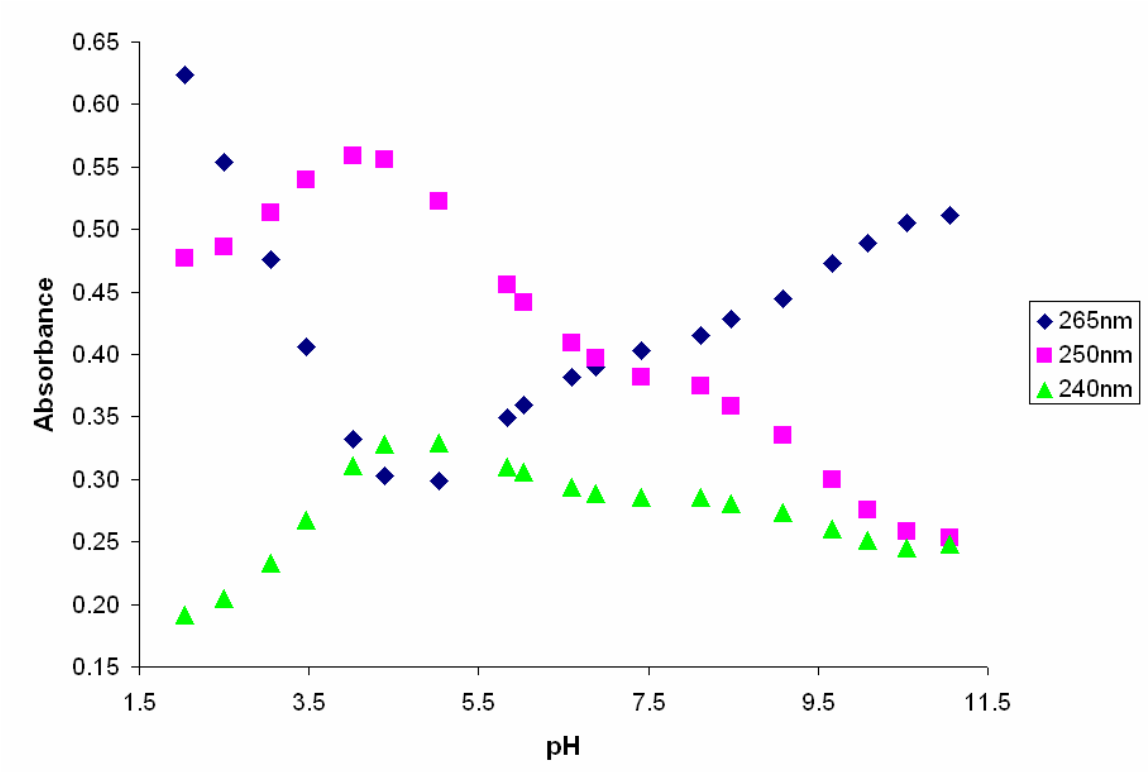

(b)

Figure 33. HQC and gadolinium UV-Vis spectra (a) and peak shifts at wavelengths 240nm, 250nm, and 265 nm (b).

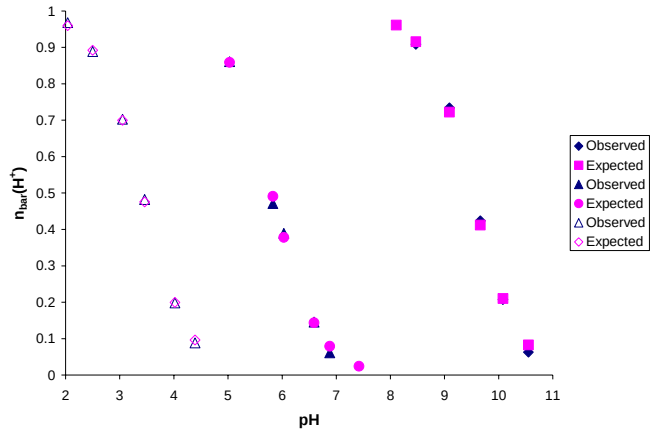

(a)

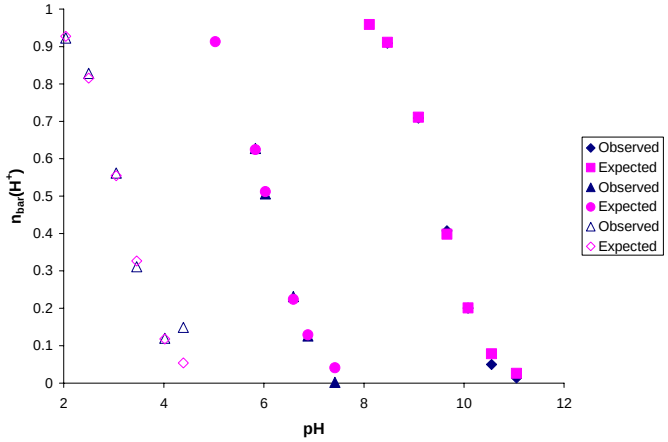

(b)

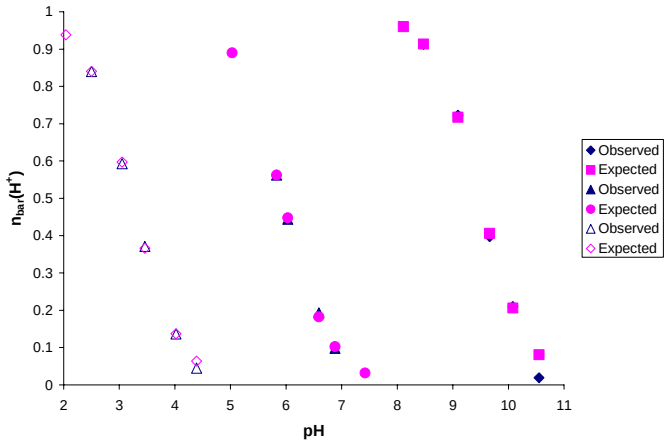

(c)

Figure 34. Observed $\bar{n}$ graphs of HQC and gadolinium at (a) 240nm, (b) 250nm, and (c) 265nm plotted against expected $\bar{n}$ values.

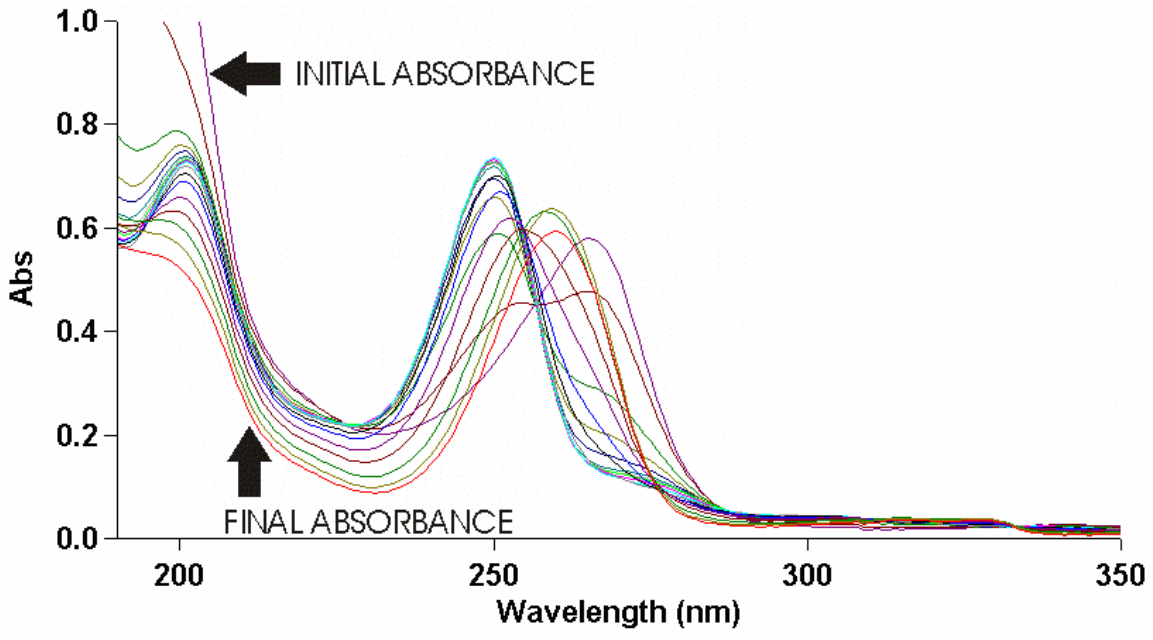

(a)

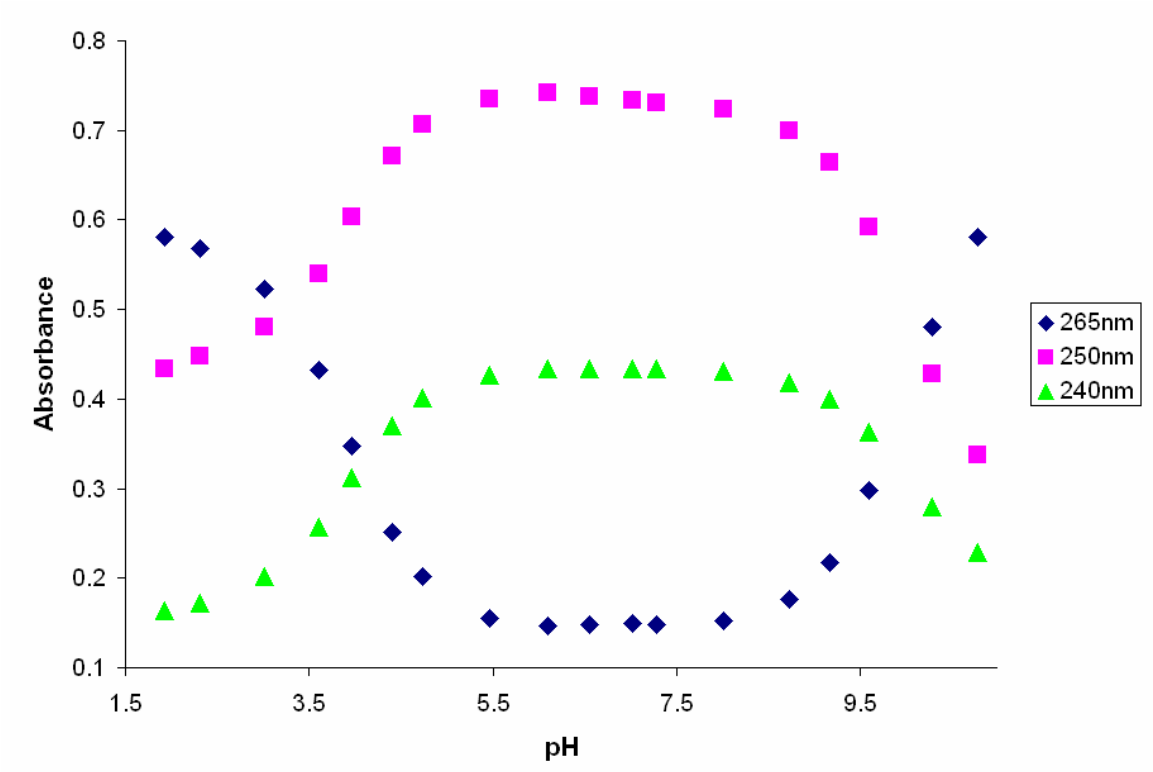

(b)

Figure 35. HQC and lead UV-Vis spectra (a) and peak shifts at wavelengths 240nm, 250nm, and 265 nm (b).

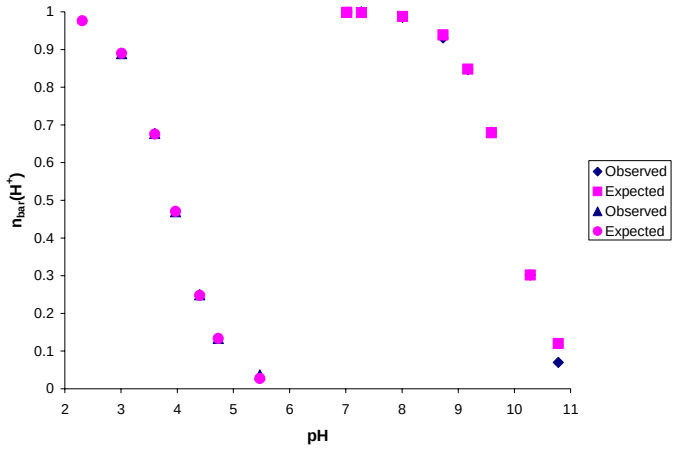

(a)

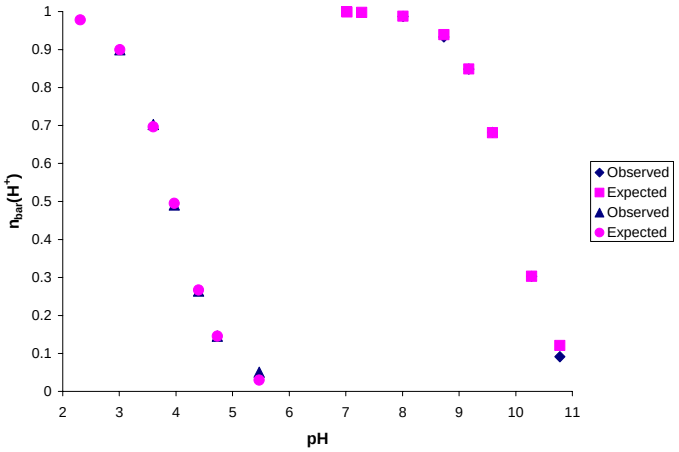

(b)

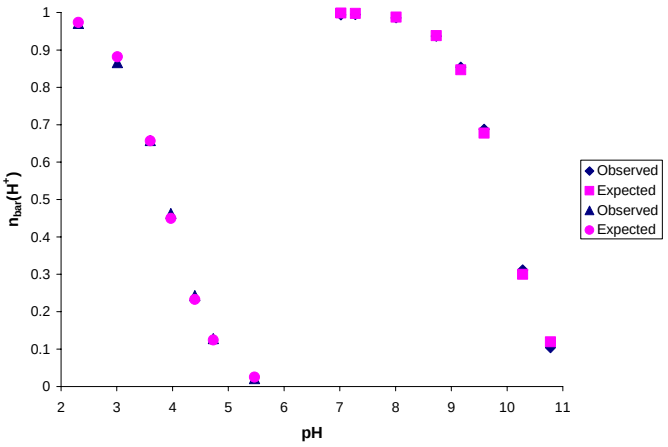

(c)

Figure 36. Observed $\bar{n}$ graphs of HQC and lead at (a) 240nm, (b) 250nm, and (c) 265nm plotted against expected $\bar{n}$ values.

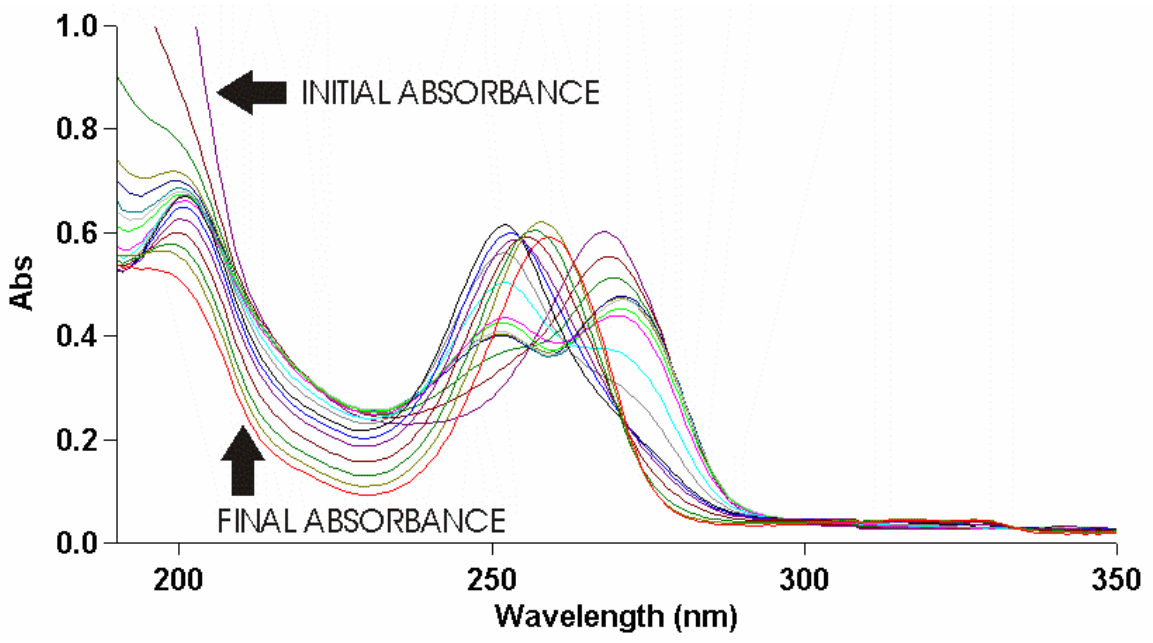

(a)

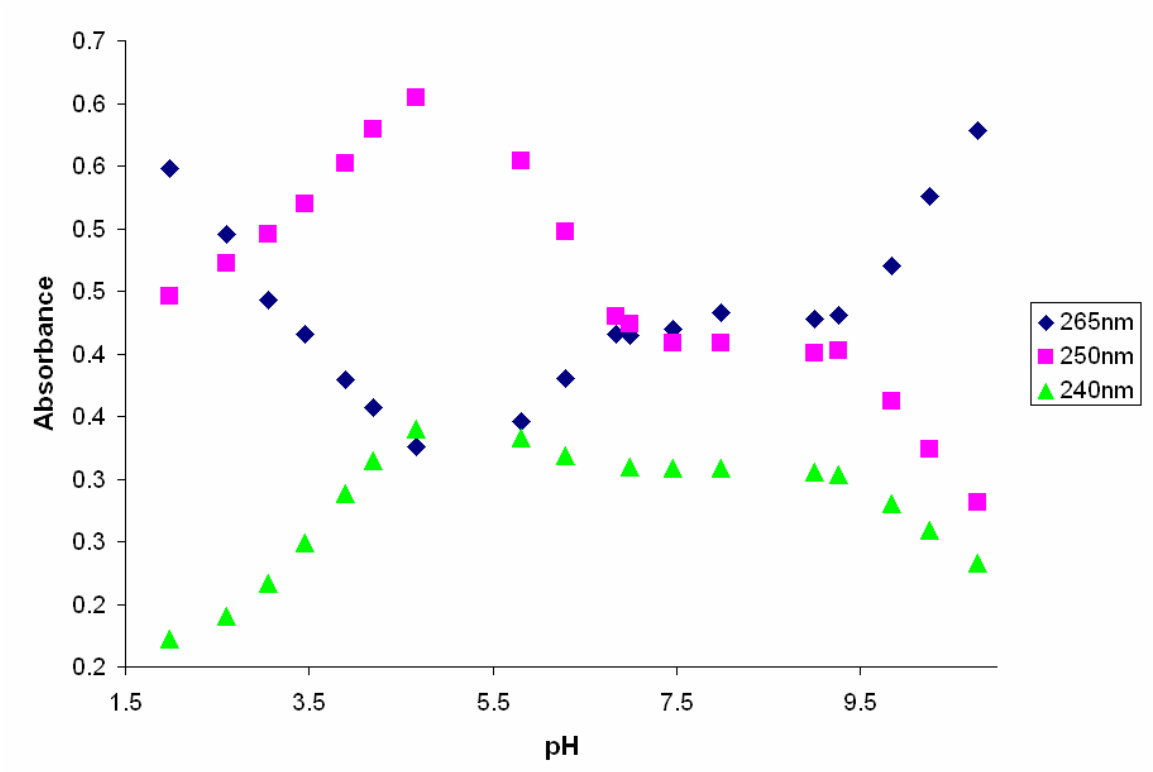

(b)

Figure 37. HQC and copper UV-Vis spectra (a) and peak shifts at wavelengths 240nm, 250nm, and 265 nm (b).

these $\bar{n}$ plots one can recognize the $\bar{n}$ observed data, gathered experimentally, agrees with the $\bar{n}$ theoretical data (Figure 38). Using equation 8, pK_1 was calculated to be 3.54 and using equation 9, pK_2 was calculated to be at least 3.54. Like lead, the actual pK_2 of the HQC – Cu complex was not observed experimentally because the copper in the complex coordinated so strongly it shifted pK_2 to a pH < 1.5. Since the phenolate is more basic and would be protonated first, it can be assumed that the greatest pK_2 could be is a value equal to pK_1. In order to calculate the formation constant of copper and HQC, the sum of differences between pK_1 and pK_2 of the free and complexed ligand was determined using equation 16, the resulting value was 12.00.

Additive properties

The formation constants calculated for HQC-metal complexes are summarized in Table 3. This can give great insight into the intricacies of the metal – ligand interactions. By creating a method to predict approximate pK_a values one could save valuable time and energy when designing ion-specific ligands.

Effect of carboxylate (Table 4 and Figure 39).

The structural difference between oxine, otherwise known as 8-hydroxyquinoline and HQC is the addition of a carboxylate on HQC. Donald Cram's proposal of preorganization proved that increasing denticity leads to an increase in preorganization thereby elevating the formation constant. The log *K* increased for every metal ligand complex studied when a carboxylate was added as a donor, with the exception of Cu^{2+}. This demonstrates how the increase in denticity from oxine to HQC did increase the formation constants. There is a noticeable trend in the change of formation constants as the size of the ligand changes. The smaller metal ions (r < 1.00 Å) have little to no change in formation constant. This is because the metal ions are not large

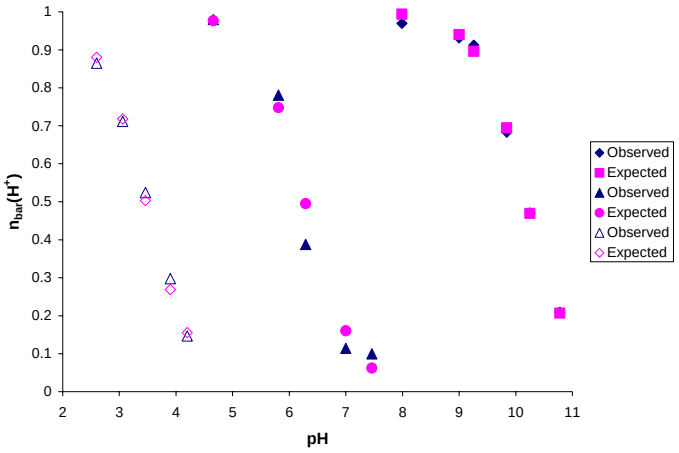

(a)

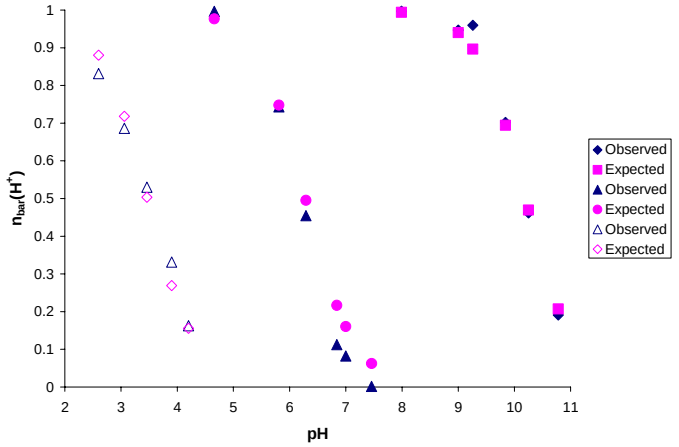

(b)

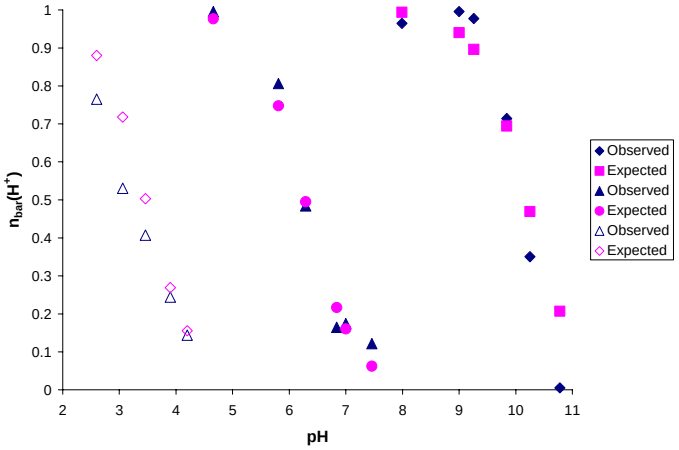

(c)

Figure 38. Observed $\bar{n}$ graphs of HQC and copper at (a) 240nm, (b) 250nm, and (c) 265nm plotted against expected $\bar{n}$ values.

Table 3. Formation constants for HQC (L) at 25 ºC and 0.1 *M* $NaClO_4$.

Equilibrium			log *K*	reference
$H+ + OH^-$	⇆	H_2O	13.78	Martell & Smith
$L^{2-} + H^+$	⇆	LH^-	10.18	this work
$LH^- + H^+$	⇆	LH_2	3.94	"
$L^{2-} + Mg^{2+}$	⇆	MgL	4.42	"
$MgL + H^+$	⇆	$MgLH^+$	7.43	"
$L^{2-} + Ca^{2+}$	⇆	CaL	6.00	"
$CaL + H^+$	⇆	$CaLH^+$	7.09	"
$L^{2-} + Sr^{2+}$	⇆	SrL	4.51	"
$SrL + H^+$	⇆	$SrLH^+$	7.69	"
$L^{2-} + Ba^{2+}$	⇆	BaL	6.00	"
$BaL + H^+$	⇆	$BaLH^+$	7.09	"
$L^{2-} + La^{3+}$	⇆	LaL^+	11.28	"
$LaL^+ + H^+$	⇆	$LaLH^{2+}$	4.89	"
$LaLOH + H^+$	⇆	LaL	8.82	"
$L^{2-} + Gd^{3+}$	⇆	GdL^+	9.89	"
$GdL^+ + H^+$	⇆	$GdLH^{2+}$	5.93	"
$GdLOH + H^+$	⇆	GdL	9.49	"
$L^{2-} + Cd^{2+}$	⇆	CdL	8.57	"
$CdL + H^+$	⇆	$CdLH^+$	6.75	"
$CdLOH + H^+$	⇆	CdL	9.38	"
$L^{2-} + Pb^{2+}$	⇆	PbL	>11.2	"

Table 3 (continued). Formation constants for HQC (L) at 25 ºC and 0.1 *M* $NaClO_4$.

Equilibrium			log *K*	reference
$PbL + H^+$	⇆	$PbLH^+$	3.92	this work
$PbLOH + H^+$	⇆	PbL	9.92	"
$L^{2-} + Ni^{2+}$	⇆	NiL	10.86	"
$NiL + H^+$	⇆	$NiLH^+$	5.64	"
$NiLOH + H^+$	⇆	NiL	9.22	"
$L^{2-} + Cu^{2+}$	⇆	CuL	12.00	"
$CuL + H^+$	⇆	$CuLH^+$	3.54	"
$CuLOH^- + H^+$	⇆	CuL	6.29	"
$CuL(OH)_2 + H^+$	⇆	$CuLOH^-$	10.15	"
$L^{2-} + Zn^{2+}$	⇆	ZnL	9.10	"
$ZnL + H^+$	⇆	$ZnLH^+$	6.13	"
$ZnLOH^- + H^+$	⇆	ZnL	8.63	"
$ZnL(OH)_2 + H^+$	⇆	$ZnLOH^-$	11.35	"

Table 4. Log of formation constants of various metals with HQC and oxine

Metal Ion	Ionic Radius	HQC	Oxine[31-34]
Cu^{2+}	0.57	12.00*	12.00
Ni^{2+}	0.69	10.58	9.27
Mg^{2+}	0.72	4.42	4.31
Zn^{2+}	0.74	9.10	8.52
Gd^{3+}	0.93	9.89	N/A
Cd^{2+}	0.95	8.57	7.34
Ca^{2+}	1.00	6.00	2.82
La^{3+}	1.03	11.28	5.90
Sr^{2+}	1.18	4.51	2.11
Pb^{2+}	1.19	11.24*	9.02
Ba^{2+}	1.35	3.93	1.62

.

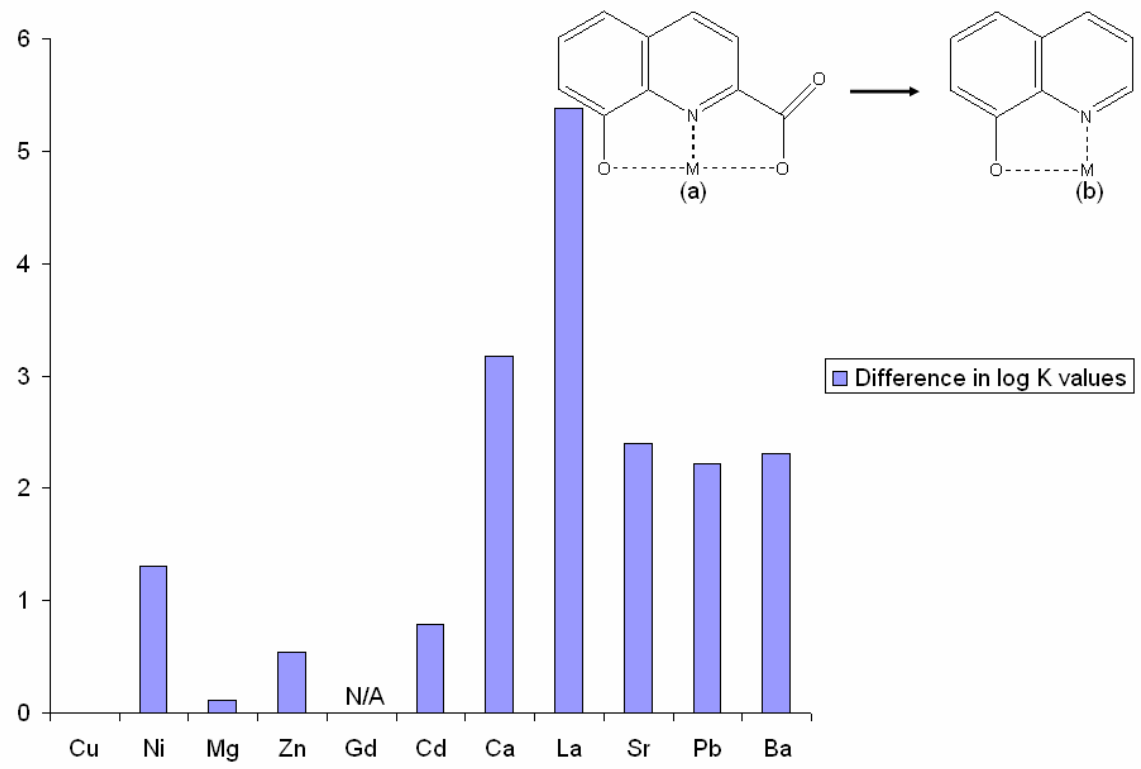

Figure 39. Graph of the difference in log *K* values for (a) HQC and (b) oxine.

enough to reach across the ligand's cavity to the carboxylate. Copper is a perfect example of this situation. Copper has a formation constant of 12.00 with oxine. However, when the denticity increased with the addition of the carboxylate (to HQC) there was no change in formation constant. This lack of change shows copper, the smallest metal ion in this study with a radius of only 0.57 Å, cannot bridge the gap to the carboxylate. This postulate was confirmed when the pK_1 and pK_2 were reviewed and the HQC – copper complex had only one protonation constant (Figure 38). Though nickel, magnesium, zinc, and cadmium complexes have two protonation constants, the same basic theory applies. As the metal becomes large enough to coordinate fully to both donor groups the change in formation constant from oxine to HQC become increasingly more pronounced. This trend continues until the metal becomes too large and the strain pushes the metal ion out of the plane. Once the metal ion is out of the plane the bond lengths and angles have increased enough to lower the stability of the complex. This in turn lowers the formation constant as seen in strontium, lead, and barium.

Effect of phenolate (Table 5 and Figure 40).

The most notable effect that the addition of a phenolate donor group has when compared to a carboxylate or alcohol is the structural rigidity it adds to the system. As compared to Δ log K for HQC and oxine and Δ log K for HQC and dipicolinic acid, HQC and picolinic acid have the largest difference in log K values. This can be attributed to the weak coordinating bond that the carboxylic acid provides. Overall the greatest differences were in the large metal ions such as Gd^{3+}, La^{3+}, and Pb^{2+}. However there was a trend in the block 2 metals where calcium seemed to have the greatest change in formation constant.

Table 5. Log of formation constants of various metals with HQC and picolinic acid.

Metal Ion	Ionic Radius	HQC	Picolinic Acid[35-38]
Cu^{2+}	0.57	12.00*	7.87
Ni^{2+}	0.69	10.58	6.72
Mg^{2+}	0.72	4.42	2.21
Zn^{2+}	0.74	9.10	5.23
Gd^{3+}	0.93	9.89	3.98
Cd^{2+}	0.95	8.57	4.35
Ca^{2+}	1.00	6.00	1.80
La^{3+}	1.03	11.28	3.51
Sr^{2+}	1.18	4.51	1.69
Pb^{2+}	1.19	11.24*	4.58
Ba^{2+}	1.35	3.93	1.65

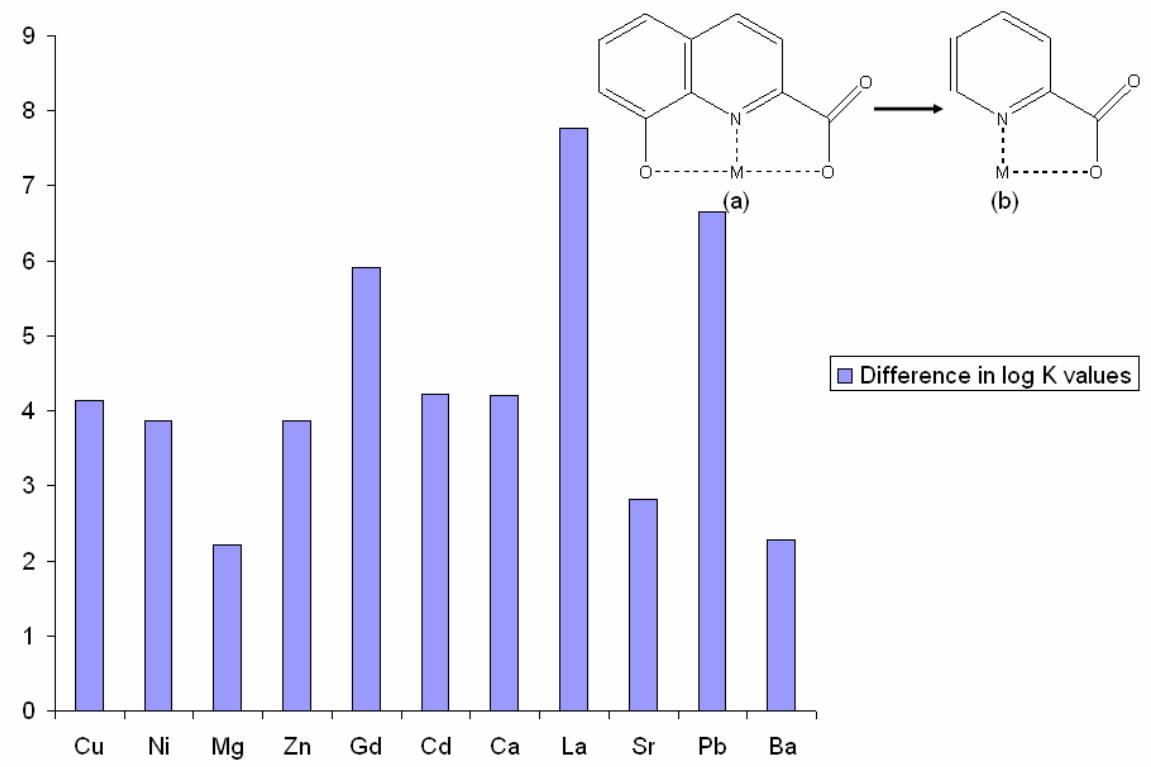

Figure 40. Graph of the difference in log *K* values for (a) HQC and (b) picolinic acid.

Effect of phenolate over carboxylate (Table 6 and Figure 41).

As noted earlier, Donald Cram defined preorganization as the more nearly a ligand is constrained to be in a specific conformation required to complex the metal ion. One such way to increase this constraint is to increase structural rigidity. This can be accomplished easily by adding a rigid backbone to the ligand.

In the case of every metal ion studied, the phenolate donor of HQC was found to increase the metal ligand formation constant over the formation constant of dipicolinic acid, which looks identical, with the exception of a second carboxylate in the place of the phenolate. The change in formation constants decreases gradually as the metal ion become larger. This trend is likely due to smaller metal ions struggling to bridge the breadth of the HQC cavity. In dipicolinic acid smaller metal ions are not forced to one carboxylate but are instead weakly coordinated to both. However in HQC the metal coordinates much more strongly to the phenolate. This pulls the metal far enough away from the carboxylate so that the carboxylate has little effect on the formation constant. The difference in this strong attraction of the smaller metal to the phenolate and the weak attraction holding the metal inside dipicolinic acid is greater the smaller the metal ion.

Large metals do not have as great a variation from coordination to dipicolinic acid to HQC. This is because these metals can completely coordinate to both carboxylates in dipicolinic acid and they also coordinate to both the phenolate and carboxylate in HQC. This makes $\Delta \log K$ less pronounced with the addition of the phenolate ion over the second carboxylate, with exception of both lanthanum and lead which seem to display a very high affinity for the phenolate donor or the increased structural rigidity it offers.

This trend can be readily identified when a group of similarly charged metals are grouped

Table 6. Log of formation constants of various metals with HQC and dipicolinic acid.

Metal Ion	Ionic Radius	HQC	Dipicolinic Acid[39-41]
Cu^{2+}	0.57	12.00*	9.10
Ni^{2+}	0.69	10.58	6.95
Mg^{2+}	0.72	4.42	2.34
Zn^{2+}	0.74	9.10	6.35
Gd^{3+}	0.93	9.89	8.69
Cd^{2+}	0.95	8.57	6.36
Ca^{2+}	1.00	6.00	4.36
La^{3+}	1.03	11.28	7.94
Sr^{2+}	1.18	4.51	3.85
Pb^{2+}	1.19	11.24*	8.70
Ba^{2+}	1.35	3.93	3.44

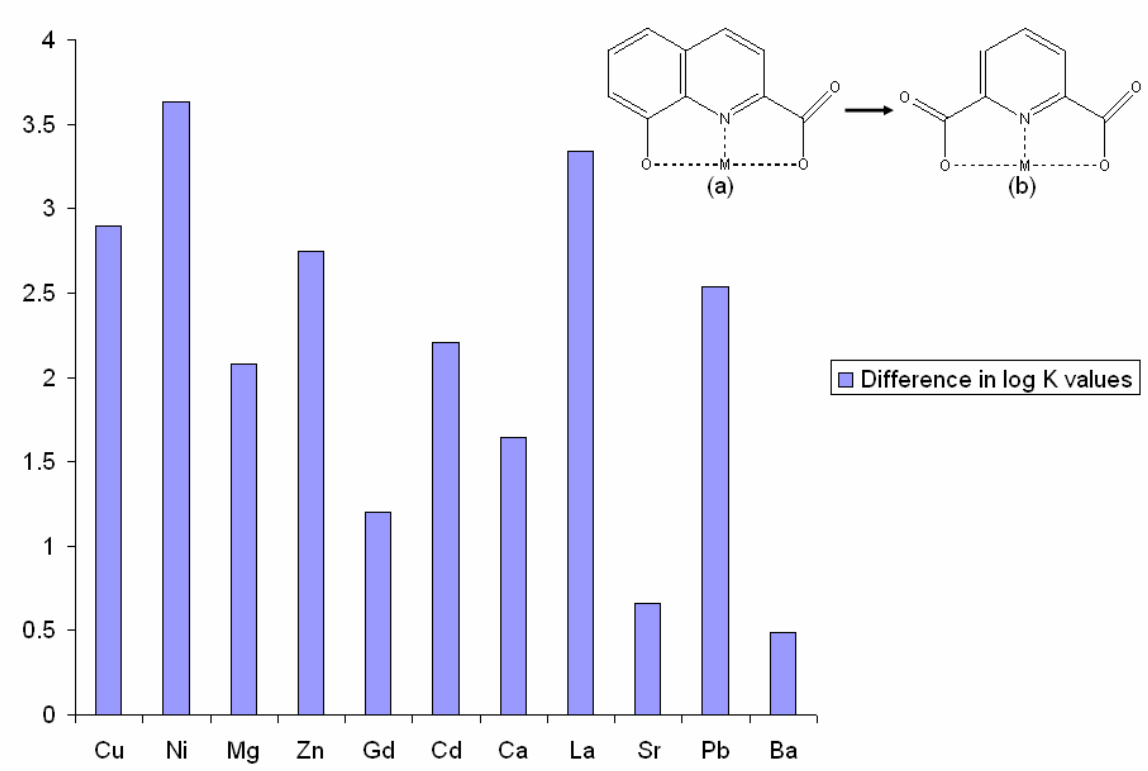

Figure 41. Graph of the difference in log *K* values for (a) HQC and (b) dipicolinic acid.

together by increasing size, such as Mg^{2+}, Ca^{2+}, Sr^{2+}, and Ba^{2+}. The reported formation constant for dipicolinic acid with Mg^{2+}, Ca^{2+}, Sr^{2+}, and Ba^{2+} was 2.34, 4.36, 3.85, and 3.44 respectively. The Δ log *K* between dipicolinic acid and HQC corresponding to the "block 2" metals was calculated to be 2.08, 1.64, 0.66, and 0.49 respectively (Table 6).

Crystal Structures

Structures of free ligand, Co^{2+}, and Ni^{2+} had been previously reported by Okabe and Muranishi[42,43]. The crystal structures of $[H_2(HQC)]$, $[Ni(HQC)_2]$, and $[Co(HQC)_2]$ are shown in Figures 42, 43 and 44. Cobalt and nickel are approximately the same size. The ionic radius of Co^{2+} is 0.74 and Ni^{2+} is 0.69 Å. Because cobalt and nickel are similar in size and charge it would be expected that the bond lengths between each metal and their respective donor atoms would be similar as well. This holds true when comparing the average bond length of Co-N ~1.973 Å to Ni-N ~1.976 Å. The difference in average bond lengths to both the carboxylate and phenolate are just as insignificant; Co-O_{phen} ~2.256 Å to Ni-O_{phen} ~2.259 Å and Co-O_{carb} ~2.102 Å to Ni-O_{carb} ~2.102 Å.

HQC allows for two five-membered rings to form, as previously stated. Five-membered rings favor larger metal ions with an ideal coordination length of ~2.5 Å and a bond angle of 70º (Figure 4 and 5). The reported bond lengths for both cobalt and nickel are shorter than ideal due to their small size. This in turn affects the bond angles formed, putting strain on the complex. This strain makes it increasingly unfavorable for the complex to form, which decreases the formation constant. The average bond angle for each complex was 76.9º for nickel and 77.0º for cobalt[42,43].

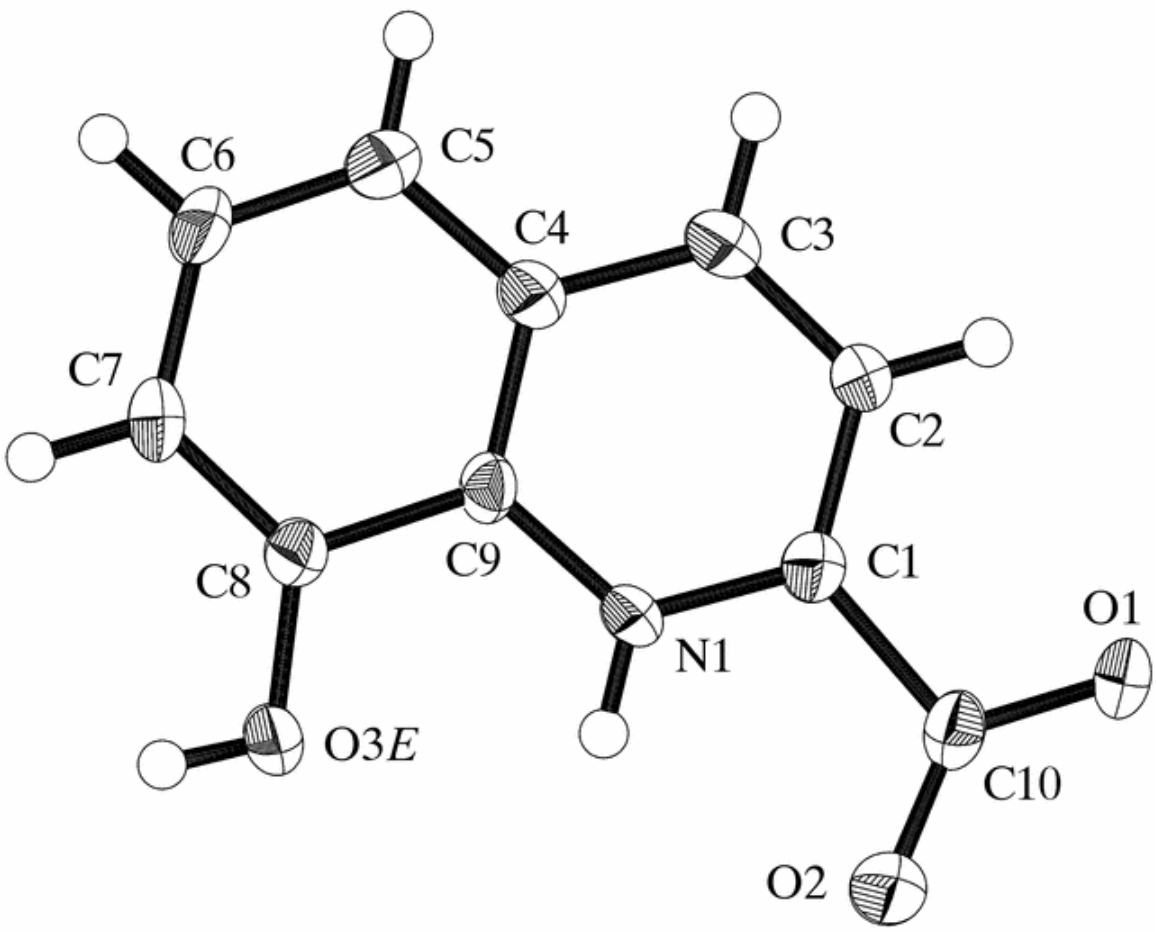

Figure 42. HQC structure as determined by Okabe[42].

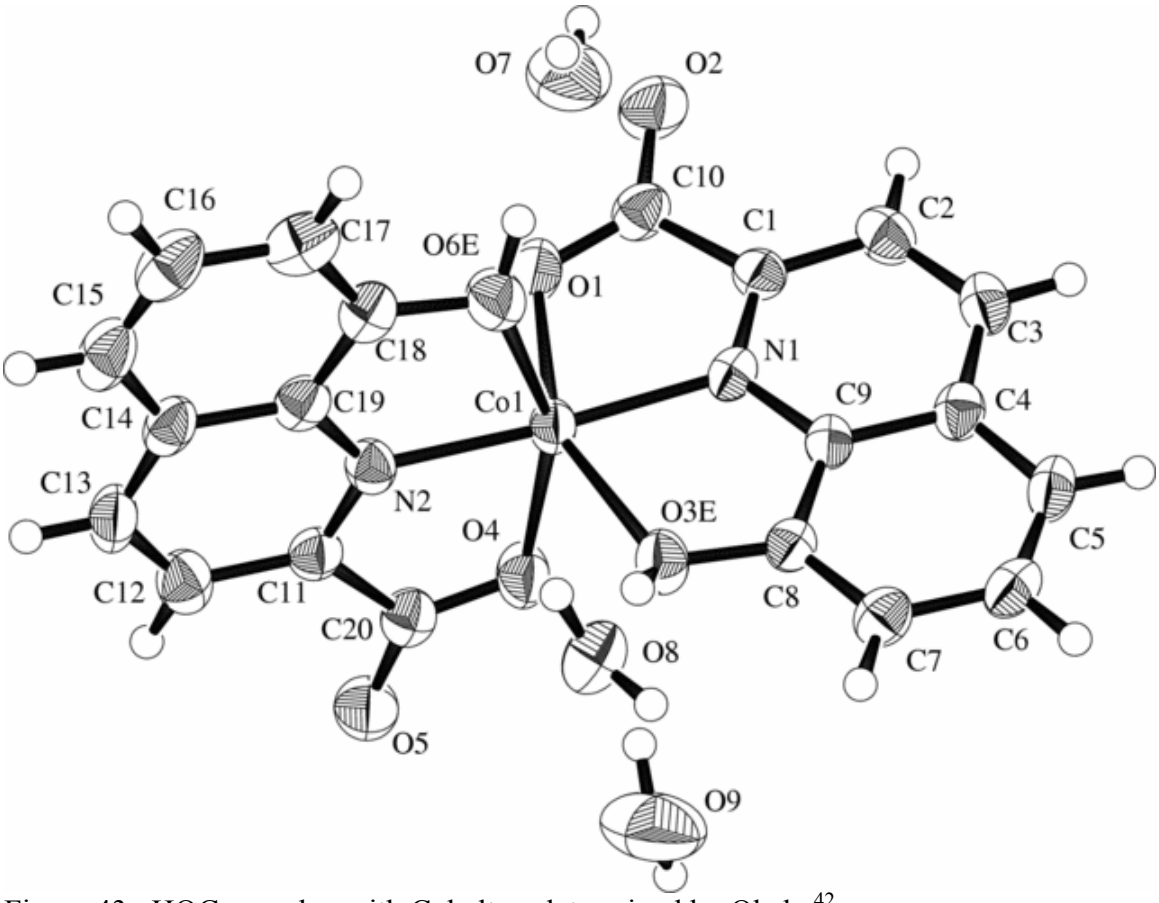

Figure 43. HQC complex with Cobalt as determined by Okabe[42].

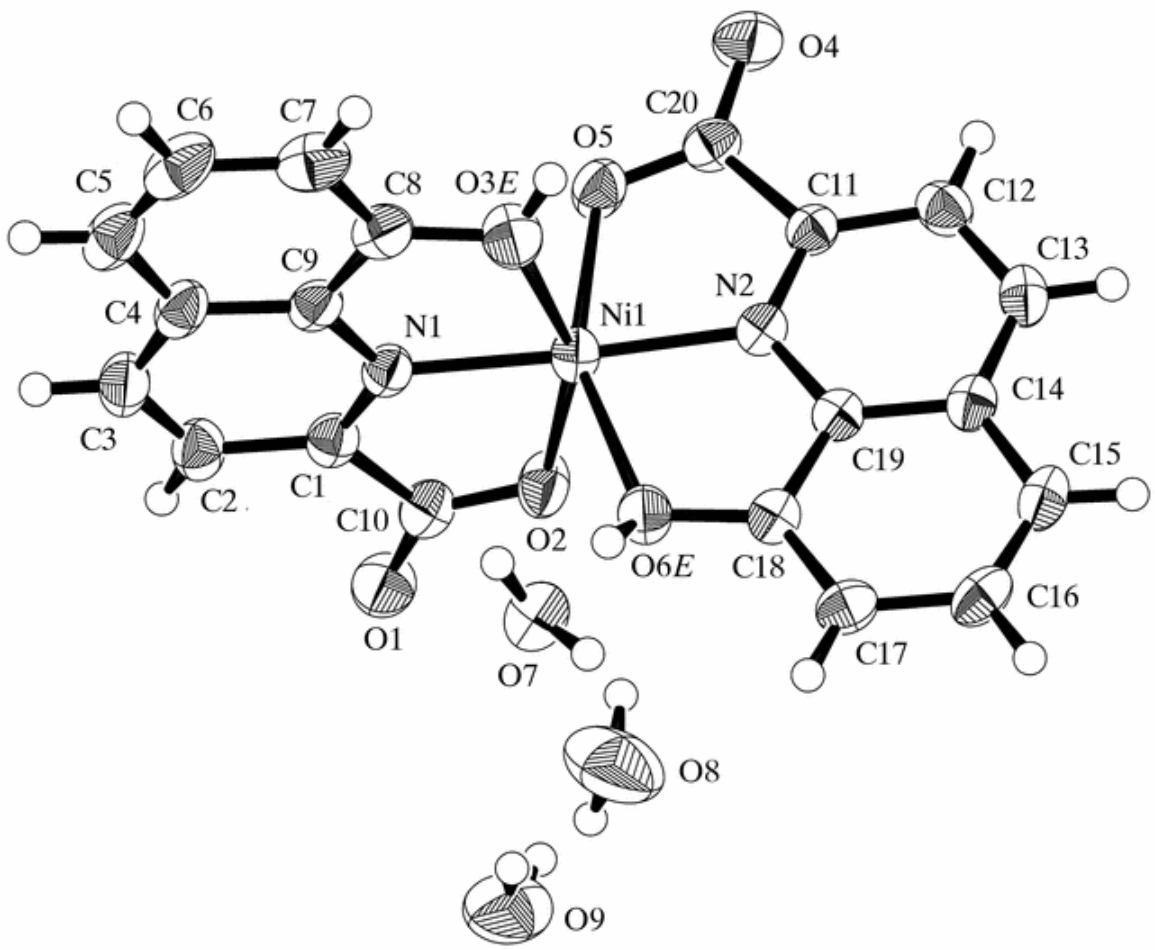

Figure 44. HQC complex with Nickel determined by Okabe[43].

[$Cd(HQC)_2$] crystal structure

The synthesis of [$Cd(HQC)_2$] produced orange plates of crystals along the water/n-butanol interface. Crystals were removed by vacuum filtration and dried on the lab bench. IR analysis was then used to confirm that product had been formed by comparing the Cd-HQC complex with an IR of the free ligand. There is a distinct peak in the IR of the free ligand seen at 3273 wave numbers which is the N – H stretch of the protonated pyridine (Figure 45a), however this peak is missing in the cadmium – HQC complex since the cadmium is coordinated to the pyridine (Figure 45b). Though it is likely that the complex is 1:1 when in solution the crystalline form of [$Cd(HQC)_2$] is 1:2 cadmium to HQC as seen in Figure 46. The cadmium in the complex is 6 coordinate, bound to two neutral nitrogen of the quinoline moiety, two phenolate oxygens, and two carboxylate oxygens. The crystal structure and refinement parameters for [$Cd(HQC)_2$] are listed in Table 7, while the spatial coordinates of the atoms are reported in Tables 8 and 9. Unlike all other reported complexes formed with HQC, cadmium has a radius of 0.95 Å making it much larger in comparison to cobalt, nickel, and zinc. Like the other reported structures cadmium was coordinated to two HQCs lying perpendicular to one another. Though the entire complex is quite 3 dimensional, the metal and ligand in 1:1 ratio continue to be planar. The bond distances for [$Cd(HQC)_2$] can be found in Table 10. The average bond distance from cadmium to a nitrogen donor was found to be 2.214 Å, the average distance from cadmium to O_{phen} was 2.398 Å and the average distance from cadmium to O_{carb} was 2.340 Å (Table 10). All bonds approached the ideal bond length of 2.5 Å for a five membered ring. The average bond angle for cadmium was reported as 71.3º which has much less steric strain than the other reported crystal structures (Table 11).

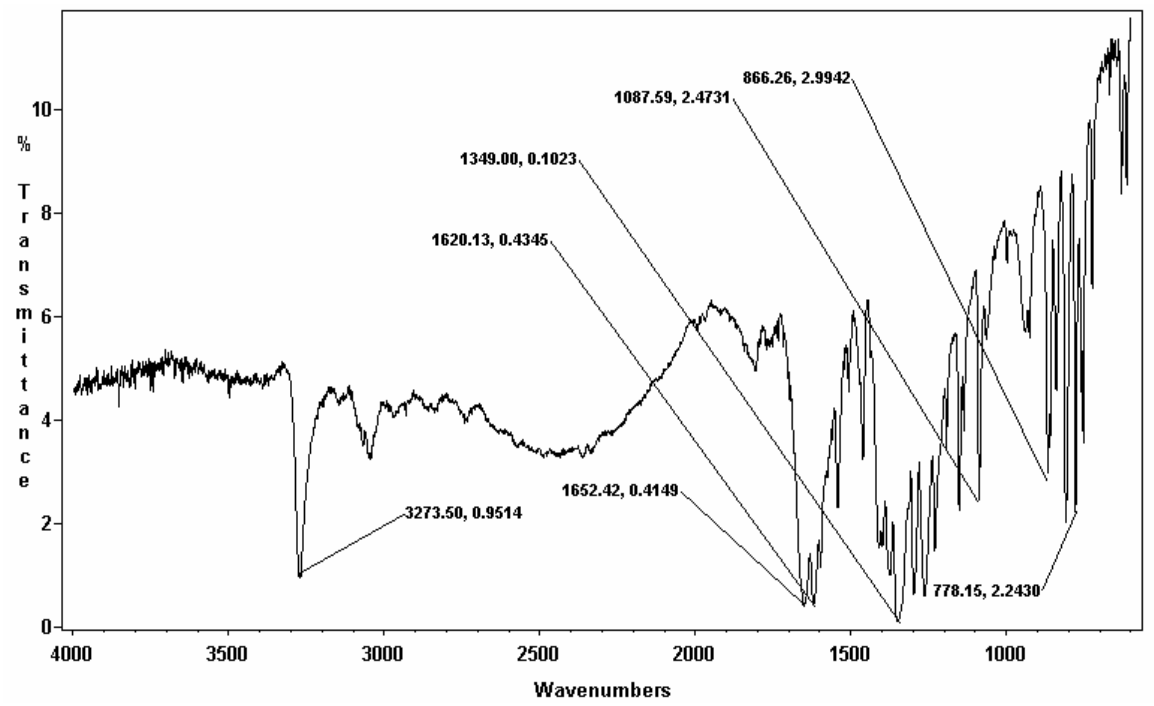

(a)

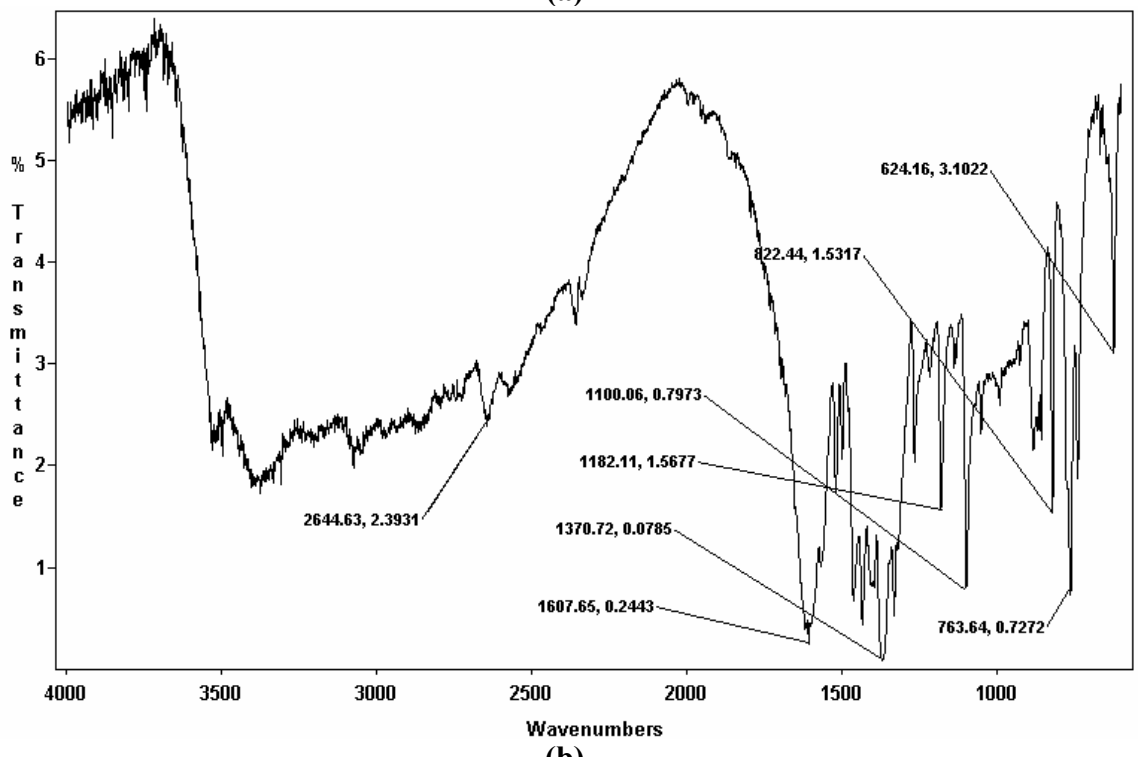

(b)

Figure 45. Infrared Spectroscopy of HQC alone (a) as compared to the $[Cd(HQC)_2]$ complex (b).

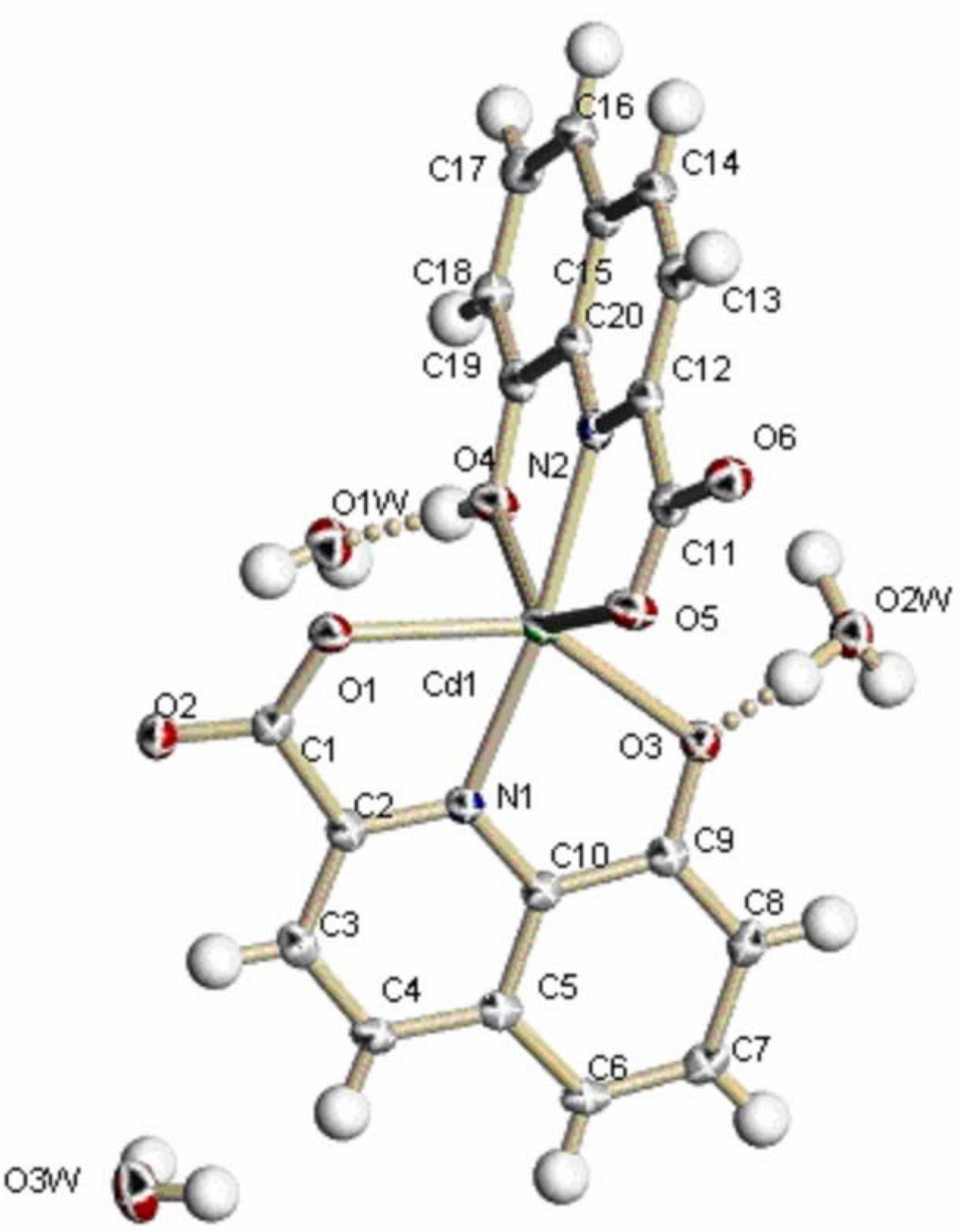

Figure 46. HQC and Cadmium Crystal Structure.

Table 7. Crystal data and structure refinement for HQC – Cd

Identification code	rh60	
Empirical formula	C20 H18 Cd N2 O9	
Formula weight	542.76	
Temperature	110(2) K	
Wavelength	0.71073 Å	
Crystal system	Triclinic	
Space group	P-1	
Unit cell dimensions	a = 7.0833(10) Å	a= 105.039(2)°.
	b = 9.1570(13) Å	b= 93.984(2)°.
	c = 16.054(2) Å	g = 107.101(2)°.
Volume	949.1(2) Å3	
Z	2	
Density (calculated)	1.899 Mg/m3	
Absorption coefficient	1.212 mm-1	
F(000)	544	
Crystal size	0.20 x 0.10 x 0.04 mm3	
Theta range for data collection	1.33 to 28.17°.	
Index ranges	-8<=h<=9, -12<=k<=11, -21<=l<=20	
Reflections collected	10812	
Independent reflections	4296 [R(int) = 0.0308]	
Completeness to theta = 28.17°	92.1 %	
Absorption correction	Semi-empirical from equivalents	
Max. and min. transmission	0.9531 and 0.7935	
Refinement method	Full-matrix least-squares on F2	
Data / restraints / parameters	4296 / 0 / 321	
Goodness-of-fit on F2	1.058	
Final R indices [I>2sigma(I)]	R1 = 0.0294, wR2 = 0.0678	
R indices (all data)	R1 = 0.0343, wR2 = 0.0702	
Largest diff. peak and hole	1.058 and -0.381 e.Å-3	

.

Table 8. Atomic coordinates (x 10^4) and equivalent isotropic displacement parameters ($Å^2$x 10^3) for HQC - Cd. U(eq) is defined as one third of the trace of the orthogonalized U^{ij} tensor.

x		y	z	U(eq)
Cd(1)	34(1)	3667(1)	2523(1)	14(1)
O(1)	-1961(3)	1208(2)	2703(1)	16(1)
O(2)	-1999(3)	-383(2)	3553(1)	17(1)
O(3)	2446(3)	6118(2)	3263(1)	15(1)
O(4)	2268(3)	2393(2)	1734(1)	18(1)
O(5)	-2414(3)	4770(2)	2300(1)	20(1)
O(6)	-4117(3)	5361(2)	1284(1)	18(1)
N(1)	883(3)	3610(2)	3856(1)	11(1)
N(2)	-559(3)	3359(2)	1096(1)	13(1)
C(1)	-1431(4)	938(3)	3398(2)	13(1)
C(2)	53(4)	2325(3)	4108(2)	13(1)
C(3)	493(4)	2299(3)	4965(2)	14(1)
C(4)	1809(4)	3637(3)	5564(2)	14(1)
C(5)	2706(3)	5020(3)	5310(2)	13(1)
C(6)	4078(4)	6465(3)	5880(2)	15(1)
C(7)	4849(4)	7722(3)	5559(2)	16(1)
C(8)	4345(4)	7645(3)	4681(2)	15(1)
C(9)	3024(4)	6278(3)	4104(2)	14(1)
C(10)	2199(3)	4947(3)	4431(2)	12(1)
C(11)	-2908(4)	4725(3)	1530(2)	14(1)
C(12)	-1974(4)	3868(3)	814(2)	14(1)
C(13)	-2538(4)	3663(3)	-74(2)	16(1)
C(14)	-1579(4)	2911(3)	-668(2)	18(1)
C(15)	-39(4)	2362(3)	-393(2)	15(1)
C(16)	1014(4)	1561(3)	-957(2)	18(1)
C(17)	2442(4)	1052(3)	-622(2)	19(1)
C(18)	2905(4)	1307(3)	281(2)	16(1)
C(19)	1924(4)	2084(3)	853(2)	15(1)
C(20)	425(4)	2626(3)	518(2)	14(1)
O(1W)	3952(3)	527(3)	2171(1)	20(1)
O(2W)	5048(3)	7325(2)	2441(1)	18(1)
O(3W)	8566(3)	1292(3)	6957(1)	27(1)

Table 9. Hydrogen coordinates (x 10^4) and isotropic displacement parameters (Å^{2}x 10^3) for HQC - Cd.

x	y	z	U(eq)
H(1)	2870(60)	1860(50)	1850(30)	55(13)
H(3)	-112	1367	5132	17
H(4)	2117	3635	6149	17
H(6)	4451	6555	6476	18
H(7)	5761	8685	5943	19
H(8)	4925	8547	4486	19
H(13)	-3563	4038	-259	19
H(14)	-1949	2754	-1273	21
H(16)	730	1376	-1570	21
H(17)	3141	511	-1009	23
H(18)	3906	938	496	20
H(1WA)	5080(60)	750(40)	2300(20)	31(10)
H(2WA)	3320(60)	-60(50)	2400(20)	38(11)
H(1WB)	4220(60)	6870(50)	2780(30)	54(12)
H(2WB)	6050(60)	7960(40)	2750(20)	35(10)
H(3WB)	5440(60)	6480(50)	1940(30)	71(14)
H(1WC)	8460(60)	2220(50)	6910(30)	53(12)
H(2WC)	9710(60)	1260(50)	6770(30)	64(14)

Table 10. Bond lengths [Å] for HQC - Cd. Symmetry transformations used to generate equivalent atoms.

Cd(1)-N(1)	2.200(2)
Cd(1)-N(2)	2.228(2)
Cd(1)-O(5)	2.2989(18)
Cd(1)-O(3)	2.3335(17)
Cd(1)-O(1)	2.3815(18)
Cd(1)-O(4)	2.4633(19)
O(1)-C(1)	1.260(3)
O(2)-C(1)	1.253(3)
O(3)-C(9)	1.341(3)
O(4)-C(19)	1.358(3)
O(5)-C(11)	1.249(3)
O(6)-C(11)	1.263(3)
N(1)-C(2)	1.329(3)
N(1)-C(10)	1.357(3)
N(2)-C(12)	1.322(3)
N(2)-C(20)	1.357(3)
C(1)-C(2)	1.521(3)
C(2)-C(3)	1.398(3)
C(3)-C(4)	1.373(4)
C(4)-C(5)	1.416(4)
C(5)-C(10)	1.412(3)
C(5)-C(6)	1.423(3)
C(6)-C(7)	1.366(4)
C(7)-C(8)	1.407(4)
C(8)-C(9)	1.375(3)
C(9)-C(10)	1.434(3)
C(11)-C(12)	1.522(3)
C(12)-C(13)	1.401(3)
C(13)-C(14)	1.368(4)
C(14)-C(15)	1.417(4)
C(15)-C(16)	1.410(4)
C(15)-C(20)	1.416(3)
C(16)-C(17)	1.364(4)
C(17)-C(18)	1.407(4)
C(18)-C(19)	1.368(4)
C(19)-C(20)	1.426(3)

Table 11. Bond angles [°] for HQC - Cd. Symmetry transformations used to generate equivalent atoms.

N(1)-Cd(1)-N(2)	169.01(7)	C(10)-C(5)-C(4)	117.3(2)
N(1)-Cd(1)-O(5)	117.81(7)	C(10)-C(5)-C(6)	118.3(2)
N(2)-Cd(1)-O(5)	72.59(7)	C(4)-C(5)-C(6)	124.4(2)
N(1)-Cd(1)-O(3)	72.47(7)	C(7)-C(6)-C(5)	119.1(2)
N(2)-Cd(1)-O(3)	111.71(7)	C(6)-C(7)-C(8)	122.6(2)
O(5)-Cd(1)-O(3)	94.30(6)	C(9)-C(8)-C(7)	120.7(2)
N(1)-Cd(1)-O(1)	70.91(7)	O(3)-C(9)-C(8)	124.3(2)
N(2)-Cd(1)-O(1)	104.86(7)	O(3)-C(9)-C(10)	118.2(2)
O(5)-Cd(1)-O(1)	99.89(6)	C(8)-C(9)-C(10)	117.4(2)
O(3)-Cd(1)-O(1)	143.25(6)	N(1)-C(10)-C(5)	121.2(2)
N(1)-Cd(1)-O(4)	100.84(7)	N(1)-C(10)-C(9)	116.9(2)
N(2)-Cd(1)-O(4)	68.83(7)	C(5)-C(10)-C(9)	121.9(2)
O(5)-Cd(1)-O(4)	141.35(6)	O(5)-C(11)-O(6)	125.4(2)
O(3)-Cd(1)-O(4)	97.59(6)	O(5)-C(11)-C(12)	118.8(2)
O(1)-Cd(1)-O(4)	92.15(6)	O(6)-C(11)-C(12)	115.8(2)
C(1)-O(1)-Cd(1)	114.98(15)	N(2)-C(12)-C(13)	122.6(2)
C(9)-O(3)-Cd(1)	113.78(14)	N(2)-C(12)-C(11)	114.7(2)
C(19)-O(4)-Cd(1)	114.72(15)	C(13)-C(12)-C(11)	122.7(2)
C(11)-O(5)-Cd(1)	115.90(15)	C(14)-C(13)-C(12)	118.5(2)
C(2)-N(1)-C(10)	120.6(2)	C(13)-C(14)-C(15)	120.8(2)
C(2)-N(1)-Cd(1)	120.87(16)	C(16)-C(15)-C(20)	118.7(2)
C(10)-N(1)-Cd(1)	118.47(16)	C(16)-C(15)-C(14)	124.7(2)
C(12)-N(2)-C(20)	119.8(2)	C(20)-C(15)-C(14)	116.5(2)
C(12)-N(2)-Cd(1)	117.81(16)	C(17)-C(16)-C(15)	119.9(2)
C(20)-N(2)-Cd(1)	122.30(16)	C(16)-C(17)-C(18)	121.6(2)
O(2)-C(1)-O(1)	125.7(2)	C(19)-C(18)-C(17)	120.5(2)
O(2)-C(1)-C(2)	116.9(2)	O(4)-C(19)-C(18)	124.9(2)
O(1)-C(1)-C(2)	117.4(2)	O(4)-C(19)-C(20)	116.2(2)
N(1)-C(2)-C(3)	121.6(2)	C(18)-C(19)-C(20)	118.9(2)
N(1)-C(2)-C(1)	114.5(2)	N(2)-C(20)-C(15)	121.8(2)
C(3)-C(2)-C(1)	123.8(2)	N(2)-C(20)-C(19)	117.8(2)
C(4)-C(3)-C(2)	119.2(2)	C(15)-C(20)-C(19)	120.4(2)
C(3)-C(4)-C(5)	120.1(2)		

$[Zn(HQC)_2]$ crystal structure

The synthesis of $[Cd(HQC)_2]$ produced green needlelike crystals along the water/n-butanol interface. Crystals were removed by vacuum filtration and dried on the lab bench. IR analysis was then used to confirm that product had been formed by comparing the Zn-HQC complex with an IR of the free ligand. There is a distinct peak in the IR of the free ligand seen at 3273 wave numbers which is the N – H stretch of the protonated pyridine (Figure 47a), however this peak is missing in the zinc – HQC complex since the zinc is coordinated to the pyridine (Figure 47b). Though it is likely that the complex is 1:1 when in solution the crystalline form of $[Zn(HQC)_2]$ is 1:2 zinc to HQC as seen in Figure 48. The zinc in the complex is 6 coordinate, bound to two neutral nitrogen of the quinoline moiety, two phenolate oxygen, and two carboxylate oxygen. The crystal structure and refinement parameters for $[Cd(HQC)_2]$ are listed in Table 12, while the spatial coordinates of the atoms are reported in Tables 13 and 14.

Zinc, having a 2+ formal charge and an ionic radius of 0.74 Å, is very similar to both cobalt and nickel. Like in all other HQC complexes, the two molecules of HQC in $[Zn(HQC)_2]$ lie perpendicular to one another with each individual HQC zinc complex remaining planar. The bond lengths for $[Zn(HQC)_2]$ can be found in Table 15. The average bond distance from zinc to a nitrogen donor was found to be 2.017 Å, the average distance from zinc to O_{phen} was 2.351 Å and the average distance from zinc to O_{carb} was 2.161 Å. Though the bond lengths were less than ideal there was a slight elongation of bond length when zinc was compared to both cobalt and nickel (Table 15). The average bond angle for zinc was 75.8º which is greater than desired but still sterically more favorable than cobalt and nickel (Table 16).

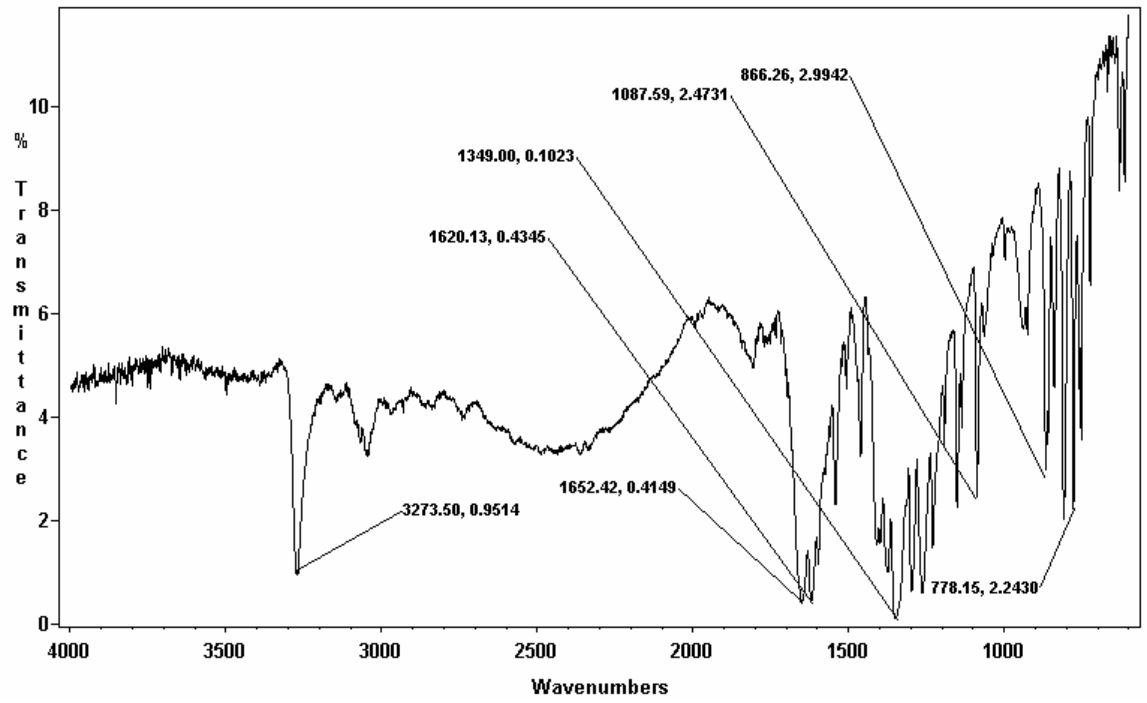

(a)

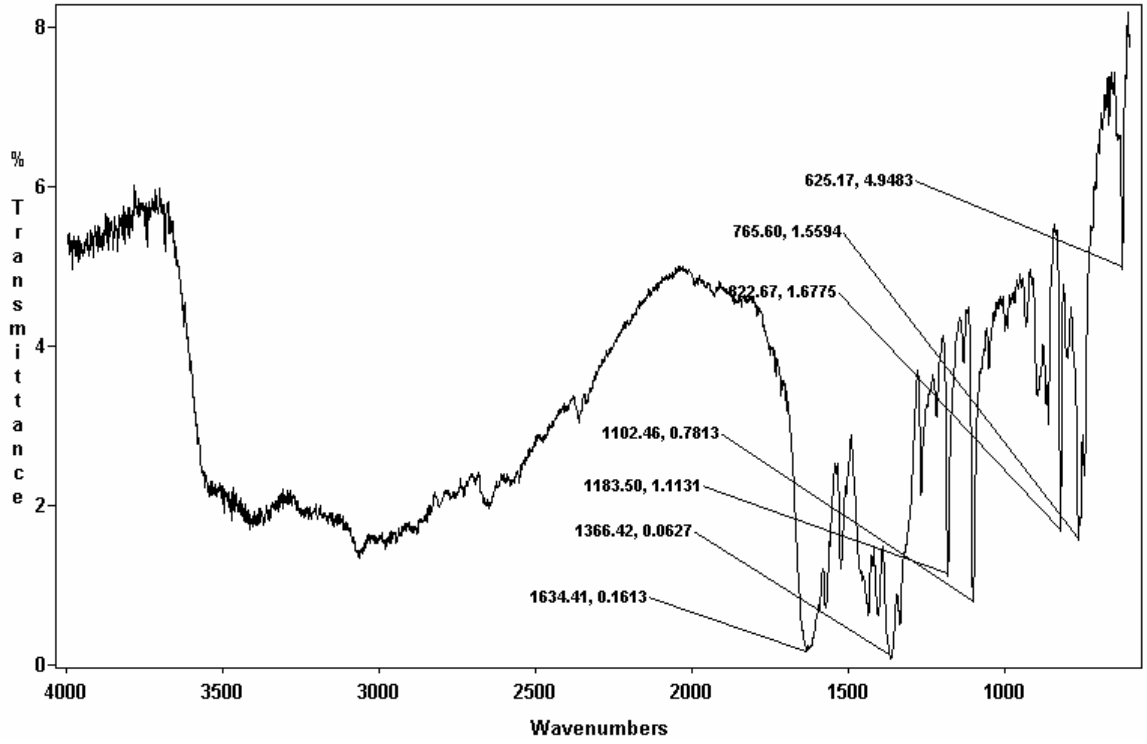

(b)

Figure 47. Infrared Spectroscopy of HQC alone (a) as compared to the complex of HQC and Zinc (b).

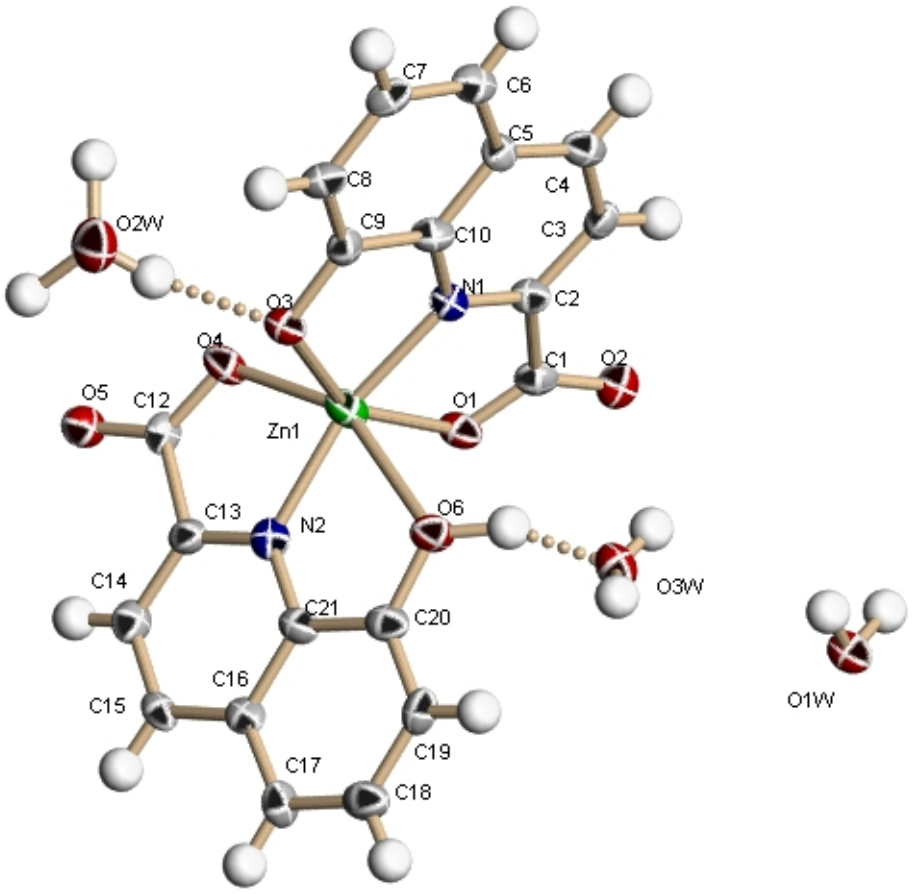

Figure 48. HQC and Zinc Crystal Structure.

Table 12. Crystal data and structure refinement for HQC - Zn.

Identification code	rh59	
Empirical formula	C20 H18 N2 O9 Zn	
Formula weight	495.73	
Temperature	110(2) K	
Wavelength	0.71073 Å	
Crystal system	Triclinic	
Space group	P-1	
Unit cell dimensions	a = 7.172(2) Å	a= 104.000(5)°.
	b = 9.253(3) Å	b= 94.829(5)°.
	c = 15.675(5) Å	g = 108.059(5)°.
Volume	945.2(5) Å3	
Z	2	
Density (calculated)	1.742 Mg/m3	
Absorption coefficient	1.361 mm-1	
F(000)	508	
Crystal size	0.10 x 0.10 x 0.05 mm3	
Theta range for data collection	4.28 to 24.99°.	
Index ranges	-8<=h<=8, -10<=k<=10, -18<=l<=18	
Reflections collected	6783	
Independent reflections	3042 [R(int) = 0.0837]	
Completeness to theta = 24.99°	91.6 %	
Absorption correction	Semi-empirical from equivalents	
Max. and min. transmission	0.9351 and 0.8759	
Refinement method	Full-matrix least-squares on F2	
Data / restraints / parameters	3042 / 0 / 289	
Goodness-of-fit on F2	1.017	
Final R indices [I>2sigma(I)]	R1 = 0.0638, wR2 = 0.1417	
R indices (all data)	R1 = 0.1043, wR2 = 0.1735	
Largest diff. peak and hole	0.983 and -0.668 e.Å-3	

Table 13. Atomic coordinates (x 10^4) and equivalent isotropic displacement parameters ($Å^2$x 10^3) for HQC - Zn. U(eq) is defined as one third of the trace of the orthogonalized U^{ij} tensor.

	x	y	z	U(eq)
Zn(1)	10085(1)	1313(1)	2495(1)	26(1)
O(1)	12023(6)	3676(4)	2422(2)	25(1)
O(2)	12187(6)	5325(5)	1571(3)	26(1)
O(3)	7713(6)	-1069(4)	1885(2)	23(1)
O(4)	12265(6)	285(5)	2631(2)	26(1)
O(5)	14045(6)	-265(5)	3677(2)	27(1)
O(6)	7728(6)	2524(5)	3130(2)	26(1)
N(1)	9213(7)	1352(5)	1253(3)	19(1)
N(2)	10497(7)	1631(5)	3832(3)	21(1)
C(1)	11538(9)	3992(7)	1725(4)	22(1)
C(2)	10025(8)	2631(6)	992(3)	20(1)
C(3)	9570(9)	2702(6)	121(4)	21(1)
C(4)	8243(9)	1357(7)	-483(4)	25(1)
C(5)	7336(9)	-19(6)	-238(3)	19(1)
C(6)	5951(9)	-1453(7)	-795(4)	26(1)
C(7)	5176(9)	-2708(6)	-458(4)	23(1)
C(8)	5707(10)	-2609(7)	456(4)	27(1)
C(9)	7052(9)	-1257(6)	1012(4)	20(1)
C(10)	7851(9)	46(7)	678(4)	23(1)
C(12)	12830(8)	309(6)	3417(4)	18(1)
C(13)	11908(9)	1131(6)	4142(4)	21(1)
C(14)	12475(9)	1369(7)	5049(4)	24(1)
C(15)	11502(9)	2098(6)	5646(3)	21(1)
C(16)	9995(9)	2617(6)	5336(3)	20(1)
C(17)	8932(9)	3388(7)	5898(4)	24(1)
C(18)	7523(10)	3878(7)	5527(4)	29(2)
C(19)	7065(9)	3615(6)	4600(4)	25(1)
C(20)	8049(9)	2842(6)	4027(4)	24(1)
C(21)	9503(9)	2335(6)	4400(4)	23(1)
O(1W)	5111(6)	7714(5)	2663(2)	25(1)
O(2W)	8708(7)	6251(5)	1868(3)	40(1)
O(3W)	6171(7)	4486(5)	2744(3)	30(1)

Table 14. Hydrogen coordinates (x 10^4) and isotropic displacement parameters ($Å^2$x 10^3) for HQC - Zn.

x	y	z	U(eq)
H(6O)	7162	3207	2812	31
H(3)	10153	3640	-48	25
H(4)	7934	1363	-1083	30
H(6)	5554	-1552	-1406	31
H(7)	4258	-3670	-845	28
H(8)	5122	-3487	676	32
H(14)	13512	1037	5256	29
H(15)	11853	2250	6267	25
H(17)	9195	3563	6526	28
H(18)	6834	4412	5908	35
H(19)	6078	3969	4365	29
H(1WA)	4164	6735	2348	30
H(2WA)	6054	8177	2264	30
H(1WB)	9648	6204	2536	48
H(2WB)	9166	5709	1200	48
H(3WB)	8849	7306	1953	48
H(1WC)	6776	4849	2357	36
H(2WC)	5066	4323	2930	36

Table 15. Bond lengths [Å] for HQC - Zn. Symmetry transformations used to generate equivalent atoms.

Zn(1)-N(1)	2.006(5)
Zn(1)-N(2)	2.028(5)
Zn(1)-O(4)	2.087(5)
Zn(1)-O(1)	2.234(4)
Zn(1)-O(3)	2.247(4)
Zn(1)-O(6)	2.454(4)
O(1)-C(1)	1.246(7)
O(2)-C(1)	1.266(7)
O(3)-C(9)	1.362(7)
O(4)-C(12)	1.257(7)
O(5)-C(12)	1.241(7)
O(6)-C(20)	1.349(7)
N(1)-C(2)	1.324(7)
N(1)-C(10)	1.349(7)
N(2)-C(13)	1.338(8)
N(2)-C(21)	1.357(8)
C(1)-C(2)	1.526(8)
C(2)-C(3)	1.400(8)
C(3)-C(4)	1.376(8)
C(4)-C(5)	1.399(8)
C(5)-C(6)	1.409(8)
C(5)-C(10)	1.433(8)
C(6)-C(7)	1.372(8)
C(7)-C(8)	1.425(8)
C(8)-C(9)	1.355(8)
C(9)-C(10)	1.409(8)
C(12)-C(13)	1.527(8)
C(13)-C(14)	1.389(8)
C(14)-C(15)	1.383(9)
C(15)-C(16)	1.407(9)
C(16)-C(17)	1.418(8)
C(16)-C(21)	1.420(7)
C(17)-C(18)	1.371(9)
C(18)-C(19)	1.407(8)
C(19)-C(20)	1.388(8)
C(20)-C(21)	1.408(9)

Table 16. Bond angles [°] for HQC - Zn. Symmetry transformations used to generate equivalent atoms.

N(1)-Zn(1)-N(2)	164.6(2)	C(4)-C(5)-C(6)	126.7(5)
N(1)-Zn(1)-O(4)	115.64(17)	C(4)-C(5)-C(10)	116.5(5)
N(2)-Zn(1)-O(4)	79.66(18)	C(6)-C(5)-C(10)	116.7(5)
N(1)-Zn(1)-O(1)	75.89(16)	C(7)-C(6)-C(5)	120.2(5)
N(2)-Zn(1)-O(1)	100.88(15)	C(6)-C(7)-C(8)	121.9(5)
O(4)-Zn(1)-O(1)	99.00(16)	C(9)-C(8)-C(7)	119.7(5)
N(1)-Zn(1)-O(3)	76.18(16)	C(8)-C(9)-O(3)	124.1(5)
N(2)-Zn(1)-O(3)	106.41(15)	C(8)-C(9)-C(10)	119.1(5)
O(4)-Zn(1)-O(3)	91.83(16)	O(3)-C(9)-C(10)	116.9(5)
O(1)-Zn(1)-O(3)	152.04(14)	N(1)-C(10)-C(9)	116.7(5)
N(1)-Zn(1)-O(6)	93.60(17)	N(1)-C(10)-C(5)	120.9(5)
N(2)-Zn(1)-O(6)	71.20(18)	C(9)-C(10)-C(5)	122.4(5)
O(4)-Zn(1)-O(6)	150.68(14)	O(5)-C(12)-O(4)	127.9(5)
O(1)-Zn(1)-O(6)	89.79(15)	O(5)-C(12)-C(13)	115.6(5)
O(3)-Zn(1)-O(6)	93.24(15)	O(4)-C(12)-C(13)	116.5(5)
C(1)-O(1)-Zn(1)	113.3(3)	N(2)-C(13)-C(14)	122.0(5)
C(9)-O(3)-Zn(1)	110.6(3)	N(2)-C(13)-C(12)	114.1(5)
C(12)-O(4)-Zn(1)	114.7(4)	C(14)-C(13)-C(12)	123.9(6)
C(20)-O(6)-Zn(1)	110.2(4)	C(15)-C(14)-C(13)	118.8(6)
C(2)-N(1)-C(10)	120.4(5)	C(14)-C(15)-C(16)	120.3(5)
C(2)-N(1)-Zn(1)	120.1(4)	C(15)-C(16)-C(17)	124.2(5)
C(10)-N(1)-Zn(1)	119.5(4)	C(15)-C(16)-C(21)	117.6(5)
C(13)-N(2)-C(21)	120.4(5)	C(17)-C(16)-C(21)	118.2(6)
C(13)-N(2)-Zn(1)	114.9(4)	C(18)-C(17)-C(16)	119.4(5)
C(21)-N(2)-Zn(1)	124.7(4)	C(17)-C(18)-C(19)	122.0(6)
O(1)-C(1)-O(2)	126.2(5)	C(20)-C(19)-C(18)	120.3(6)
O(1)-C(1)-C(2)	116.3(5)	O(6)-C(20)-C(19)	125.4(6)
O(2)-C(1)-C(2)	117.5(5)	O(6)-C(20)-C(21)	116.5(5)
N(1)-C(2)-C(3)	122.9(5)	C(19)-C(20)-C(21)	118.2(5)
N(1)-C(2)-C(1)	113.5(5)	N(2)-C(21)-C(20)	117.3(5)
C(3)-C(2)-C(1)	123.6(5)	N(2)-C(21)-C(16)	120.8(6)
C(4)-C(3)-C(2)	117.3(5)	C(20)-C(21)-C(16)	121.8(5)
C(3)-C(4)-C(5)	121.9(5)		

Hydronium importance

The structures of the Zn(II) and Cd(II) HQC complexes, together with those of the Co(II) and Ni(II) HQC structures reported by Okabe and Muranishi[42,43] show an interesting progression in the nature of the H-bonds. In all four structures one of the phenols is protonated in a normal way, with a somewhat longer M-O bond to the phenolic oxygen. For the second phenolic oxygen from an HQC ligand, the proton is somewhat removed from the phenolic oxygen, and shorter M-O bonds result. This supports the idea that this phenolate is different in the Zn^{2+} and Cd^{2+} structures reported here. In contrast, the Co^{2+} and Ni^{2+} structures reported by Okabe *et al.* do not show significantly different M-O bond lengths to the phenolates, and accordingly the protons appear to be attached at normal bond lengths to the coordinated phenolate oxygens. In contrast, for the Zn^{2+} structure, the proton appears to be placed symmetrically between the second coordinated phenolate oxygen and the H-bonded water molecule, giving a short low-energy bond. Such H-bonds are of interest[44] in biology, where they catalytically lower the barrier to reaction and speed up reactions. The Cd^{2+} structure is of particular interest in that the proton appears to be attached to the water molecule (Figure 49) rather than the phenolic oxygen. It is remarkable that a hydronium ion could be extracted from aqueous solution at pH ~5 when it is held in place only by a H-bond, and the concentration of hydronium ions at pH 5 is obviously rather low (10^{-5} *M*). One has to understand that the energy of short H-bonds as seen here is very high. One normally thinks of the energy of an H-bond as being quite weak at ~ 7 kcal·mol^{-1} [44]. However, such H-bonds typically involve O-- distances of about 2.7 Å. Very strong H-bonds involve more symmetrically placed H-atoms in the O--H--O bonding arrangement. Very strong H-bonds with energies of perhaps 90 kcal·mol^{-1} are found when the O--O distance contracts to

less than 2.5 Å[44] as found in the present structures. Thus, a hydronium ion could easily be held in place in the Cd(II)/HQC structure by such a very strong H-bond, even at a pH as high as 5.0.

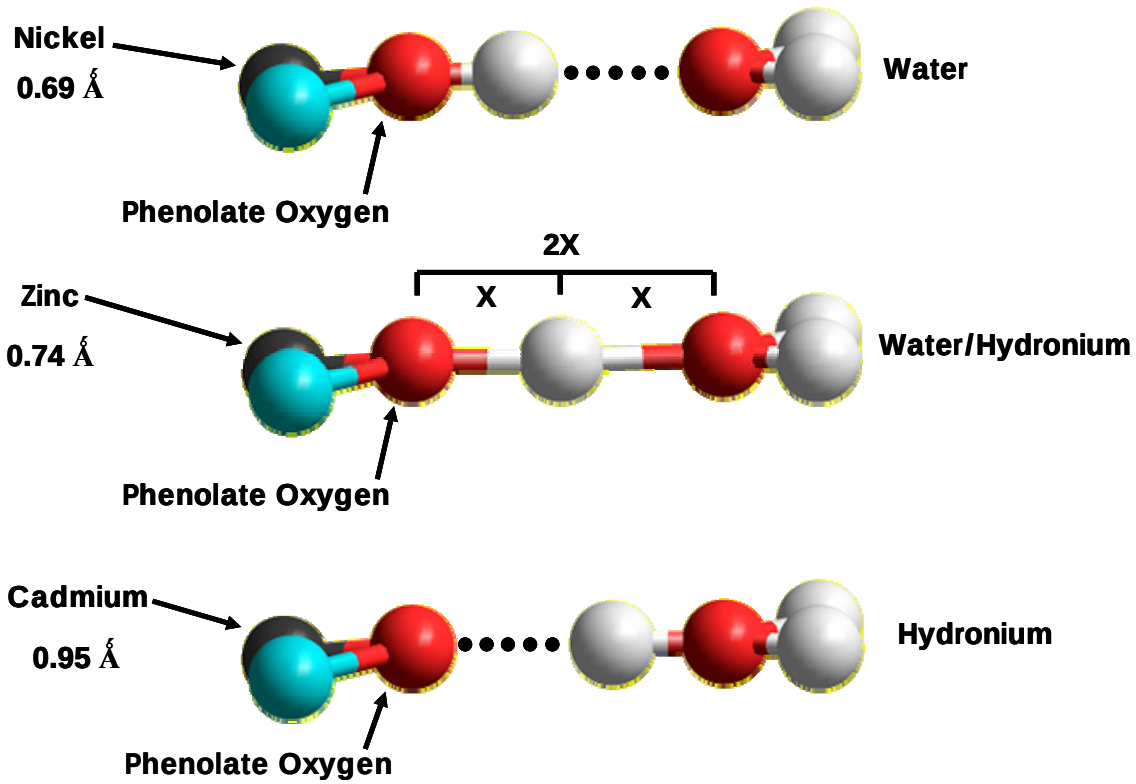

Figure 49. Distance of bonding hydrogen related to the size of the metal ion complexed Ni^{2+} < Zn^{2+} < Cd^{2+}.

Table 17. Important distances in bis-HQC complexes of various metal ions, showing the bonding distances to the phenolate oxygens, accompanying O-H bond lengths, and O--O separations of the H-bonded water molecules (O(w)). Note that for Ni(II) and Co(II) both phenolate oxygens are at normal bond lengths. For Zn(II) one phenolate has a short M-O(2) bond length, where the O-H bond is long with the proton placed symmetrically between the two O-atoms involved in the H-bond. For Cd(II) the long M-O(2) bond has the proton even further removed and forming a hydronium ion with the water molecule present. (Bond lengths in Å).

Metal ion:	Cd(II)	Zn(II)	Ni(II)[a]	Co(II)[a]
M-O(1)	2.465	2.431	2.290	2.285
O(1)-H	0.706	0.843	0.781	0.905
M-O(2)	2.334	2.220	2.227	2.226
O(2)-H	1.671	1.214	0.806	0.916
O(2)—O(w)	2.496	2.452	2.465	2.495

[a]Reference 42 and 43 Okabe and Muranishi.

CONCLUSION

UV-Visible spectroscopy is a highly effective method for studying complex formation of ligands such as 8-hydroxyquinoline-2-carboxylic acid which are of low water solubility and have extended aromatic system that give intense absorption in the 200-350 nm range. Studying metal – ligand (HQC) complex formation by UV spectroscopy, allows spectra of 1:1 metal – ligand solution as a function of pH to give successive protonation events that can be used to calculate equilibrium such as:

$$ML + H^+ \leftrightarrows MLH$$

$$MLH + H^+ \leftrightarrows M + LH_2$$

$$\underline{ML + OH^- \leftrightarrows MLOH}$$

$$M + L \leftrightarrows ML$$

The UV analysis of M – L equilibria involving HQC shows that there is a protonation event that occurs before further protonation causes the metal ion to be removed from the ligand. Crystal structures for Zn^{2+} and Cd^{2+} show that this proton is attached to a phenolic oxygen, so that a coordinated protonated oxygen of this type is determined. In other words, the crystallography supports our interpretation of the UV-Visible spectra.

HQC is a highly preorganized ligand that shows strong selectivity for larger metal ions such as Pb^{2+} and La^{2+}, with an ionic radius in the vicinity of 1.0 Å. This relates to chelate ring size rules. HQC has two five-membered rings in its complexes, which predicts this would be the case. The carboxylate of HQC causes considerable stabilization compared to oxine complexes, again mostly for larger metal ions that can span the gap between the oxygen donors of HQC. The more basic phenolate group on the HQC leads to complexes of conceivably enhanced thermodynamic stability compared to its analog, dipicolinic acid. Replacement of a carboxylate

of dipicolinic acid with a phenolate increases log K_1 greatly for larger more acidic metal ions such as Pb^{2+}.

WORKS CITED

1. D.J. Cram, *TheDesign of Molecular Hosts, Guests, and their Complexes*, 1987, Nobel Lecture.

2. N. Uchida, H. Kasai, Y. Takeda, R. Maekawa, K. Sugita, T. Yoshioka, *Anticancer Res.,* 1998, 18, 247

3. J.L. Misset, *Br. J. Cancer.,* 1998, 77, 4

4. B.K. Keppler, D. Schmähl, *Arzneim. Forsch*., 1986, 36, 1822

5. S.J. Berners-Price, R.J. Bowen, P. Galettis, P.C. Healy, M.J. McKeage, *Coord. Chem Rev.*, 1999, 185, 823

6. P. Collery, M. Morel, B. Desoize, H. Millart, D. Perdu, A. Prevost, H. Vallerand, C. Pechery, H. Choisy, J.C. Etienne, J.M.D. Demontreynaud, *Anticancer Res.,* 1991, 11, 1529

7. F. Kratz, M. Hartmann, B.K. Keppler, L. Messori, *J. Bio. Chem.*, 1994, 269, 2581

8. C.F. Shaw III in *Gold – Progress in Chemistry, Biochemistry, and Technology*, Wiley, New York, 1999.

9. G.F. Baxter, *Chem. B*r., 1992, 28, 445

10. J.L. Clement, P.S. Jarrett, *Met. Based Drugs*, 1994, I, 467

11. Z.I. Cabantchik, H. Glickstein, J. Golenser, M. Loyevsky, A. Tsafack, *Acta Haematol.,* 1996, 95, 70

12. J.S. Bishop, J.K. Guycaffey, J.O. Ojwang, S.R. Smith, M.E. Hogan, P.A. Cossum, R.F. Rando, N. Chaundhary, *J. Biol. Chem.,* 1996, 271, 5698

13. I.H. Tuzal, *J. Clin. Pharmacol.,* 1974, 14, 494

14. M. Nicolini, G. Bandoli, U. Mazzi, *Technetium and Rhenium in Chemistry and Nulsear Medicine.* SG Editorali, Padova, Italy, 1995.

15. P.F. Sharp, F.W. Smith, H.G. Gemmell, D. Lyall, N.T.S. Evans, D. Gvozdanovic, J. Davidson, D.A. Tyrell, R.D. Pickett, R.D. Neirinckx, *J. Nucl. Med*., 1986, 27, 171

16. E. Deutsch, W. Bushong, K.A.Glavan, R.C. Elder, V.J. Sodd, K.L.Scholz, D.L. Fortman, S.J. Lukes, *Science.,* 1981, 214, 85

17. T.W. Redpath, *Br. J. Radiol.*, 1997, 70, S70

18. B. Gallez, G. Bacic, H.M. Swartz, *Magn. Resn. Med*., 1996, 35, 14

19. S.M. Rocklage, W.P. Cacheris, S.C. Quay, K.N. Raymond, *Inorg. Chem.,* 1989, 28, 477

20. A.E. Martell and R.D. Hancock, *Metal Complexes in Aqueous Solutions*, Plenum, New York, 1996.

21. Ahrland, S., Chatt, J., Davies, N.R. *Quart. Rev.* London, 1958, 12, 265

22. Edwards, J.O., Pearson, R.G. *J. Am. Chem. Soc*., 1962, 84, 16

23. Pearson, R.G. *J. Am. Chem. Soc*., 1963, 85, 3533

24. Pearson, R.G. *Science*, 1966, 151, 172-177

25. Pearson, R.G. *J. Chem. Ed*., 1968, 45, 581

26. Pearson, R.G. *J. Chem. Ed*., 1968, 45, 643

27. Pearson, R.G. *Chem. Comm*., 1968, 65

28. Leden and Chatt, J., 1955, 2936

29. A.E. Martell and R.M. Smith, *Critical Stability Constants*, Plenum, New York, Vols. 1-6. 1974-1989.

30. R.D. Hancock, *J. Chem. Ed*., 1992, 615

31. M. Borrel and R. S. Paris, Anal. Chim. Acta, 1952, 6, 389

32. E. S. Tinovskaya, Zh. Anal. Khim., 1950, 5, 345; Chem Abstr., 1951, 45, 930g

33. R. Nasanen, Acta Chem. Scand., 1951, 5, 1293

34. D. Dyrssen, Svensk Kem. Tidskr., 1954, 66, 234

35. F. Holmes and W. R. C. Crimmin, J. Amer. Chem. Soc., 1955, 1175

36. P. O. Lumme, Suomen Kem., 1957, B10, 182

37. L. C. Thompson. Inorg. Chem., 1964, 3, 1319L.

38. Moyne and G. Thomas, Anal. Chim. Acta, 1964, 31, 583

39. R. M Tichane and W. E. Bennett, J. Amer. Chem. Soc., 1957, 79, 1293

40. K. Suzuki and Y. Yamasaki, Naturwiss., 1957, 44, 396

41. I. Grenthe, J. Amer. Chem. Soc., 1961, 83, 360

42. N. Okabe and Y, Muranishi. *Acta Cryst.,* 2002, *C*58, 475-477.

43. N. Okabe and Y, Muranishi. *Acta Cryst.,* 2002, E58, 352-353.

44. F. Hibbert, J. Emsley, *Adv. Phys. Org. Chem.,* 1990, *26*, 255.

45. R.D. Hancock, *J. Chem. Ed.,* 1992, 69, 615-620.